Construction of C^∞ Surfaces from Triangular Meshes Using Parametric Pseudo-Manifolds

Marcelo Siqueira
Departamento de Computação e Estatística
Universidade Federal de Mato Grosso do Sul
Campo Grande, MS 79002-204, Brazil
email: marcelo@dct.ufms.br

Dianna Xu
Department of Computer Science
Bryn Mawr College
Bryn Mawr, PA 19010, USA
email: dxu@cs.brynmawr.edu

Jean Gallier
Department of Computer and Information Science
University of Pennsylvania
Philadelphia, PA 19104, USA
email: jean@cis.upenn.edu

Technical Report MS-CIS-08-14

University of Pennsylvania
Department of Computer and Information Science

ACKNOWLEDGMENTS

This manuscript was the result of a collaborative work initiated at INRIA, Sophia-Antipolis, France, during the summer of 2007. We are grateful to Nicholas Ayache and the members of the ASCLEPIOS group for their hospitality.

Some people have read incomplete versions of the manuscript, pointed out several mistakes, and given useful suggestions. In particular, we thank Dimas Martínez, Luis Gustavo Nonato, and Luiz Velho for that. All of them are currently working with us on some extensions of the results described in this manuscript. In addition, Luis Gustavo Nonato generated the curvature plots in Chapter 6. We are also very grateful to Jos Stam for providing us with his own code for exact evaluation of Loop subdivision surfaces.

Almost all triangle meshes used in the experiments described in this manuscript belong to the repository of 3D digital models of the AIM@SHAPE project. We also relied upon several open source and freely available softwares, such as `MeshLab`, `Geomview`, `SurfRemesh` and `Blender`, for preprocessing the triangle meshes we used. Luiz Velho also provided us with a software for mesh simplification based on his Four-Face Clusters algorithm.

Marcelo Siqueira would like to thank CNPq for partially supporting his research (Grant 475703/2006-5).

ABSTRACT

We present a new constructive solution for the problem of fitting a smooth surface to a given triangle mesh. Our construction is based on the manifold-based approach pioneered by Grimm and Hughes. The key idea behind this approach is to define a surface by overlapping surface patches via a gluing process, as opposed to stitching them together along their common boundary curves. The manifold-based approach has proved to be well-suited to fit with relative ease, C^k-continuous parametric surfaces to triangle and quadrilateral meshes, for any arbitrary finite k or even $k = \infty$. Smooth surfaces generated by the manifold-based approach share some of the most important properties of splines surfaces, such as local shape control and fixed-sized local support for basis functions. In addition, the differential structure of a manifold provides us with a natural setting for solving equations on the surface boundary of 3D shapes.

Our new manifold-based solution possesses most of the best features of previous constructions. In particular, our construction is simple, compact, powerful, and flexible in ways of defining the geometry of the resulting surface. Unlike some of the most recent manifold-based solutions, ours has been devised to work with triangle meshes. These meshes are far more popular than any other kind of mesh encountered in computer graphics and geometry processing applications. We also provide a mathematically sound theoretical framework to undergird our solution. This theoretical framework slightly improves upon the one given by Grimm and Hughes, which was used by most manifold-based constructions introduced before.

Contents

List of Figures

Chapter 1

Introduction

The use of triangle meshes for the representation of surfaces with highly complex geometry and arbitrary topology has become the *de facto* standard in many different areas of computer graphics and geometry processing. This is mainly due to (1) their geometric simplicity, (2) the existence of efficient algorithms for displaying, editing, smoothing, simplifying, remeshing, parametrizing and compressing them, and (3) the advent and progress of 3D laser range scanner technologies [1]. In addition, most techniques for manipulating traditional industry-standard smooth surface representations, such as NURBS [2], are now available for triangle meshes.

Triangle meshes can represent surfaces with arbitrary topology with much more ease than smooth surfaces. In addition, triangle meshes have always been used in several stages of a typical pipeline in geometric design applications. Thus, it would seem attractive to replace smooth surfaces with triangle meshes in all stages, avoiding inter-stage, error-prone representation conversion and accelerating the production pipeline. On the other hand, in certain applications smooth surface representations are still preferable over triangle meshes for reasons of compactness, manufacturability, appearance, and high-degree continuity:

- Smooth surface representations offer a more compact way of representing fine geometric features, which would typically require an enormous amount of small triangles to achieve the same level of detail [3, 4, 5, 6, 7].

- Many shapes designed by CAD systems are physically realized by numerically controlled (NC) machines. To meet aesthetic and functional requirements, shapes are often represented by smooth surfaces [8].

- It is well known that C^2-continuity is important for visual quality, as it guarantees smooth normal variation.

- Higher degrees of continuity are desirable for numerical purposes. For instance, C^k-continuous surfaces, for any finite integer k, are used in [9] to enable smooth calculations in the quantification of joint kinematics, ligament strains, and distances between joint surfaces. In turn, C^∞-continuous surfaces are used in [10] to achieve high-order convergence rates in the numerical solution of boundary integral equations.

Therefore, algorithms to convert a triangle mesh representation into a smooth surface one and vice-versa are still necessary in the processing pipeline of certain applications related to computer graphics and scientific computing. In this paper, we are only interested in converting triangle mesh representations into smooth surfaces ones. In particular, we regard this conversion as a *surface fitting* problem, whose solution is a smooth surface with the same topology as the triangle mesh that closely approximates the mesh vertices.

Fitting a surface with guaranteed topology and continuity to the vertices of a mesh (triangle or quadrilateral) of arbitrary topology has been a topic of major research interest for many years. This is mainly due to the fact that, in general, meshes of arbitrary topology cannot be parametrized on a single rectangular domain and have no restriction on vertex connectivity. Much of the previous research efforts has been focused on stitching parametric polynomial patches together along their seams (see Figure 1.1). Each patch is the image of a distinct parametrization of a closed, planar domain. Because the patches need to be "pieced" together, there are natural smoothness concerns along the borders where they join. It turns out that ensuring continuity along the borders has proved to be a difficult problem, in particular for closed[1] meshes.

Although there is a large number of C^k constructions, where k is a finite integer, based on the "stitch-

[1]Meshes without boundary, or equivalently, in which each edge is shared by exactly two triangles (or quadrilaterals).

ing" paradigm and catered to triangle meshes[2] (see [11, 12, 13, 14, 15, 16, 17, 18, 19, 20, 21, 22, 23, 24, 25, 26]), only a few go beyond C^2-continuity (i.e., [19, 21, 26]). However, higher order constructions suffer from the following drawbacks:

- **High order polynomial patches**. To enforce high order continuity, high order polynomial patches, whose degree rapidly grows with the desired degree, k, of continuity, are required. A recent exception is the construction in [26], which is capable of producing G^k-continuous surfaces of low degree.

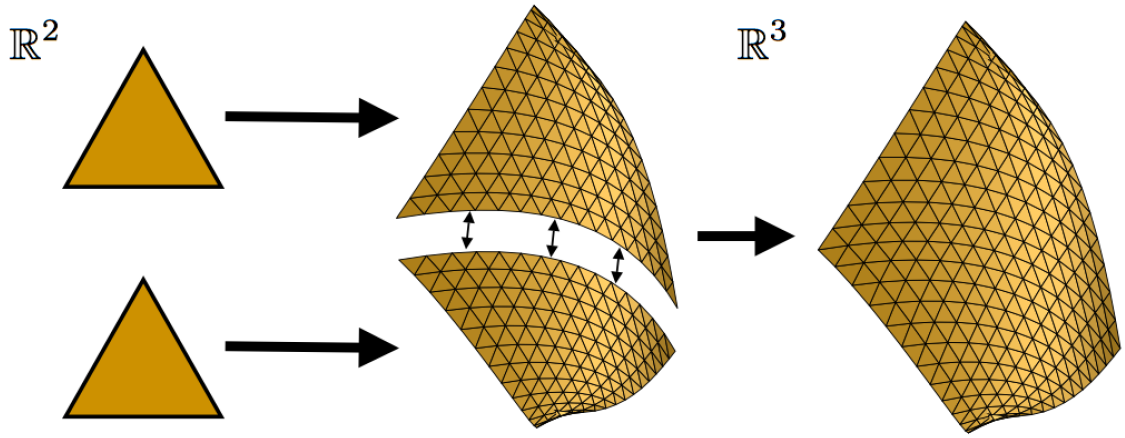

Figure 1.1: Two parametric surface patches joining together along their common boundary.

- **Free parameters**. The geometry of the polynomial patches is defined by a finite amount of points, called *control points*, whose locations are determined by *free parameters* of the construction. Free parameters can be used to adjust and fair the shape of the patches. However, an automatic procedure for optimizing these parameters is rarely found among the majority of the constructions. As a result, shape tuning is up to the designer and it can become an extremely laborious task if the triangle mesh has a large number of triangles (as the number of patches is in general no smaller than the number of triangles).

- **Lack of shape control**. Continuity is ensured by maintaining constraints on the position of the control points, which limits the freedom to move those points freely to achieve a desirable shape.

[2]Some of them are actually G^k-continuous, which is a measure of continuity that subsumes strict parametric continuity.

- **Lack of simplicity**. Higher order constructions are in general complex. Very few of them were ever implemented, and the visual quality of their resulting surfaces was typically inferior to lower degree constructions.

Subdivision surfaces are another common approach to fit a smooth surface to triangle or quadrilateral meshes of arbitrary topology, and they have been extensively investigated in the recent past [27, 28, 29, 30, 31, 32, 33]. These surfaces are limit surfaces obtained by repeatedly subdividing a given polygonal mesh. The subdivision process requires nothing else than vertex positions and connectivity information, is in general very simple, can easily handle meshes with arbitrary topology, and produces smooth surfaces with good visual quality in an intuitive sense, except near vertices of high degree[3]. These are the main reasons for the success of subdivision surfaces in the computer graphics and geometric modeling communities.

Despite their advantages for modeling surfaces of arbitrary topology, subdivision surfaces also have drawbacks. For instance, surface evaluation is often carried out by explicit, recursive subdivision, as most subdivision schemes do not possess a closed-form, analytic formulation (the Catmull-Clark subdivision scheme [27] is a notable exception [34]). In addition, most existing subdivision schemes yield G^k- or C^k-continuous surfaces, for $k = 1, 2$, only. If the input mesh has *extraordinary* vertices[4], then the resulting subdivision surface is not even C^1 at those vertices, and it may also present shape artifacts around them [35, 36]. Although it is possible to produce subdivision surfaces with C^2 or even higher continuity order at extraordinary vertices, previous efforts by Prautzsch and Reif [37, 38] have shown that subdivision schemes to produce such surfaces cannot be as simple and elegant as existing subdivision schemes. Finally, there is also no easy way to parametrize a subdivision surface for purposes such as texture mapping.

Implicit functions have also been used to fit smooth surfaces to triangle meshes [4, 5]. Implicit and parametric representations have complementary properties, and hence the advantages and drawbacks of each is highly dependent on the application [39]. In particular, implicit functions have been successfully used for fitting surfaces to dense and unorganized point sets [40, 41, 42]. This is because unorganized point sets have no explicit topological information, and this information is not required for defining an

[3]The degree of a vertex is the number of edges incident to it.

[4]For triangle (resp. quadrilateral) mesh based schemes, this means a vertex of degree different from six (resp. four).

implicit surface that interpolates or closely approximates the points. However, in general the topology of the resulting surface cannot be anticipated, unless the point set is very dense and satisfies some special constraints [43]. Although the topology is known *a priori* in the surface fitting problem we are interested here (i.e., it is the mesh topology), ensuring that the implicit surface will have this exact topology remains very difficult, and we are not aware of any result that provides such a guarantee for *any* triangle mesh of arbitrary topology.

Finally, a manifold-based approach pioneered by Grimm and Hughes [44] has proved to be well-suited to fit with relative ease, C^k-continuous parametric surfaces to triangle and quadrilateral meshes, for any arbitrary finite k or even $k = \infty$ [45, 46, 47, 48]. Manifold-based constructions also share some of the most important properties of splines surfaces, such as local shape control and fixed-sized local support for basis functions. In addition, the differential structure of a manifold provides us with a natural setting for solving equations on surfaces with complex topology and geometry. Thus, as pointed out in [49], a manifold is a very attractive surface representation form for a handful of applications in computer graphics, such as reaction-diffusion texture [50], texture synthesis [51, 52], fluid simulation [53], and surface deformation [54].

The main **contributions** of our work are two-fold:

(1) A new manifold-based construction for fitting a C^∞-continuous surface to a triangle mesh of arbitrary topology. Our construction combines, in the same framework, *most* of the best features of previous constructions. In particular, it is simpler and more compact than the ones in [44, 45, 48], does not contain singular points as the construction in [47], and shares with [46], a construction devised for quadrilateral meshes, the ability of producing C^∞-continuous surfaces and the flexibility in ways of defining the geometry of the resulting surface.

(2) A theoretical framework that provides a sound justification for the correctness of our construction. This framework is a slight improvement upon the one in [44], which was also used to undergird the constructions in [45, 46, 48].

After a review of prior work, given in Chapter 2, we review some basic mathematical notions in Chapter 3, and introduce the theoretical framework that supports our manifold-based construction. In Chap-

ter 4 and Chapter 5, we describe in detail our manifold-based construction for fitting a C^∞-continuous surface to a triangle mesh. In Chapter 6, we give details of an implementation of our construction, and present and discuss experimental results. Finally in Chapter 7, we offer some concluding remarks and directions for future work.

Chapter 2

Background and Prior Work

The formal definition of a manifold can be found in standard mathematics textbooks [55, 56, 57], and is also given in Chapter 3. Informally, manifolds are spaces that locally behave like the familiar n-dimensional Euclidean space, and on which we one can do calculus (e.g., compute derivatives, integrals, volumes, and curvatures). For that, each manifold, M, is equipped with a differentiable structure called an *atlas*. An atlas, $\mathcal{A}$, is a collection of *charts*. Each chart is a pair, (U, φ), where U is an open set of M and $\varphi : U \to \varphi(U) \subseteq \mathbb{R}^n$ is a continuous and bijective map whose inverse is also continuous. This means that $\varphi(U)$ is also an open set of $\mathbb{R}^n$. Furthermore, every point of the manifold, M, belongs to the open set, U, of at least one chart of its atlas, $\mathcal{A}$. Thus, the atlas, $\mathcal{A}$, establishes a correspondence between one neighborhood (i.e., some U) of every point of M and an open set (i.e., the set $\varphi(U)$) of $\mathbb{R}^n$. That's why we say that, locally, M looks like $\mathbb{R}^n$.

An atlas also enables us to do calculus on $\varphi(U)$ as we were doing on U. However, because the open sets, U_1 and U_2, of two distinct charts, (U_1, φ_1) and (U_2, φ_2), can overlap, we must also establish a correspondence between the subsets, $\varphi_1(U_1 \cap U_2)$ and $\varphi_2(U_1 \cap U_2)$, of $\mathbb{R}^n$ in order to do calculus on $\varphi_1(U_1)$ and $\varphi_2(U_2)$ in a consistent manner. This is done by defining *transition functions*, $\varphi_{21} : \varphi_1(U_1 \cap U_2) \to \varphi_2(U_1 \cap U_2)$ and $\varphi_{12} : \varphi_2(U_1 \cap U_2) \to \varphi_1(U_1 \cap U_2)$, which are required to satisfy the following two conditions (refer to Figure 2.1):

$$\varphi_{21} = \varphi_2 \circ \varphi_1^{-1} \quad \text{and} \quad \varphi_{12} = \varphi_1 \circ \varphi_2^{-1} .$$

Transition functions are usually required to be C^k-continuous, for some finite, non-negative integer k or

even $k = \infty$, so that the necessary degree of "smoothness" to compute certain differential properties of M is ensured. Transition functions define which points in $\varphi_1(U_1 \cap U_2)$ and $\varphi_2(U_1 \cap U_2)$ are the "same", i.e., correspond to the same point in M under φ_1^{-1} and φ_2^{-1}. They also provide us with a means of "moving" along M without actually being on M, which ultimately allows us to consistently do global calculations on M.

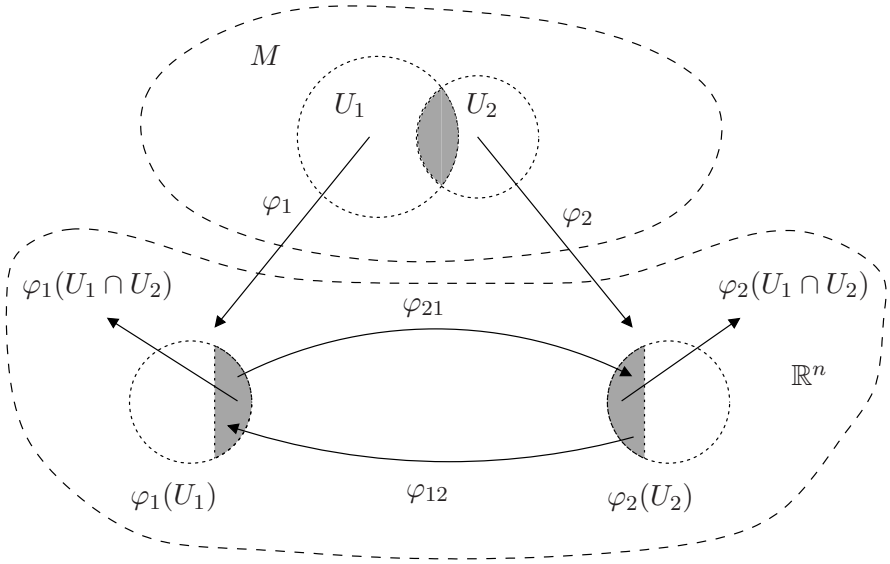

Figure 2.1: Illustration of the definition of a manifold.

Grimm and Hughes [44] offers a very elucidating real-world analogy to a manifold. In a world atlas, portions of the earth, i.e., Europe (the open set U_1) and Asia (the open set U_2), are laid flat to paper maps (the open sets $\varphi_1(U_1)$ and $\varphi_2(U_2)$), as illustrated by Figure 2.2. Every bit of the world must be laid down to at least one paper map in the atlas (i.e., every point of M belongs to an open set, U, of a chart). Overlaps of the open sets of two charts are represented by Europe and Asia both containing the country of Russia. The navigation from the map of Asia to the map of Europe does not require additional construct in real life, but is mathematically achieved via a transition function. Also, we can walk around the world, without being physically there, by moving from a position in one map to its counterpart position in an overlapping map.

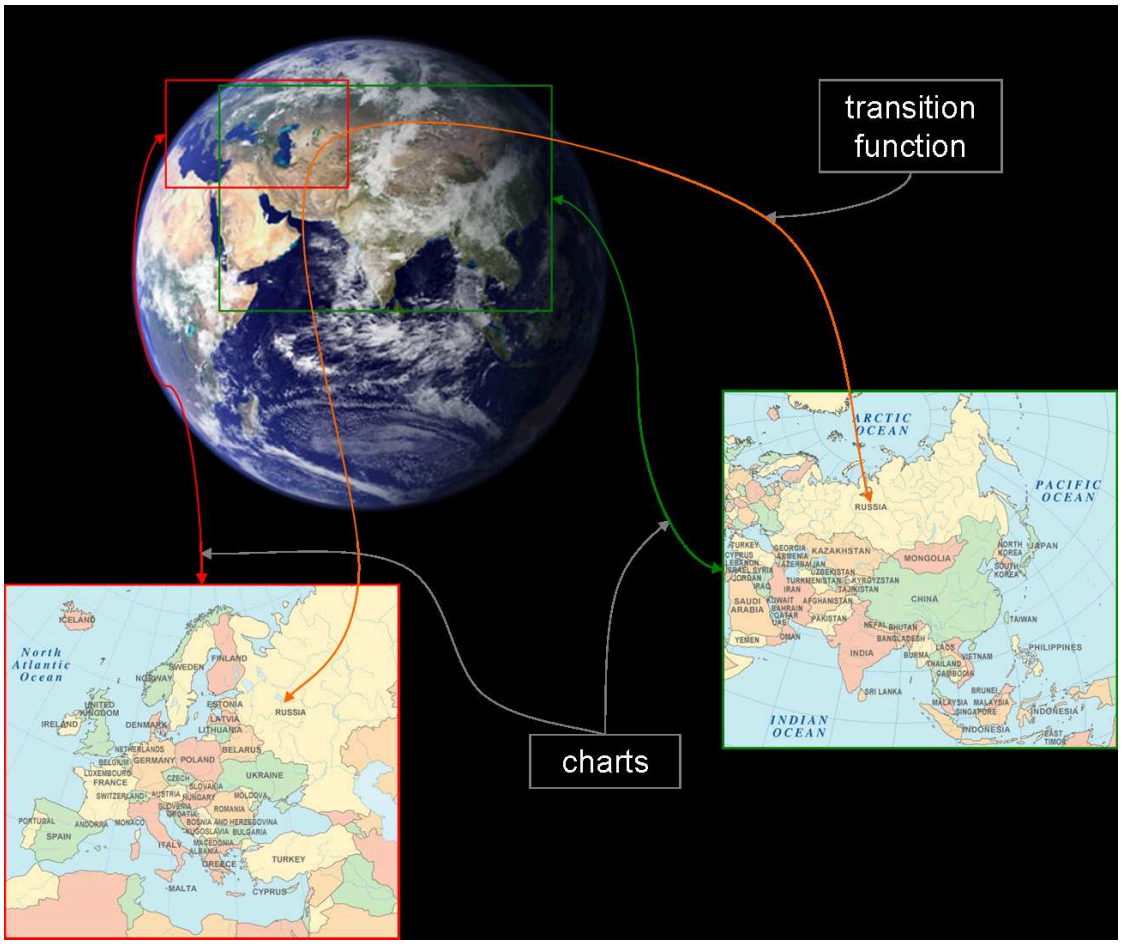

Figure 2.2: Manifold and the World Atlas

A manifold-based approach for surface construction aims at building a manifold, M, which is a smooth surface in $\mathbb{R}^3$. The classic definition of a manifold assumes the existence of a manifold *a priori*, which is not very helpful from the constructive point of view. Fortunately, it is possible to define M in a constructive way from what we call a *set of gluing data* and a set of *parametrizations*. A set of gluing data consists of a collection of open sets in $\mathbb{R}^n$, called *parametrizations domains* (or *p-domains* for short), a collection of *gluing domains*, which are open subsets of p-domains, and a collection of transition functions, which are functions from gluing domains to gluing domains. In turn, each parametrization is a map from a p-domain to a subset, M, of $\mathbb{R}^m$. There is a simple correspondence between the constituents of the traditional definition of a manifold and the ones of a set of gluing data and a set of parametrizations (refer to Figure 2.3):

- each p-domain, $\Omega_i \subseteq \mathbb{R}^n$, is the image, $\Omega_i = \varphi_i(U_i)$, of an open set, U_i, of M under the map φ_i of the chart (U_i, φ_i) of an atlas of M;

- each gluing domain, $\Omega_{ij} \subseteq \Omega_i$, is the image, $\Omega_{ij} = \varphi_i(U_i \cap U_j)$, of the overlapping subset, $U_i \cap U_j$, of U_i and U_j;

- each transition function, $\varphi_{ji} : \Omega_{ij} \to \Omega_{ji}$, is a function from $\varphi_i(U_i \cap U_j) = \Omega_{ji}$ to $\varphi_j(U_i \cap U_j) = \Omega_{ij}$; and

- each parametrization, $\theta_i : \Omega_i \to M$, is the inverse, φ_i^{-1}, of the map $\varphi_i : U_i \to \varphi_i(U_i) \subseteq \mathbb{R}^n$, of the chart, (U_i, φ_i).

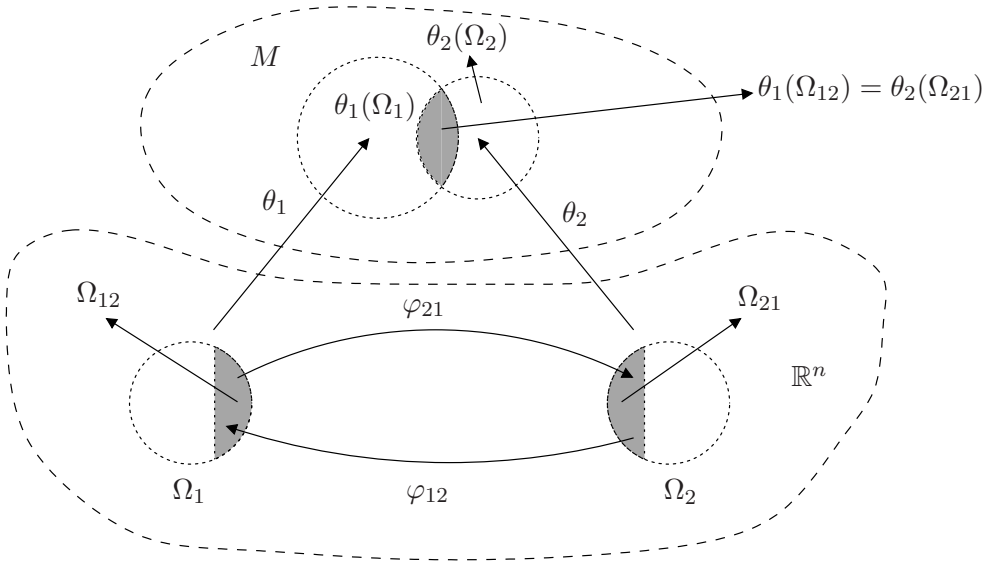

Figure 2.3: Illustration of p-domains, gluing domains, transition functions, and parametrizations.

The key idea behind a manifold-based approach for surface construction is to define a set of gluing data and a set of parametrizations from the given triangle mesh. The idea of defining manifolds from a set of gluing data and a set of parametrizations is not new. André Weil introduced this idea to define abstract algebraic varieties by gluing irreducible affine sets in his book [58] published in 1946. The same idea is well-known in bundle theory and can be found in standard texts such as Steenrod [59], Bott and Tu [60], Morita [61], and Wells [62]. However, Grimm and Hughes [44, 63] were the first to have realized the power of the gluing process in surface modeling. We wish to emphasize that this is a very significant

discovery and that their work inspired our construction, which is described in chapters 4 and 5 of this manuscript.

The body of work on manifold-based constructions to surface modeling has been reviewed in detail in the recent SIGGRAPH 2006 course notes [49]. Grimm and Hughes [44] introduced the first manifold-based construction for surface modeling, and their basic framework has been adopted in almost all subsequent constructions [45, 46, 48], including ours. In their basic framework, a set of gluing data is defined from the given mesh by associating p-domains with mesh vertices, edges, or triangles. Gluing domains and transition functions are determined by the mesh connectivity. Finally, a set of parametrizations is defined using the mesh geometry. The efficiency of a manifold-based construction depends upon the size of the set of gluing data and the complexity of the transition functions and parametrizations. The smaller the set of gluing data is and the simpler the transition functions and parametrizations are, the more efficient the construction is.

The construction in [44] takes a triangle mesh as input, subdivides the mesh by one step of the Catmull-Clark subdivision scheme, and then considers the dual of the subdivided mesh (which is no longer a triangle mesh). So, if the input mesh has v vertices, e edges, and t triangles, the dual mesh will have $3v$ vertices, $3e$ edges, and $v + e + t$ faces. A set of gluing data is defined from the dual mesh by assigning a p-domain with each vertex, edge, and face of the mesh, which gives a total of $v + 4e + 4t$ p-domains. The p-domains associated with the vertices differ from the ones associated with the edges and faces, which in turn are also distinct. Furthermore, there are three distinct types of transition functions. The construction in [44] yields C^2-continuous surfaces only, but it was later simplified and improved [9] to produce C^k-continuous surfaces, for any finite integer k. Subsequent efforts [45, 46] aimed at providing a construction that requires a smaller set of gluing data, consists of simpler transition functions, and achieves C^∞-continuity.

Navau and Pla-Garcia [45] introduced a construction that takes a quadrilateral mesh and two integers, k and n, as input. The integer k specifies the finite degree of continuity of the resulting surface, while n is related to the extent of p-domains and gluing domains. The construction assigns a p-domain with each vertex of the mesh. A p-domain is said to be regular if its associated vertex is regular (i.e., the degree of the vertex is 4); otherwise, it is said to be irregular. Transition functions map gluing domains from regular to regular, regular (resp. irregular) to irregular (resp. regular), and irregular to irregular p-domains. So, like

in [44], there are also three types of transition functions, but the one from regular to regular p-domains is trivial.

The size of the gluing data, however, depends on n and on the topology of the input mesh, as an irregular vertex cannot be in the neighborhood consisting of the $n + 1$ "layers" of quadrilaterals surrounding another irregular vertex. In addition, the graph consisting of the vertices and edges of the $n + 1$ layers of quadrilaterals surrounding each vertex of the mesh must be planar. If any of these two requirements is not satisfied, the mesh is subdivided by the Catmull-Clark scheme, resulting in a larger mesh. So, for input triangle and quadrilateral meshes of comparable sizes, the construction in [45] may construct a set of gluing domain larger than the one constructed by the construction in [44]. This is true even for small values of n, with $n \geq 2$, as the quadrilateral mesh may contain an edge whose endpoints are irregular vertices.

Both constructions in [44] and [45] define the geometry of the resulting surfaces by means of control points, which is the usual way of defining the geometry of surfaces constructed by the parametric approach. In particular, the parametrizations in [44, 45] are expressed as convex sums of control points whose weights are given by *blending* functions. These functions are compositions of piecewise polynomials (e.g., B-splines) and transition functions. Since the transition functions may not be polynomial, parametrizations need not be polynomial. Nevertheless, the resulting surfaces share an important property with the polynomial surfaces constructed by the parametric approaches: they are contained in the convex hull of *all* control points, which allows us to optimize for speed ray tracing and collision detection algorithms.

Ying and Zorin [46] devised another manifold-based construction, which also takes a quadrilateral mesh as input and considerably improves upon the two previous constructions in several ways. First, the number of p-domains is fixed and equals the number of vertices of the input mesh (which is never subdivided). Second, there is only one type of transition function, which greatly simplifies their construction. Third, the resulting surface is C^∞-continuous. Fourth, control points are replaced by general polynomials in the expression defining the parametrizations. This allows their construction to produce a C^∞-continuous surface that closely approximates a visually pleasant surface defined from the same mesh, but in general with a finitely small degree of continuity. Furthermore, the polynomials allow the user to prescribe derivatives at certain points of the resulting surface, and to enforce mesh vertex interpolation.

So, the construction in [46] offers a more flexible control of the geometry of the resulting surface than the ones in [44, 45]. However, this construction was designed to work with quadrilateral meshes. Although extension to triangle meshes is possible, it is not obvious how certain elements of the proto-manifold should be adjusted.

More recently, Gu, He, and Qin [47] introduced another manifold-based construction for building C^k surfaces from triangle meshes, for any finite k. Unlike previous constructions [44, 45, 46], the construction in [47] is based on a novel theoretical framework, which undergirds what the authors called *manifold splines*. The main advantage of manifold splines over previous constructions is that their transition functions are affine and the parametrizations are either polynomial or rational polynomial functions. Manifold splines are in general more compact to represent and cheaper to evaluate than the surfaces produced by any other construction (including ours). However, according to a classical result from characteristic class theory [64], closed surfaces (except tori) cannot be covered by an *affine atlas*, i.e., an atlas in which every transition function is affine. In particular, such surfaces contain points, called *singular points* or *singularities*, that cannot belong to the open set of any chart of any affine atlas. These points are removed and traditional spline hole-filling techniques are used to patch the resulting surface.

The construction in [47] yields manifold splines with at most $2g - 2$ singular points, where g is the genus of the input triangle mesh. The resulting manifold splines have two main drawbacks. First, they are difficult to construct in the neighborhood of singular points, and they are not differentiable there. Second, there are distortions in the parametrizations near singular points, which may affect the visual quality of the surface. Furthermore, the algorithm for constructing manifold splines is based on the computation of holomorphic 1-forms, which is equivalent to solving an elliptic partial differential equation on the mesh using the finite element method [65]. So, even though the transition functions used by the construction in [47] are simpler than the ones in [44, 45, 46], its manifold structure is a lot more complicated to compute.

An improvement upon the construction in [47] was recently described in [66]. By using the concept of discrete Ricci flow, the improved construction computes a metric on a mesh parametric domain. The parametric domain is computed by a global parametrization procedure that requires the mesh be cut open along a set of closed curves [65]. This metric induces an affine atlas covering the entire manifold, except for one singular point. A single point is the theoretical lower bound for the number of singular points. So, the construction in [66] is optimal as far as affine atlases are concerned. However, the complexity of

the surface construction process, which involves mesh segmentation and parametrization, remains large when compared to the complexity of ones in [44, 45, 46]. Moreover, even though the problems caused by singular points on the manifold splines are reduced to one neighborhood of the surface, they are not eliminated.

It is important to remark that the constructions in [47, 66] can also yield C^k-continuous surfaces, for $k = \infty$. This is the case when the (rational) polynomial parametrizations are replaced by non-polynomial C^∞ functions (including the functions used to patch the holes caused by the removal of singular points). However, in this case, the resulting surface is no longer polynomial, as the parametrizations are not polynomial.

Very recently, Vecchia, Jüttler, and Kim [48] introduced another triangle-based manifold construction, which also represents the resulting surface with a rational polynomial. However, unlike the constructions in [47, 66], the surface does not contain any singular points. However, the construction in [48] suffers from the same problem as the one in [44]: it makes use of an intricate mechanism to define its transition functions and their domains. Moreover, there is no proof of correctness for the construction in [48], although the experimental evidences given in [48] indicate that the construction indeed produces C^k surfaces, for any finite k.

The new manifold-based construction described here is also based on the basic framework developed by Grimm and Hughes [44]. Our construction shares with the one in [46] its main improvements upon the constructions in [44, 45, 48], namely: (1) it is simpler than the constructions in [44, 45, 48], as there is only type of p-domain and only one type of transition function, and the number of p-domains (resp. parametrizations) is fixed and equals the number of vertices in the input mesh; (2) the resulting surface is C^∞-continuous; (3) parametrizations are defined as convex sums of polynomial functions rather than control points; (4) the geometry of the resulting surface closely approximates the geometry of a given surface defined on the same input mesh. This surface must be continuous and must have an empty boundary.

There are two main differences from our construction to the one in [46]. First, ours was devised to work with triangle meshes, which are far more popular than quadrilateral meshes in computer graphics and geometry processing applications [1]. Second, the polynomials used in the definition of our

parametrizations are rectangular Bézier patches. This means that the resulting smooth surface is contained in the convex hull of *all* control points defining the patches. As we mentioned before, this property has been used to optimize for speed ray tracing and collision detection algorithms, and it is also present in the constructions given in [44, 45]. Since the construction in [46] is based on more general polynomials, the convex hull property may not hold for the surfaces generated by it. Unlike the surfaces generated by the construction in [47], the ones generated by our construction are not given by polynomials or rational polynomials. However, they do not contain singularities and do not present the aforementioned shortcomings caused by them. Furthermore, our construction is a lot more simpler to implement than the ones in [47, 66].

Chapter 3

Mathematical Preliminaries

This chapter introduces basic mathematical concepts that are important for the understanding of our manifold-based construction. Most concepts were borrowed from standard textbooks on differentiable manifolds, such as [55, 56, 57].

3.1 Simplicial Surfaces

The input of the problem we are dealing with in this manuscript, a triangle mesh, is formally known as a *simplicial surface*. The goal of this section is to introduce the formal definition of a simplicial surface as well as some of its important properties. All concepts presented in this section can be found in the book by Bloch [67].

Definition 3.1.1. Let $v_0, \ldots, v_d$ be any $d+1$ affinely independent points in $\mathbb{R}^n$, where d is a non-negative integer. The *simplex* σ spanned by the points $v_0, \ldots, v_d$ is the convex hull of these points, and is denoted by $[v_0, \ldots, v_d]$. The points $v_0, \ldots, v_d$ are called the *vertices* of σ. The *dimension* of σ, denoted by $dim(\sigma)$, is d, and σ is called a d-simplex.

In $\mathbb{R}^n$, the largest number of affinely independent points is $n+1$, and we have simplices of dimension $0, 1, \ldots, n$. Note that a 0-simplex is a single point, a 1-simplex is a line segment, a 2-simplex is a triangle, and a 3-simplex is a tetrahedron. Note also that the convex hull of any non-empty subset of vertices of

a simplex is again a simplex. This is a generalization of the observation that the boundary of a triangle consists of edges and vertices, and these edges and vertices are spanned by subsets of the vertices of the triangle.

Definition 3.1.2. Let $\sigma = [v_0, \ldots, v_d]$ be a d-simplex in $\mathbb{R}^n$. A *face* of σ is a simplex spanned by a non-empty subset of $\{v_0, \ldots, v_d\}$; if this subset is proper the face is called a *proper face*. A face of σ that is a k-simplex, where k is a non-negative integer, is called a *k-face*. The *combinatorial boundary of σ*, denoted by $bd(\sigma)$, is the union of all proper faces of σ. The *combinatorial interior of σ*, denoted by $int(\sigma)$, is defined to be $\sigma - bd(\sigma)$.

Simplices are used as building blocks for defining simplicial complexes, which are the most general objects we can construct from simplices. Simplicial complexes are built by gluing simplices together along their common faces. A simplicial surface is a particular type of simplicial complex built out of vertices, edges, and triangles. In what follows we give a definition of simplicial complex and some related concepts:

Definition 3.1.3. A *simplicial complex* $\mathcal{K}$ in $\mathbb{R}^n$ is a finite collection of simplices in $\mathbb{R}^n$ such that

(i) if a simplex is in $\mathcal{K}$, then all its faces are in $\mathcal{K}$;

(ii) if $\sigma, \tau \in \mathcal{K}$ are simplices such that $\sigma \cap \tau \neq \emptyset$, then $\sigma \cap \tau$ is a face of each σ and τ.

The *dimension* of $\mathcal{K}$, denoted by $dim(\mathcal{K})$, is the largest dimension of a simplex in $\mathcal{K}$, i.e., $dim(\mathcal{K}) = \max\{dim(\sigma) \mid \sigma \in \mathcal{K}\}$. We refer to a d-dimensional simplicial complex as simply a *d-complex*. The set consisting of the union of all points in the simplices of $\mathcal{K}$ is called the *underlying space* of $\mathcal{K}$, and it is denoted by $|\mathcal{K}|$.

Figure 3.1 shows three sets of simplices in $\mathbb{R}^2$. The set on the left is not a simplicial complex because it is missing an edge and a vertex. The set in the middle contains two simplices that intersect each other but the intersection is not a face of either one, and therefore it cannot be a simplicial complex. The set on the right is a simplicial complex. Note that the underlying space, $|\mathcal{K}|$, of any simplicial complex, $\mathcal{K}$, is a compact set, for K is a finite collection of simplices.

Definition 3.1.4. Let $\mathcal{K}$ be a simplicial complex in $\mathbb{R}^n$. For each integer i, with $0 \leq i \leq dim(\mathcal{K})$, we define $\mathcal{K}^{((i))}$ to be the collection of all i-simplices of $\mathcal{K}$.

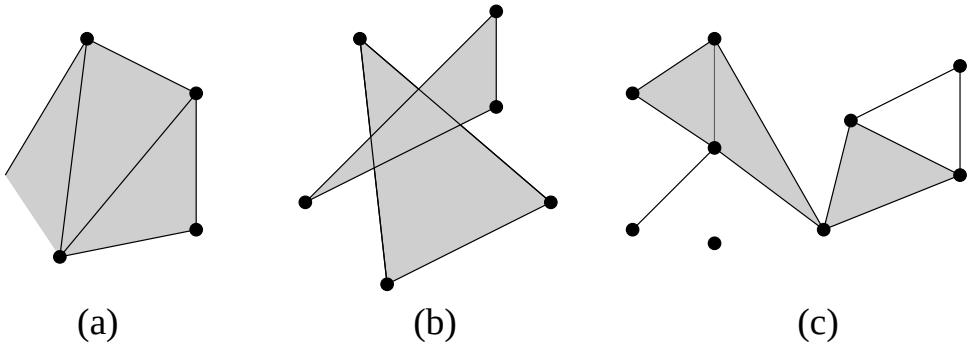

Figure 3.1: Collections of simplices in $\mathbb{R}^2$. (a) and (b) are not simplicial complexes, but (c) is.

Definition 3.1.5. Let $\mathcal{K}$ be a simplicial complex in $\mathbb{R}^n$. Then, if σ is a simplex in $\mathcal{K}$, the *star* and *link* of σ, denoted $st(\sigma, \mathcal{K})$ and $lk(\sigma, \mathcal{K})$, respectively, are defined to be

$$st(\sigma, \mathcal{K}) = \{\tau \in \mathcal{K} \mid \exists \eta \text{ in } \mathcal{K} \text{ such that } \sigma \text{ is a face of } \eta \text{ and } \tau \text{ is a face of } \eta\}$$

and

$$lk(\sigma, \mathcal{K}) = \{\tau \in \mathcal{K} \mid \tau \text{ is in } st(\sigma, \mathcal{K}) \text{ and } \tau \text{ and } \sigma \text{ have no face in common}\}.$$

Let $\mathcal{K}$ be the simplicial complex in Figure 3.2(a). Then, $\mathcal{K}^{((0))}$ consists of the 0-simplices $[p]$, $[q]$, $[r]$, $[s]$, $[t]$, $[u]$, $[v]$, $[x]$, $[y]$, and $[z]$; $\mathcal{K}^{((1))}$ consists of the 1-simplices $[p, q]$, $[p, s]$, $[p, v]$, $[q, r]$, $[q, s]$, $[r, s]$, $[r, v]$, $[s, v]$, $[t, u]$, $[t, v]$, $[t, x]$, $[u, x]$, $[v, x]$, $[v, z]$, $[x, y]$, $[x, z]$, and $[y, z]$; and $\mathcal{K}^{((2))}$ consists of the 2-simplices $[p, q, s]$, $[p, s, v]$, $[q, r, s]$, $[r, s, v]$, $[t, u, x]$, $[t, x, v]$, $[x, z, v]$, and $[x, y, z]$. The star $st([v], \mathcal{K})$ of $[v]$ consists of $[v]$, $[r]$, $[s]$, $[p]$, $[z]$, $[z]$, $[x]$, and $[t]$; 1-simplices $[p, v]$, $[r, v]$, $[r, s]$, $[s, p]$, $[s, v]$, $[t, v]$, $[x, v]$, $[z, v]$, $[z, v]$, $[z, x]$, and $[x, t]$; and 2-simplices $[r, s, v]$, $[p, s, v]$, $[t, v, x]$, and $[x, z, v]$, as illustrated by Figure 3.2(b). The link $lk([v], \mathcal{K})$ of $[v]$ consists of the 0-simplices $[p]$, $[r]$, $[s]$, $[t]$, $[x]$, $[z]$, and 1-simplices $[p, s]$, $[r, s]$, $[x, z]$, and $[t, x]$, as illustrated by Figure 3.2(c).

Definition 3.1.6. A 2-complex $\mathcal{K}$ is called a *simplicial surface* if every 1-simplex of $\mathcal{K}$ is the face of precisely two simplices of $\mathcal{K}$, and the underlying space of the link of each 0-simplex of $\mathcal{K}$ is homeomorphic to the unit 1-sphere, $\mathbb{S}^1 = \{x \in \mathbb{R}^2 \mid \|x\| = 1\}$. The underlying space of a simplicial surface is called the *underlying surface* of the simplicial surface.

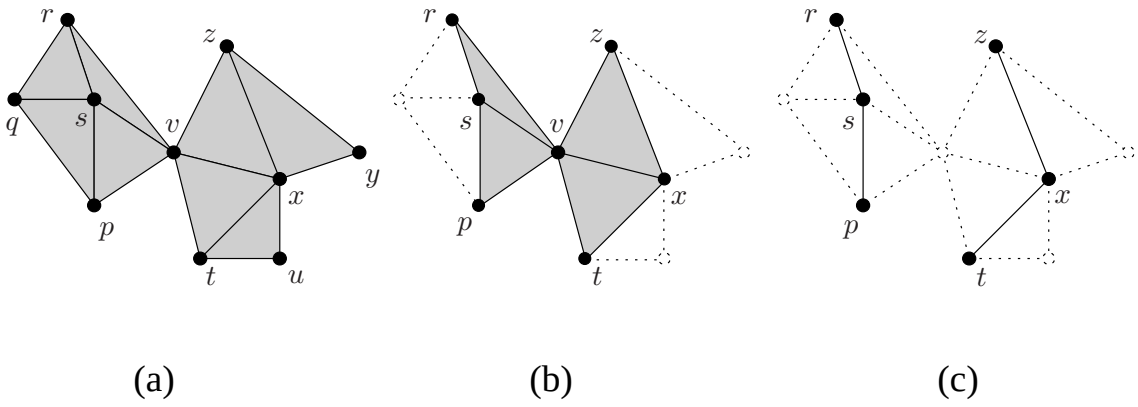

Figure 3.2: (a) A simplicial complex. (b) The star of vertex v in (a). (c) The link of vertex v in (a).

For instance, the simplicial complex consisting of all proper faces of a tetrahedron is a simplicial surface. However, the simplicial complex consisting of all proper faces of the two tetrahedra in Figure 3.3 is not a simplicial surface, as the link of $[v]$ is not homeomorphic to $\mathbb{S}^1$. Recall that a subset $S \subset \mathbb{R}^n$ is called a topological surface (or surface, for short) if for every point $p \in S$, there exists an open ball, $B_\delta(p, \mathbb{R}^n)$, in $\mathbb{R}^n$, centered at p and with radius δ, where $\delta \in \mathbb{R}$ and $\delta > 0$, such that $B_\delta(p, \mathbb{R}^n) \cap S$ is homeomorphic to the open unit disk, $\mathbb{D} = \{p \in \mathbb{R}^2 \mid \|p\| < 1\}$, in $\mathbb{R}^2$. The following lemma from [67] states an important property of simplicial surfaces:

Lemma 3.1.1. *Let $\mathcal{K}$ be a simplicial complex in $\mathbb{R}^n$. Then $|\mathcal{K}|$ is a topological surface if and only if $\mathcal{K}$ is a simplicial surface.*

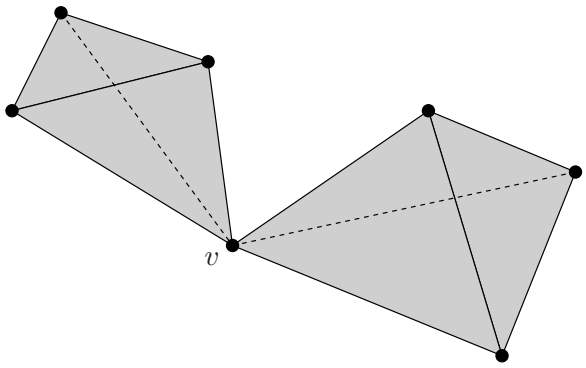

Figure 3.3: The 2-complex consisting of the proper faces of the two tetrahedra is not a simplicial surface.

Definition 3.1.7. Let $\mathcal{K}$ be a simplicial complex in $\mathbb{R}^n$, and let $\mathcal{L}$ be a simplicial complex in $\mathbb{R}^m$. A map $f : \mathcal{K}^{((0))} \to \mathcal{L}^{((0))}$ is a *simplicial map* if whenever $[v_0, \ldots, v_d]$ is a simplex in $\mathcal{K}$, then $[f(v_0), \ldots, f(v_d)]$ is a

simplex in $\mathcal{L}$. A simplicial map is a *simplicial isomorphism* if it is a bijective map on the set of vertices, and if its inverse is also a simplicial map. If there is a simplicial isomorphism from $\mathcal{K}$ to $\mathcal{L}$ then we say that $\mathcal{K}$ and $\mathcal{L}$ are *simplicially isomorphic*.

For instance, let $\mathcal{K}$ be a tetrahedron. Since any subset of two or three vertices of $\mathcal{K}$ is the set of vertices of a simplex in $\mathcal{K}$, it follows that any map $f : \mathcal{K}^{((0))} \to \mathcal{K}^{((0))}$ is a simplicial map, which is also a simplicial isomorphism.

3.2 Topological Spaces and Homeomorphisms

Definition 3.2.1. Let M be a set. A *topology* on M is a collection $\mathcal{T}_M$ of subsets of M satisfying three axioms:

(1) $\emptyset$ and M belong to $\mathcal{T}_M$;

(2) if $U_1, \ldots, U_n \in \mathcal{T}_M$ then $\left(\bigcap_{i=1}^{n} U_i\right) \in \mathcal{T}_M$; and

(3) if I is any (possibly infinite) indexing set and $U_i \in \mathcal{T}_M$, for all $i \in I$, then $\left(\bigcup_{i \in I} U_i\right) \in \mathcal{T}_M$.

Each $U \in \mathcal{T}_M$ is called an *open set* of $\mathcal{T}_M$. In short, a topology on M is a family of subsets of M (the *open sets*), containing $\emptyset$ and M, which is closed under the operation of union and finite intersection. A *topological space* is a pair, $(M, \mathcal{T}_M)$, consisting of a set, M, and a topology, $\mathcal{T}_M$, on M. We often speak of the topological space M and its open sets, omitting $\mathcal{T}_M$ from the notation when it is clear what topology is intended.

For instance, the set $\mathbb{R}^n$ is often regarded as a topological space equipped with the "usual" topology: the open sets are $\mathbb{R}^n$, $\emptyset$, and all nonempty proper subsets $U \subset \mathbb{R}^n$ such that for every $p = (p_1, \ldots, p_n) \in U$, there exists a real number δ, with $\delta > 0$, such that the *open ball, $B_\delta(p, \mathbb{R}^n)$, in $\mathbb{R}^n$ of center p and radius δ*, i.e.,

$$B_\delta(p, \mathbb{R}^n) = \{(x_1, \ldots, x_n) \in \mathbb{R}^n \mid \left(\sum_{i=1}^{n} (x_i - p_i)^2\right) < \delta^2\},$$

is a subset of U. It can be shown that the "usual" topology is indeed a topology, i.e., it satisfies conditions (1)-(3) of Definition 3.2.1.

Definition 3.2.2. If M and N are topological spaces[1], a function $f : M \to N$ is *continuous* if, for every open set $U \subset N$, the set $f^{-1}(U) \subset M$ is also open. A function $f : M \to N$ is a *homeomorphism* if f is bijective, and both f and f^{-1} are continuous. If $f : M \to N$ is a homeomorphism, we say that M and N are *homeomorphic*, and we denote this fact by $M \simeq N$.

3.3 Manifolds

Given $\mathbb{R}^n$, recall that the projection functions, $pr_i : \mathbb{R}^n \to \mathbb{R}$, are defined by

$$pr_i(x_1, \ldots, x_n) = x_i, \quad \text{for all } 1 \leq i \leq n.$$

Definition 3.3.1. Given a topological space, M, a *chart* (or *local coordinate function*) is a pair, (U, φ), where U is an open subset of M and $\varphi : U \to \Omega$ is a homeomorphism onto an open subset, $\Omega = \varphi(U)$, of $\mathbb{R}^{n_\varphi}$ (for some $n_\varphi \geq 1$). For any $p \in M$, a chart, (U, φ), is a *chart at* p if and only if $p \in U$. If (U, φ) is a chart, then the functions $x_i = pr_i \circ \varphi$ are called *local coordinates* and for every $p \in U$, the tuple $(x_1(p), \ldots, x_n(p))$ is the set of *coordinates of* p with respect to the chart. The pair (Ω, φ^{-1}), the "inverse" of (U, φ), is called a *local parametrization*.

Definition 3.3.2. Given a topological space, M, and any two charts, (U_1, φ_1) and (U_2, φ_2), where U_1 and U_2 are open subsets of M, if $U_1 \cap U_2 \neq \emptyset$, we define the *transition functions*, $\varphi_{ji} : \varphi_i(U_i \cap U_j) \to \varphi_j(U_i \cap U_j)$ and $\varphi_{ij} : \varphi_j(U_i \cap U_j) \to \varphi_i(U_i \cap U_j)$, as

$$\varphi_{ji} = \varphi_j \circ \varphi_i^{-1} \quad \text{and} \quad \varphi_{ij} = \varphi_i \circ \varphi_j^{-1}.$$

Figure 2.1 illustrates Definition 3.3.2.

Note that $\varphi_{ij} = (\varphi_{ji})^{-1}$ and that the transition functions φ_{ji} (resp. φ_{ij}) are functions between open sets of $\mathbb{R}^n$. This is good news, as the whole arsenal of calculus is available for functions on $\mathbb{R}^n$, and many important results of calculus can be promoted to manifolds by imposing suitable conditions on transition functions.

[1]Notice that we are already omitting mention of the topologies $\mathcal{T}_M$ and $\mathcal{T}_N$.

Definition 3.3.3. Given a topological space, M, given some integer $n \geq 1$, and given some k such that k is either an integer, with $k \geq 1$, or $k = \infty$, a C^k *n-atlas* (or *n-atlas of class* C^k), $\mathcal{A}$, on M is a family of charts, $\{(U_i, \varphi_i)\}_{i \in I}$, where I is a non-empty (possibly infinite) countable set, such that the following holds:

(1) $\varphi_i(U_i) \subseteq \mathbb{R}^n$, for all i;

(2) the family $\{U_i\}_{i \in I}$ is an open cover for M, i.e.,

$$M = \bigcup_{i \in I} U_i \,;$$

and

(3) whenever $U_i \cap U_j \neq \emptyset$, the transition function φ_{ji} (resp. φ_{ij}) is a C^k diffeomorphism.

For an example, consider the sphere $\mathbb{S}^n \subset \mathbb{R}^{n+1}$,

$$\mathbb{S}^n = \{(x_1, \ldots, x_{n+1}) \in \mathbb{R}^{n+1} \mid \sum_{i=1}^{n+1} x_i^2 = 1\}.$$

We can regard $\mathbb{S}^n$ as a topological space by giving $\mathbb{S}^n$ the topology consisting of all subsets U of $\mathbb{S}^n$ such that, for every $p = (p_1, \ldots, p_{n+1}) \in U$, there exists a real number δ, with $\delta > 0$, such that $(\mathbb{S}^n \cap B_\delta(p, \mathbb{R}^{n+1})) \subseteq U$, where $B_\delta(p, \mathbb{R}^{n+1})$ is the open ball in $\mathbb{R}^{n+1}$ of center p and radius δ. Using the stereographic projections (from the north pole and south pole), we can define two charts on $\mathbb{S}^n$. Denote the points $(0, \ldots, 0, 1) \in \mathbb{R}^{n+1}$ and $(0, \ldots, 0, -1) \in \mathbb{R}^{n+1}$ by N (the north pole) and S (the south pole), respectively, and let $\varphi_N : \mathbb{S}^n - \{N\} \to \mathbb{R}^n$ and $\varphi_S : \mathbb{S}^n - \{S\} \to \mathbb{R}^n$ be the functions

$$\varphi_N(x_1, \ldots, x_{n+1}) = \frac{1}{1 - x_{n+1}}(x_1, \ldots, x_n) \quad \text{and} \quad \varphi_S(x_1, \ldots, x_{n+1}) = \frac{1}{1 + x_{n+1}}(x_1, \ldots, x_n)\,,$$

which are called *stereographic projection from the north pole* and *stereographic projection from the south pole*, respectively. The inverse stereographic projections are given by

$$\varphi_N^{-1}(x_1, \ldots, x_n) = \frac{1}{\left(\sum_{i=1}^n x_i^2\right) + 1}\Big(2x_1, \ldots, 2x_n, \Big(\sum_{i=1}^n x_i^2\Big) - 1\Big)$$

and

$$\varphi_S^{-1}(x_1, \ldots, x_n) = \frac{1}{\left(\sum_{i=1}^n x_i^2\right) + 1}\Big(2x_1, \ldots, 2x_n, -\Big(\sum_{i=1}^n x_i^2\Big) + 1\Big)\,.$$

Note that φ_N and φ_S are homeomorphisms that map open sets of $\mathbb{S}^n$ to open sets of $\mathbb{R}^n$ (regarding $\mathbb{R}^n$ as a topological space equipped with the usual topology). So, (U_N, φ_N) and (U_S, φ_S) are charts. Furthermore, if we let $U_N = \mathbb{S}^n - \{N\}$ and $U_S = \mathbb{S}^n - \{S\}$, we see that (1) $\varphi_N(U_N) = \mathbb{R}^n$ and $\varphi_S(U_S) = \mathbb{R}^n$, (2) $\{U_N, U_S\}$ is an open cover for $\mathbb{S}^n$, and (3) it is easily checked that on the overlap, $U_N \cap U_S = \mathbb{S}^n - \{N, S\}$, the transition functions,

$$\varphi_{SN} = \varphi_S \circ \varphi_N^{-1} \quad \text{and} \quad \varphi_{NS} = \varphi_N \circ \varphi_S^{-1}$$

are given by

$$(x_1, \ldots, x_n) \mapsto \frac{1}{\sum_{i=1}^n x_i^2}(x_1, \ldots, x_n),$$

which is a smooth bijection on $\mathbb{R}^n - \{O\}$. So, we conclude that (U_N, φ_N) and (U_S, φ_S) form a smooth n-atlas on $\mathbb{S}^n$.

The existence of a C^k n-atlas on a topological space, M, is sufficient to establish that M is an n-dimensional C^k manifold, but there is still a minor subtlety in the actual definition of a manifold. This has to do with the fact that there may be many choices of atlases, but it is useful to think of a manifold as an object independent of the choice of atlas. To do so, we define the notion of atlas compatibility. Given a C^k n-atlas, $\mathcal{A}$, on M, for any other chart, (U, φ), we say that (U, φ) is *compatible* with the atlas $\mathcal{A}$ if and only if every function $\varphi_i \circ \varphi^{-1}$ (resp. $\varphi \circ \varphi_i^{-1}$) is C^k (whenever $U \cap U_i \neq \emptyset$). Two atlases, $\mathcal{A}$ and $\mathcal{A}'$, on M are *compatible* if and only if every chart of one atlas is compatible with the other atlas. This is equivalent to saying that the union of the two atlases is still an atlas. It can be shown that compatibility induces an equivalence relation on C^k n-atlases on M. In fact, given an atlas, $\mathcal{A}$, on M, the collection, $\tilde{\mathcal{A}}$, of all charts compatible with $\mathcal{A}$ is a maximal atlas in the equivalence class of charts compatible with $\mathcal{A}$. Finally, we define a manifold as follows:

Definition 3.3.4. Given an integer $n \geq 1$ and given some k such that k is either an integer, with $k \geq 1$, or $k = \infty$, a C^k *manifold of dimension* n consists of a topological space, M, together with an equivalence class, $\overline{\mathcal{A}}$, of C^k n-atlases on M. Any atlas, $\mathcal{A}$, of $\overline{\mathcal{A}}$ is called a *differentiable structure of class* C^k (*and dimension* n) on M. When $k = \infty$, we say that M is a *smooth manifold*.

To avoid pathological cases and to ensure that a manifold is embeddable in $\mathbb{R}^n$, for some $n \geq 1$, we require that the topology of M be *Hausdorff* and *second-countable*. Hausdorff means that for every distinct points, $x \neq y$ in M, there are disjoint open subsets, U_x and U_y, with $x \in U_x$ and $y \in U_y$. Second-countable

means that there is a countable set of open subsets of M such that every open subset of M is a union of opens from this countable set. Thus, as it is customary, in this paper, manifolds are required to be Hausdorff and second-countable.

Definition 3.3.4 relates to our informal discussion in Chapter 2 as follows: The manifold, M, can be viewed as the world; an atlas $\mathcal{A}$ on M correspond to a collection of regions of the world (the open sets $\{U_i\}_{i\in I}$), so that each region U_i is associated with a map, $\varphi_i : U_i \to \Omega_i$, from the region to a rectangular page of the World Atlas, Ω_i; and the functions φ_{ji} and φ_{ij} provide us with a way of moving from one page to another page of the World Atlas in a consistent manner. In particular, given the "local coordinates" of a location, p, in a rectangular page, $\Omega_i = \varphi(U_i)$, of the world atlas, we can move to another page of the atlas, say $\Omega_j = \varphi(U_j)$, which covers another region, U_j, of the world containing $\varphi_i^{-1}(p)$ (i.e., $\varphi_i^{-1}(p) \in (U_i \cap U_j)$), by using φ_{ji}. The transition φ_{ji} can be viewed as a two-step move: (1) go from the World Atlas to the world using φ_i^{-1} and then (2) return to the atlas page, $\Omega_j = \varphi_j(U_j)$, that covers U_j using φ_j. However, once we have φ_{ji}, we do not need the world in order to moving from one page to another page of the World Atlas. This is actually the key idea behind the *gluing process* for constructing manifolds from sets of gluing data.

3.4 Sets of Gluing Data for Manifolds

Recall that the goal of this work is to build a C^k surface, S, where $S \subset \mathbb{R}^3$, and $k \geq 1$ or $k = \infty$, that approximates the underlying surface of a given simplicial surface in $\mathbb{R}^3$. To that end, we propose a new construction that defines the surface S as a manifold. However, for our purposes, the traditional definition of a manifold (see Definition 3.3.4) is not very helpful. The reason is that the standard definition assumes that the object we want to build, the manifold, already exists. Remarkably, manifolds can also be defined by a gluing process, using what is often called a set of gluing data. In what follows, we define the notion of gluing data and show that it is possible, in principle, to construct a manifold from any given set of gluing data.

Definition 3.4.1. Let n be an integer with $n \geq 1$ and let k be either an integer with $k \geq 1$ or $k = \infty$. A *set of gluing data* is a triple,

$$\mathcal{G} = \left((\Omega_i)_{i\in I}, (\Omega_{ij})_{(i,j)\in I\times I}, (\varphi_{ji})_{(i,j)\in K}\right),$$

satisfying the following properties, where I and K are (possibly infinite) countable sets, and I is non-empty:

(1) For every $i \in I$, the set Ω_i is a non-empty open subset of $\mathbb{R}^n$ called *parametrization domain*, for short, *p-domain*, and the Ω_i are pairwise disjoint (i.e., $\Omega_i \cap \Omega_j = \emptyset$ for all $i \neq j$).

(2) For every pair $(i, j) \in I \times I$, the set Ω_{ij} is an open subset of Ω_i. Furthermore, $\Omega_{ii} = \Omega_i$ and $\Omega_{ji} \neq \emptyset$ if and only if $\Omega_{ij} \neq \emptyset$. Each non-empty Ω_{ij} (with $i \neq j$) is called a *gluing domain*.

(3) If we let

$$K = \{(i, j) \in I \times I \mid \Omega_{ij} \neq \emptyset\},$$

then $\varphi_{ji} : \Omega_{ij} \to \Omega_{ji}$ is a C^k bijection for every $(i, j) \in K$ called a *transition function* (or *gluing function*) and the following conditions hold:

(a) $\varphi_{ii} = \mathrm{id}_{\Omega_i}$, for all $i \in I$,

(b) $\varphi_{ij} = \varphi_{ji}^{-1}$, for all $(i, j) \in K$, and

(c) For all i, j, k, if $\Omega_{ji} \cap \Omega_{jk} \neq \emptyset$, then $\varphi_{ji}^{-1}(\Omega_{ji} \cap \Omega_{jk}) \subseteq \Omega_{ik}$ and $\varphi_{ki}(x) = \varphi_{kj} \circ \varphi_{ji}(x)$, for all $x \in \varphi_{ji}^{-1}(\Omega_{ji} \cap \Omega_{jk})$ (see Figure 3.4).

(4) For every pair $(i, j) \in K$, with $i \neq j$, for every $x \in \partial(\Omega_{ij}) \cap \Omega_i$ and $y \in \partial(\Omega_{ji}) \cap \Omega_j$, there are open balls, V_x and V_y, centered at x and y, so that no point of $V_y \cap \Omega_{ji}$ is the image of any point of $V_x \cap \Omega_{ij}$ by φ_{ji} (see Figure 3.5).

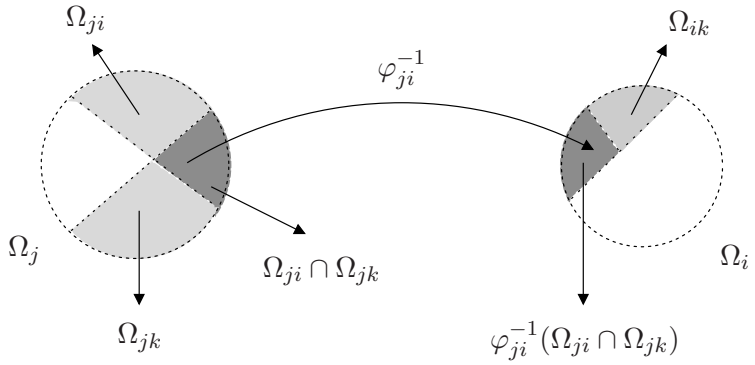

Figure 3.4: Illustration of condition 3(c) of Definition 3.4.1.

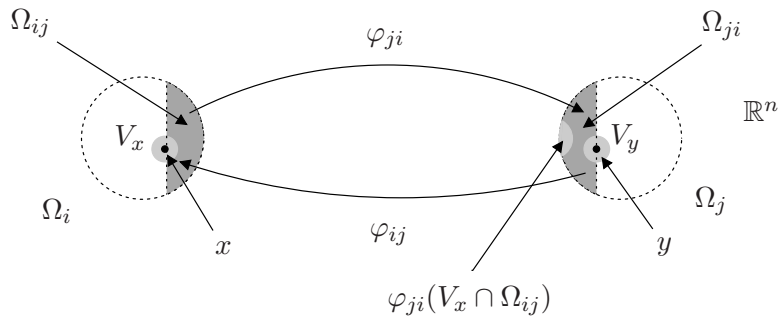

Figure 3.5: Illustration of condition 4 of Definition 3.4.1.

We can think of the p-domains Ω_i as the images $\varphi_i(U_i)$ of the charts (U_i, φ_i) of the manifold, M, we want to define. Likewise, we can think of the gluing domains Ω_{ij} and Ω_{ji} as the images $\varphi_i(U_i \cap U_j)$ and $\varphi_j(U_i \cap U_j)$, under the maps φ_i and φ_j, of the overlap region $U_i \cap U_j$, respectively. Finally, the gluing functions $\varphi_{ji} : \Omega_{ij} \to \Omega_{ji}$ can be thought of as the transition functions of M. Observe that $\Omega_{ij} \subseteq \Omega_i$ and $\Omega_{ji} \subseteq \Omega_j$. If $i \neq j$, as Ω_i and Ω_j are disjoint, so are Ω_{ij} and Ω_{ji}. Observe also that both conditions 3(a) and 3(b) of Definition 3.4.1 follow from 3(c). More specifically, to get 3(a), set $i = j = k$ in 3(c). Then, 3(b) follows from 3(a) and 3(c) by setting $k = i$. Condition 3(c) is called the *cocycle condition* and it plays a crucial role in Theorem 3.4.1, which states that an n-dimensional C^k manifold can be constructed from the set of gluing data, $\mathcal{G}$. This condition may seem overly complicated, but it is actually needed to guarantee the transitivity of the relation, $\sim$, defined in the proof of Theorem 3.4.1. The problem is that $\varphi_{kj} \circ \varphi_{ji}$ is a partial function whose domain, $\varphi_{ji}^{-1}(\Omega_{ji} \cap \Omega_{jk})$, is not necessarily related to the domain, Ω_{ik}, of φ_{ki}. Consequently, in order to ensure the transitivity of $\sim$, we must assert that whenever the composition $\varphi_{kj} \circ \varphi_{ji}$ has nonempty domain, this domain is contained in the domain of φ_{ki} and that $\varphi_{kj} \circ \varphi_{ji}$ and φ_{ki} agree.

Theorem 3.4.1. For every set of gluing data,

$$\mathcal{G} = \left((\Omega_i)_{i\in I}, (\Omega_{ij})_{(i,j)\in I\times I}, (\varphi_{ji})_{(i,j)\in K}\right),$$

there is an n-dimensional C^k manifold, $M_{\mathcal{G}}$, whose transition functions are the φ_{ji}'s.

Proof. Define the binary relation, $\sim$, on the disjoint union, $\coprod_{i\in I} \Omega_i$, of the open sets, Ω_i, as follows: For all $x, y \in \coprod_{i\in I} \Omega_i$,

$$x \sim y \quad \text{iff} \quad (\exists (i,j) \in K)(x \in \Omega_{ij}, y \in \Omega_{ji}, y = \varphi_{ji}(x)).$$

Note that if $x \sim y$ and $x \neq y$, then $i \neq j$, as $\varphi_{ii} = \mathrm{id}$. But then, as $x \in \Omega_{ij} \subseteq \Omega_i$, $x \in \Omega_{ji} \subseteq \Omega_j$ and $\Omega_i \cap \Omega_j = \emptyset$ when $i \neq j$, if $x \sim y$ and $x, y \in \Omega_i$, then $x = y$. We claim that $\sim$ is an equivalence relation. This follows easily from the co-cocycle condition but to be on the safe side, we provide the crucial step of the proof. Clearly, condition 3(a) of Definition 3.4.1 ensures reflexivity and condition 3(b) ensures symmetry. The crucial step is to check transitivity. Assume that $x \sim y$ and $y \sim z$. Then, there are some i, j, k such that

(i) $x \in \Omega_{ij}$, $y \in \Omega_{ji} \cap \Omega_{jk}$, $z \in \Omega_{kj}$, and

(ii) $y = \varphi_{ji}(x)$ and $z = \varphi_{kj}(y)$.

Consequently, $\Omega_{ji} \cap \Omega_{jk} \neq \emptyset$ and $x \in \varphi_{ji}^{-1}(\Omega_{ji} \cap \Omega_{jk})$, so by 3(c), we get $\varphi_{ji}^{-1}(\Omega_{ji} \cap \Omega_{jk}) \subseteq \Omega_{ik}$ and thus, $\varphi_{ki}(x)$ is defined and by 3(c) again,

$$\varphi_{ki}(x) = \varphi_{kj} \circ \varphi_{ji}(x) = z\,,$$

that is, $x \sim z$, as desired. Since $\sim$ is an equivalence relation let

$$M_{\mathcal{G}} = \Big(\coprod_{i \in I} \Omega_i \Big) / \sim$$

be the quotient set and let $p : \coprod_{i \in I} \Omega_i \to M_{\mathcal{G}}$ be the quotient map, with $p(x) = [x]$, where $[x]$ denotes the equivalence class of x (see Figure 3.6). Also, for every $i \in I$, let $\mathrm{in}_i : \Omega_i \to \coprod_{i \in I} \Omega_i$ be the natural injection and let

$$\tau_i = p \circ \mathrm{in}_i : \Omega_i \to M_{\mathcal{G}}\,.$$

Since we already noted that if $x \sim y$ and $x, y \in \Omega_i$, then $x = y$, we conclude that every τ_i is injective. We give $M_{\mathcal{G}}$ the coarsest topology that makes the bijections, $\tau_i : \Omega_i \to \tau_i(\Omega_i)$, into homeomorphisms. Then, if we let $U_i = \tau_i(\Omega_i)$ and $\varphi_i = \tau_i^{-1}$, it is immediately verified that the (U_i, φ_i) are charts and this collection of charts forms a C^k atlas for $M_{\mathcal{G}}$. As there are countably many charts, $M_{\mathcal{G}}$ is second-countable. Therefore, for $M_{\mathcal{G}}$ to be a manifold it only remains to check that the topology is Hausdorff. For this, we use the following:

Claim. For all $(i, j) \in I \times I$, we have $\tau_i(\Omega_i) \cap \tau_j(\Omega_j) \neq \emptyset$ iff $(i, j) \in K$ and if so,

$$\tau_i(\Omega_i) \cap \tau_j(\Omega_j) = \tau_i(\Omega_{ij}) = \tau_j(\Omega_{ji})\,.$$

Proof of Claim. Assume that $\tau_i(\Omega_i) \cap \tau_j(\Omega_j) \neq \emptyset$ and let $[z] \in \tau_i(\Omega_i) \cap \tau_i(\Omega_j)$. Observe that $[z] \in \tau_i(\Omega_i) \cap \tau_i(\Omega_j)$ iff $z \sim x$ and $z \sim y$, for some $x \in \Omega_i$ and some $y \in \Omega_j$. Consequently, $x \sim y$, which implies that $(i, j) \in K$, $x \in \Omega_{ij}$ and $y \in \Omega_{ji}$. We have $[z] \in \tau_i(\Omega_{ij})$ iff $z \sim x$, for some $x \in \Omega_{ij}$. Then, either $i = j$ and $z = x$ or $i \neq j$ and $z \in \Omega_{ji}$, which shows that $[z] \in \tau_j(\Omega_{ji})$ and so,

$$\tau_i(\Omega_{ij}) \subseteq \tau_j(\Omega_{ji})\,.$$

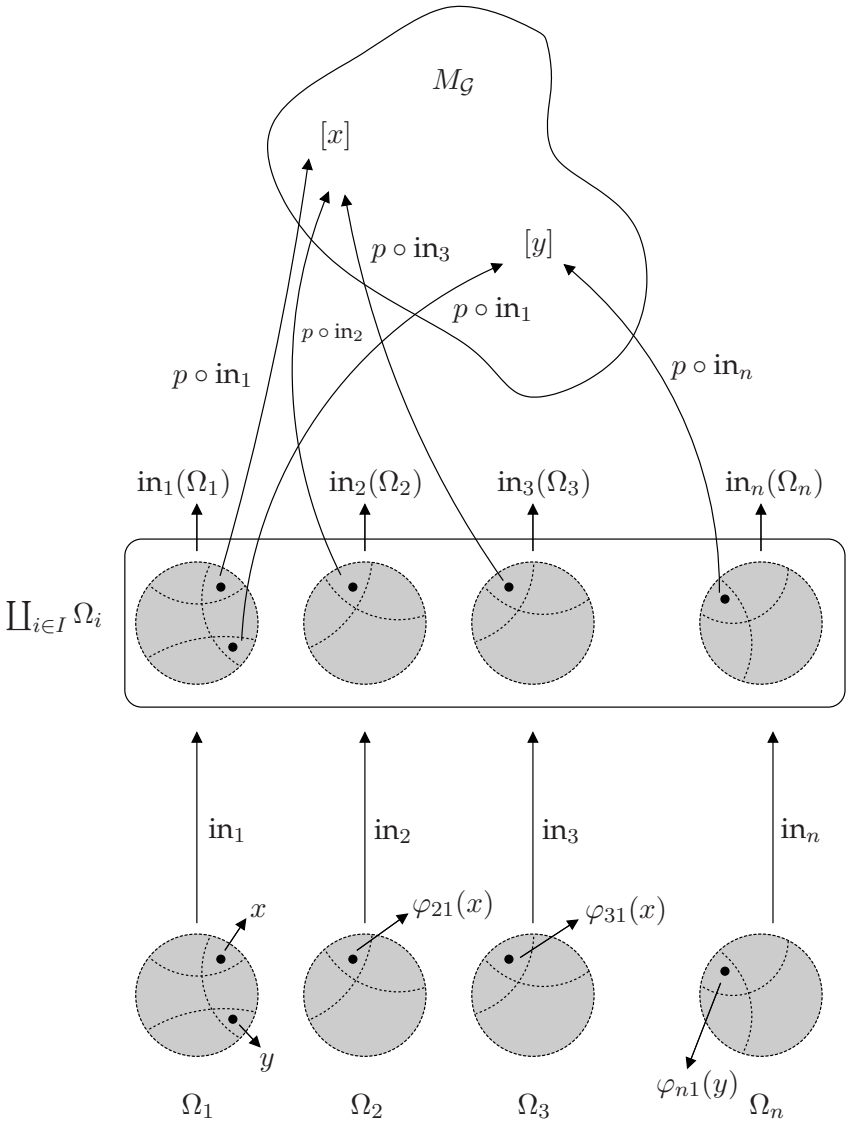

Figure 3.6: The quotient construction.

Since the same argument applies by interchanging i and j, we have

$$\tau_i(\Omega_{ij}) = \tau_j(\Omega_{ji})\,,$$

for all $(i,j) \in K$. Since $\Omega_{ij} \subseteq \Omega_i$, $\Omega_{ji} \subseteq \Omega_j$, and $\tau_i(\Omega_{ij}) = \tau_j(\Omega_{ji})$, for all $(i,j) \in K$, we have

$$\tau_i(\Omega_{ij}) = \tau_j(\Omega_{ji}) \subseteq \tau_i(\Omega_i) \cap \tau_j(\Omega_j)\,,$$

for all $(i,j) \in K$. For the reverse inclusion, if $[z] \in \tau_i(\Omega_i) \cap \tau_j(\Omega_j)$, then we know that there is some $x \in \Omega_{ij}$ and some $y \in \Omega_{ji}$ such that $z \sim x$ and $z \sim y$, so $[z] = [x] \in \tau_i(\Omega_{ij})$ and $[z] = [y] \in \tau_j(\Omega_{ji})$, and then we get

$$\tau_i(\Omega_i) \cap \tau_j(\Omega_j) \subseteq \tau_i(\Omega_{ij}) = \tau_j(\Omega_{ji})\,.$$

This proves that if $\tau_i(\Omega_i) \cap \tau_j(\Omega_j) \neq \emptyset$, then $(i,j) \in K$ and

$$\tau_i(\Omega_i) \cap \tau_j(\Omega_j) = \tau_i(\Omega_{ij}) = \tau_j(\Omega_{ji})\,.$$

Finally, assume that $(i,j) \in K$. Then, for any $x \in \Omega_{ij} \subseteq \Omega_i$, we have $y = \varphi_{ji}(x) \in \Omega_{ji} \subseteq \Omega_j$ and $x \sim y$, so that $\tau_i(x) = \tau_j(y)$, which proves that $\tau_i(\Omega_i) \cap \tau_j(\Omega_j) \neq \emptyset$ and our claim is proved.
End of Proof of Claim.

We now prove that the topology of $M_{\mathcal{G}}$ is Hausdorff. Pick $[x], [y] \in M_{\mathcal{G}}$ with $[x] \neq [y]$, for some $x \in \Omega_i$ and some $y \in \Omega_j$. Either $\tau_i(\Omega_i) \cap \tau_j(\Omega_j) = \emptyset$, in which case, as τ_i and τ_j are homeomorphisms, $[x]$ and $[y]$ belong to the two disjoint open sets $\tau_i(\Omega_i)$ and $\tau_j(\Omega_j)$. If not, then by the Claim, $(i,j) \in K$ and

$$\tau_i(\Omega_i) \cap \tau_j(\Omega_j) = \tau_i(\Omega_{ij}) = \tau_j(\Omega_{ji})\,.$$

There are several cases to consider (refer to Figure 3.7):

(1) If $i = j$ then x and y can be separated by disjoint opens, V_x and V_y, and as τ_i is a homeomorphism, $[x]$ and $[y]$ are separated by the disjoint open subsets $\tau_i(V_x)$ and $\tau_j(V_y)$.

(2) If $i \neq j$, $x \in \Omega_i - \overline{\Omega_{ij}}$ and $y \in \Omega_j - \overline{\Omega_{ji}}$, then $\tau_i(\Omega_i - \overline{\Omega_{ij}})$ and $\tau_j(\Omega_j - \overline{\Omega_{ji}})$ are disjoint open subsets separating $[x]$ and $[y]$, where $\overline{\Omega_{ij}}$ and $\overline{\Omega_{ji}}$ are the closures of Ω_{ij} and Ω_{ji}, respectively.

(3) If $i \neq j$, $x \in \Omega_{ij}$ and $y \in \Omega_{ji}$, as $[x] \neq [y]$ and $y \sim \varphi_{ij}(y)$, then $x \neq \varphi_{ij}(y)$. We can separate x and $\varphi_{ij}(y)$ by disjoint open subsets, V_x and V_y, and $[x]$ and $[y] = [\varphi_{ij}(y)]$ are separated by the disjoint open subsets $\tau_i(V_x)$ and $\tau_i(V_y)$.

(4) If $i \neq j$, $x \in \partial(\Omega_{ij}) \cap \Omega_i$ and $y \in \partial(\Omega_{ji}) \cap \Omega_j$, then we use condition (4) of Definition 3.4.1. This condition yields two disjoint open subsets, V_x and V_y, with $x \in V_x$ and $y \in V_y$, such that no point of $V_x \cap \Omega_{ij}$ is equivalent to any point of $V_y \cap \Omega_{ji}$, and so $\tau_i(V_x)$ and $\tau_j(V_y)$ are disjoint open subsets separating $[x]$ and $[y]$.

Therefore, the topology of $M_{\mathcal{G}}$ is Hausdorff and $M_{\mathcal{G}}$ is indeed a manifold. Finally, it is trivial to verify that the transition functions of $M_{\mathcal{G}}$ are the original gluing functions, φ_{ij}. □

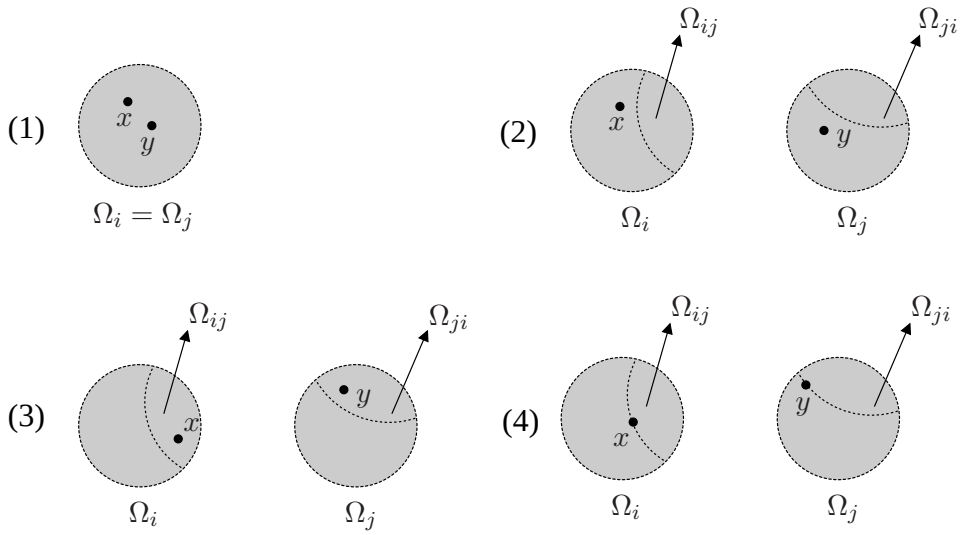

Figure 3.7: The four cases of the proof of Condition (4) of Definition 3.4.1.

The beauty of the idea of defining gluing data for constructing a manifold, M, is that it allows the construction of M without having prior knowledge of its topology (that is, without explicitly having the underlying topological space M). The construction is carried out by gluing open subsets of $\mathbb{R}^n$ (the Ω_i's) according to prescribed gluing instructions (namely, glue Ω_i and Ω_j by identifying Ω_{ij} and Ω_{ji} using φ_{ji}). This way of specifying a manifold clearly separates the local structure of the manifold (given by the Ω_i's) from its global structure, which is specified by the gluing functions. Furthermore, the construction ensures that M is C^k (even for $k = \infty$) with no extra effort, as the gluing functions φ_{ji} are assumed to be C^k.

In [44, 63], a set of gluing data is called a *proto-manifold*. However, there are two subtle differences between our definition of gluing data and the definition of a proto-manifold in [44, 63]. First, the cocycle

condition (condition 3(c)) of both definitions are slightly different, as the one used in the definition of a proto-manifold is too weak to imply transitivity of the relation $\sim$ in the proof of Theorem 3.4.1 (see Appendix A). Second, in the definition of a proto-manifold, there is no condition similar to condition 4 of Definition 3.4.1. However, in order to ensure that a Hausdorff manifold can always be constructed from a proto-manifold (in a way much like $M_{\mathcal{G}}$ is in Theorem 3.4.1), Grimm [63] requires that the manifold be embeddable in $\mathbb{R}^n$. This requirement is stronger than condition 4 of Definition 3.4.1, and it prevents us from obtaining certain manifolds such as a 2-sphere resulting from gluing two open discs in $\mathbb{R}^2$ along an annulus (see [63], Appendix C).

3.5 Parametric Pseudo-Manifolds

It should be noted that as nice as it is, the proof of Theorem 3.4.1 gives us a theoretical construction, which yields an "abstract" manifold, $M_{\mathcal{G}}$, but does not yield any information on the geometry of this manifold. Furthermore, $M_{\mathcal{G}}$ may not be orientable or compact, even if we start with a finite set of p-domains. However, for the problem we are dealing with, we are given a simplicial surface and we want to build a "concrete" manifold: a surface in $\mathbb{R}^3$ that approximates the underlying surface of the simplicial surface. It turns out that it is always possible to define what we call a "pseudo-surface" from any given set of gluing data, which under certain conditions is a surface in $\mathbb{R}^3$, as we shall show later on in this section.

Definition 3.5.1. Let n, d, and k be three integers with $n > d \geq 1$ and $k \geq 1$ or $k = \infty$. A *parametric C^k pseudo-manifold of dimension d in $\mathbb{R}^n$* is a pair, $\mathcal{M} = (\mathcal{G}, (\theta_i)_{i\in I})$, such that $\mathcal{G} = \big((\Omega_i)_{i\in I}, (\Omega_{ij})_{(i,j)\in I\times I}, (\varphi_{ji})_{(i,j)\in K}\big)$ is a set of gluing data, for some finite set I, and each θ_i is a C^k function, $\theta_i : \Omega_i \to \mathbb{R}^n$, called a *parametrization* such that the following holds:

(C) For all $(i, j) \in K$, we have

$$\theta_i = \theta_j \circ \varphi_{ji}\,.$$

For short, we use the terminology *parametric pseudo-manifold*. The subset, $M \subset \mathbb{R}^n$, given by

$$M = \bigcup_{i \in I} \theta_i(\Omega_i)$$

is called the *image* of the parametric pseudo-manifold, $\mathcal{M}$. When $n = 3$ and $d = 2$, we say that $\mathcal{M}$ is a *parametric pseudo-surface*.

Condition (C) obviously implies that

$$\theta_i(\Omega_{ij}) = \theta_j(\Omega_{ji})\,,$$

for all $(i, j) \in K$. Consequently, θ_i and θ_j are consistent parametrizations of the overlap $\theta_i(\Omega_{ij}) = \theta_j(\Omega_{ij})$. Thus, the shape, M, whatever it is, is covered by pieces, $U_i = \theta_i(\Omega_i)$, not necessarily open, with each U_i parametrized by θ_i and where the overlapping pieces, $U_i \cap U_j$, are parametrized consistently. The local structure of M is given by the θ_i's and its global structure is given by the gluing data. More importantly, we can give M a manifold structure if we require the θ_i's to be bijective and to satisfy the following additional conditions:

(C′) For all $(i, j) \in K$,

$$\theta_i(\Omega_i) \cap \theta_j(\Omega_j) = \theta_i(\Omega_{ij}) = \theta_j(\Omega_{ji})\,.$$

(C″) For all $(i, j) \notin K$,

$$\theta_i(\Omega_i) \cap \theta_j(\Omega_j) = \emptyset\,.$$

If conditions (C′) and (C″) do not hold, we may not be able to give M a manifold structure. So, these conditions are actually necessary. Interestingly, regardless of the veracity of conditions (C′) and (C″), we can still show that M is the image in $\mathbb{R}^n$ of the abstract manifold, $M_{\mathcal{G}}$, as stated by Proposition 3.5.1 below:

Proposition 3.5.1. Let $\mathcal{M} = (\mathcal{G}, (\theta_i)_{i \in I})$ be a parametric C^k pseudo-manifold of dimension d in $\mathbb{R}^n$, where $\mathcal{G} = \big((\Omega_i)_{i \in I}, (\Omega_{ij})_{(i,j) \in I \times I}, (\varphi_{ji})_{(i,j) \in K}\big)$ is a set of gluing data, for some finite set I. Then, the parametrization maps, θ_i, induce a surjective map, $\Theta : M_{\mathcal{G}} \to M$, from the abstract manifold, $M_{\mathcal{G}}$, specified by $\mathcal{G}$ to the image, $M \subseteq \mathbb{R}^n$, of the parametric pseudo-manifold, $\mathcal{M}$, and the following property holds: for every Ω_i, $\theta_i = \Theta \circ \tau_i$, where $\tau_i : \Omega_i \to M_{\mathcal{G}}$ are the parametrization maps of the manifold $M_{\mathcal{G}}$ (see the proof of Theorem 3.4.1 for the definition of τ_i).

Proof. Recall that

$$M_{\mathcal{G}} = \Big(\coprod_{i\in I} \Omega_i\Big)/\sim,$$

where $\sim$ is the equivalence relation defined so that, for all $x, y \in \coprod_{i\in I}\Omega_i$,

$$x \sim y \quad \text{iff} \quad (\exists (i,j)\in K)(x\in\Omega_{ij},\ y\in\Omega_{ji},\ y=\varphi_{ji}(x))\,.$$

The proof of Theorem 3.4.1 also showed that $\tau_i(\Omega_i)\cap\tau_j(\Omega_j)\neq\emptyset$ iff $(i,j)\in K$ and if so,

$$\tau_i(\Omega_i)\cap\tau_j(\Omega_j) = \tau_i(\Omega_{ij}) = \tau_j(\Omega_{ji})\,.$$

In particular,

$$\tau_i(\Omega_i-\Omega_{ij})\cap\tau_j(\Omega_j-\Omega_{ji}) = \emptyset$$

for all $(i,j)\in I\times I$ ($\Omega_{ij}=\Omega_{ji}=\emptyset$ when $(i,j)\notin K$). These properties with the fact that the τ_i's are injections show that for all $(i,j)\notin K$, we can define $\Theta_i : \tau_i(\Omega_i)\to\mathbb{R}^n$ and $\Theta_j:\tau_j(\Omega_j)\to\mathbb{R}^n$ by

$$\Theta_i([x]) = \theta_i(x),\ x\in\Omega_i-\Omega_{ij} \quad \text{and} \quad \Theta_j([y]) = \theta_i(y),\ y\in\Omega_j-\Omega_{ji}\,.$$

It remains to define Θ_i on $\tau_i(\Omega_{ij})$ and Θ_j on $\tau_j(\Omega_{ji})$ in such a way that they agree on $\tau_i(\Omega_{ij})=\tau_j(\Omega_{ji})$. However, condition (C) in Definition 3.5.1 says that for all $x\in\Omega_{ij}$,

$$\theta_i(x) = \theta_j(\varphi_{ji}(x))\,.$$

Consequently, if we define Θ_i on $\tau_i(\Omega_{ij})$ and Θ_j on $\tau_j(\Omega_{ji})$ by

$$\Theta_i([x]) = \theta_i(x),\ x\in\Omega_{ij} \quad \text{and} \quad \Theta_j([y]) = \theta_j(y),\ y\in\Omega_{ji}\,,$$

as $x\sim\varphi_{ji}(x)$, we have

$$\Theta_i([x]) = \theta_i(x) = \theta_j(\varphi_{ji}(x)) = \Theta_j([\varphi_{ji}(x)]) = \Theta_j([x])\,,$$

which means that Θ_i and Θ_j agree on $\tau_i(\Omega_{ij})=\tau_j(\Omega_{ji})$. But then, the functions, Θ_i, agree whenever their domains overlap and consequently, they patch to yield a function, Θ, with domain $M_{\mathcal{G}}$ and image M, as desired. □

From our discussion above, we have that the image, $M\subseteq\mathbb{R}^n$, of any parametric pseudo-manifold, $\mathcal{M}=(\mathcal{G},(\theta_i)_{i\in I})$, defined from the same set of gluing data, $\mathcal{G}$, is the image of the abstract manifold, $M_{\mathcal{G}}$, in $\mathbb{R}^n$. So, the abstract manifold, $M_{\mathcal{G}}$, can be viewed as a "universal" manifold for the set $\mathcal{G}$. Moreover, whenever the θ_i's are bijective and conditions (C') and (C") hold, the subset M can be given the structure of a manifold.

3.6 Statement of the Problem

We are now ready to formalize the surface fitting problem we are dealing with: *given a simplicial surface, $\mathcal{K}$, in $\mathbb{R}^3$, a positive real number, ϵ, and a positive integer, k (or $k = \infty$), find a C^k surface, S, in $\mathbb{R}^3$ such that (1) S is homeomorphic to the underlying space, $|\mathcal{K}|$, of $\mathcal{K}$, and (2) there exists a homeomorphism, $h : |\mathcal{K}| \rightarrow S$, such that $\|p - h(p)\| \leq \epsilon$, for every vertex p of $\mathcal{K}$.* Condition (1) requires the surfaces S and $|\mathcal{K}|$ be topologically equivalent, while condition (2) formalizes the requirement regarding the geometric proximity of S and the vertices of $\mathcal{K}$. We can view ϵ as an upper bound for the *approximation error* at the vertices of $\mathcal{K}$ with respect to h.

We solve the above problem by constructing a set of gluing data, $\mathcal{G}$, and a pseudo-parametric surface, $\mathcal{M} = (\mathcal{G}, (\theta_i)_{i \in I})$, from the given simplicial surface, $\mathcal{K}$, and its underlying space, $|\mathcal{K}|$, respectively. Our solution is a C^∞ surface, S, which is defined to be the image, M, of pseudo-parametric surface, $\mathcal{M}$. Unfortunately, our solution is not guaranteed to satisfy conditions (1) and (2). However, both conditions can in principle be enforced by a geometric procedure that checks for surface patch (self-)intersections and removes them by subdividing the input simplicial surface, $\mathcal{K}$. We further comment on these issues in Chapter 6. Chapters 4 and 5 describe the construction of the set, $\mathcal{G}$, and the pseudo-surface, $\mathcal{M}$, respectively.

Chapter 4

Building Sets of Gluing Data

This chapter describes a new construction to build a set of gluing data,

$$\mathcal{G} = \big((\Omega_i)_{i\in I}, (\Omega_{ij})_{(i,j)\in I\times I}, (\varphi_{ji})_{(i,j)\in K}\big)$$

from a given simplicial surface, $\mathcal{K}$, in $\mathbb{R}^3$. The triple $\mathcal{G}$ depends only on the topology of $\mathcal{K}$. The proofs of most propositions and lemmas in this chapter are technically simple, but long and tedious to follow. So, to make the chapter shorter and more enjoyable to read, we provide the longer and more tedious proofs in Appendix A.

4.1 p-Domains, Gluing Domains, and Transition Functions

Let $\mathcal{K}$ be any given simplicial surface in $\mathbb{R}^3$, and let

$$\mathcal{G} = \big((\Omega_i)_{i\in I}, (\Omega_{ij})_{(i,j)\in I\times I}, (\varphi_{ji})_{(i,j)\in K}\big)$$

denote the set of gluing data we want to define. Hereafter, assume that the *degree* of every vertex v of K (i.e., the number of edges of $\mathcal{K}$ incident to v) is at least three. We now describe the construction of the set of p-domains, $(\Omega_i)_{i\in I}$, and the set of gluing domains, $(\Omega_{ij})_{(i,j)\in I\times I}$, of $\mathcal{G}$. Roughly speaking, each p-domain, Ω_i, in $(\Omega_i)_{i\in I}$ is the interior of a circle in $\mathbb{R}^2$; in turn, each gluing domain, Ω_{ij}, in $(\Omega_{ij})_{(i,j)\in I\times I}$ is defined by means of two abstractions, P-polygon and its canonical triangulation, and a composition of bijective functions.

Let

$$I = \{v \mid v \text{ is a vertex of } \mathcal{K}\}.$$

Definition 4.1.1. For every $v \in I$, the *p-domain* Ω_v is the set

$$\Omega_v = \left\{(x, y) \in \mathbb{R}^2 \mid x^2 + y^2 < \left(\cos\left(\frac{\pi}{m_v}\right)\right)^2\right\},$$

where m_v is the degree of vertex v.

Note that Ω_v is simply the interior of a circle of radius $\cos(\pi/m_v)$ centered at the origin of $\mathbb{R}^2$.

For any two $u, w \in I$, **we assume that Ω_u and Ω_w belong to distinct "copies" of** $\mathbb{R}^2$. This assumption ensures that $\Omega_u \cap \Omega_w = \emptyset$, so that condition (1) of Definition 3.4.1 holds. To build gluing domains and transition functions, we define the notions of a P-polygon and its canonical triangulation, as well as a bijective function that is a composition of two rotations around the origin, an analytic function, and a double reflection.

Definition 4.1.2. For each vertex v of $\mathcal{K}$, the *P-polygon, P_v, associated with v* is the regular polygon in $\mathbb{R}^2$ given by the vertices

$$v_i' = \left(\cos\left(\frac{2\pi \cdot i}{m_v}\right), \sin\left(\frac{2\pi \cdot i}{m_v}\right)\right),$$

for each $i \in \{0, \ldots, m_v - 1\}$, where m_v is the degree of of v.

Figure 4.1 illustrates Definition 4.1.2. **We assume that P_v resides in the copy of $\mathbb{R}^2$ that contains the *p*-domain Ω_v.** So, Ω_v is the interior, int(C_v), of the circle, C_v, inscribed in the P-polygon, P_v, i.e., $\Omega_v = \text{int}(C_v)$.

Definition 4.1.3. We can triangulate P_v by adding m_v diagonals and the vertex, $v' = (0, 0)$, to P_v. Each diagonal connects v' to a vertex, v_i', of P_u, for each $i = 0, \ldots, m_v - 1$. The resulting triangulation, denoted by T_v, is the *canonical triangulation of P_v*.

Figure 4.1 illustrates Definition 4.1.3.

Let v be any m-degree vertex in $\mathcal{K}$. Since $\mathcal{K}$ is a simplicial surface, the link, $lk(v, \mathcal{K})$, of v in $\mathcal{K}$ is homeomorphic to $\mathbb{S}^1$ (see Definition 3.1.6). So, $lk(v, \mathcal{K})$ is a simple, closed polygonal chain in $\mathbb{R}^3$. Let

$v_0, \ldots, v_{m-1}$ be any enumeration of the vertices of $lk(v, \mathcal{K})$ such that $[v_i, v_{i+1}]$ is an edge of $lk(v, \mathcal{K})$, for each $i \in \{0, \ldots, m-1\}$, where the index $(i+1)$ should be always considered congruent modulo m (unless stated otherwise).

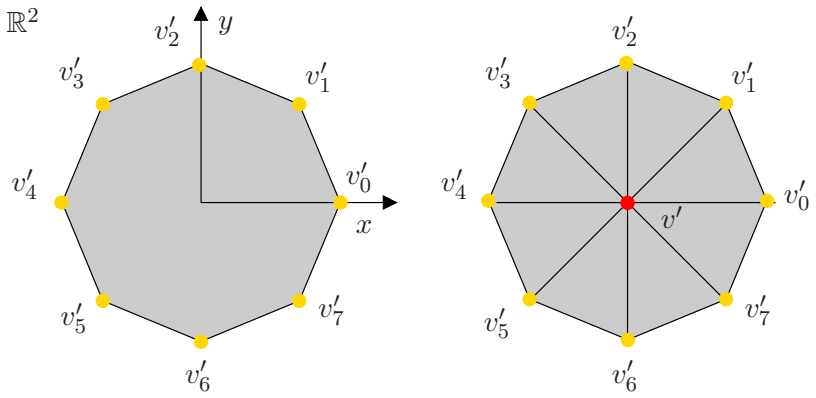

Figure 4.1: A P-polygon (left) and its canonical triangulation (right).

Definition 4.1.4. Given $st(v, \mathcal{K})$ and T_v, we define the function

$$s_v : st(v, \mathcal{K})^{((0))} \to T_v^{((0))}$$

such that $s_v(v) = v'$ and $s_v(v_i) = v'_i$, for every $i \in \{0, \ldots, m-1\}$. Note that for any $x, y, z \in st(v, \mathcal{K})$, we have that $[s_v(x), s_v(y)]$ is an edge of T_v if and only if $[x, y]$ is an edge of $st(v, \mathcal{K})$, and $[s_v(x), s_v(y), s_v(z)]$ is a triangle of T_v if and only if $[x, y, z]$ is a triangle of $st(v, \mathcal{K})$. This is to say that s_v is a simplicial isomorphism and that $st(v, \mathcal{K})$ and T_v are isomorphic. We can extend the bijection s_v to mapping triangles in $st(v, \mathcal{K})$ onto triangles in T_v. In particular, if $\sigma = [v, v_i, v_{i+1}]$ is in $st(v, \mathcal{K})$ then $s_v(\sigma) = [v', s_v(v_i), s_v(v_{i+1})]$ is its "image" in T_v.

Hereafter, we occasionally denote vertex $s_v(v)$ by v', for every $v \in st(v, \mathcal{K})$.

Definition 4.1.5. Let

$$\Pi : \mathbb{R}^2 - \{(0,0)\} \to (-\pi, \pi] \times \mathbb{R}_+$$

be the map that converts Cartesian to polar coordinates and is given by

$$\Pi(p) = \Pi((x, y)) = (\theta, r)\,,$$

for every $p \in \mathbb{R} - \{(0,0)\}$, where $\theta \in (-\pi, \pi]$ is the *angle* uniquely determined by

$$\cos\left(\frac{x}{r}\right) \quad \text{and} \quad \sin\left(\frac{y}{r}\right),$$

and $r \in \mathbb{R}_+$ is the *length*, with

$$r = \sqrt{x^2 + y^2}\,.$$

Note that Π is bijective and its inverse,

$$\Pi^{-1} : (-\pi, \pi] \times \mathbb{R}_+ \to \mathbb{R}^2 - \{(0,0)\}\,,$$

is given by

$$\Pi^{-1}((\theta, r)) = (r \cdot \cos(\theta), r \cdot \sin(\theta))\,.$$

Note also that both Π and Π^{-1} are C^∞ functions. We use Π and Π^{-1} to define a map associated with each vertex of $\mathcal{K}$:

Definition 4.1.6. For each v in I and for each $p \in \mathbb{R}^2$, let

$$g_v : \mathbb{R}^2 - \{(0,0)\} \to \mathbb{R}^2 - \{(0,0)\}$$

be given by

$$g_v(p) = \Pi^{-1} \circ f_v \circ \Pi(p)$$

for every $p \in \mathbb{R}^2 - \{(0,0)\}$, where $f_v : (-\pi, \pi] \times \mathbb{R}_+ \to (-\pi, \pi] \times \mathbb{R}_+$ is given by

$$f_v((\theta, r)) = \left(\frac{m_v}{6} \cdot \theta, \frac{\cos(\pi/6)}{\cos(\pi/m_v)} \cdot r\right),$$

(θ, r) are the polar coordinates of p and m_v is the degree of vertex v in $\mathcal{K}$.

Function g_v has the following interpretation (refer to Figure 4.2): it maps the circular sector, A, of C_v onto the circular sector, B, of the circle of radius $\cos(\pi/6)$ and centers at $(0,0)$, where A consists of $(0,0)$ and all points with polar coordinates $(\theta, r) \in [-2\pi/m_v, 2\pi/m_v] \times (0, \cos(\pi/m_v)]$ and B consists of $(0,0)$ and all points with polar coordinates $(\beta, s) \in [-\pi/3, \pi/3] \times (0, \cos(\pi/6)]$. Note that A is contained in the quadrilateral given by the vertices v', $s_v(v_{m_v-1})$, $s_v(v_0)$, and $s_v(v_1)$ of T_v. We say that B is the *canonical sector*.

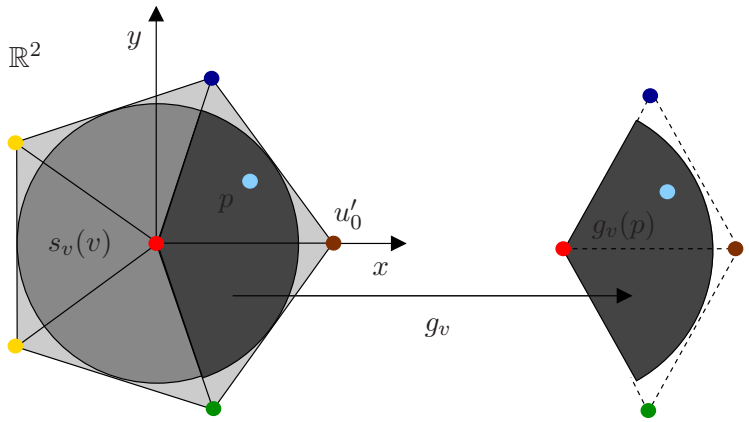

Figure 4.2: The action of g_v upon a point $p \in C_v$.

Function g_v is bijective and its inverse,

$$g_v^{-1} : \mathbb{R}^2 - \{(0,0)\} \to \mathbb{R}^2 - \{(0,0)\}\,,$$

is given by

$$g_v^{-1}(q) = \Pi^{-1} \circ f_v^{-1} \circ \Pi(q)$$

for every $q \in \mathbb{R}^2 - \{(0,0)\}$, where $f_v^{-1} : (-\pi, \pi] \times \mathbb{R}_+ \to (-\pi, \pi] \times \mathbb{R}_+$ is given by

$$f_v^{-1}((\beta, s)) = \left(\frac{6}{m_v} \cdot \beta, \frac{\cos(\pi/m_v)}{\cos(\pi/6)} \cdot s \right)\,,$$

(β, s) are the polar coordinates of q and m_v is the degree of vertex v in $\mathcal{K}$. Since f_v is clearly C^∞, so is g_v.

Definition 4.1.7. Let

$$h : \mathbb{R}^2 \to \mathbb{R}^2$$

be the function

$$h(p) = h((x,y)) = (1-x, -y)\,,$$

for every point $p \in \mathbb{R}^2$ with rectangular coordinates (x, y).

Function h is a "double" reflection: $p = (x, y)$ is reflected over the line $x = 0.5$ and then over the line $y = 0$.

Definition 4.1.8. For any two u, w of I such that $[u, w]$ is an edge of $\mathcal{K}$, we define the function

$$g_{(u,w)} : \Omega_u - \{(0,0)\} \to g_{(u,w)}(\Omega_u - \{(0,0)\})$$

as

$$g_{(u,w)}(p) = R^{-1}_{(w,u)} \circ g_w^{-1} \circ h \circ g_u \circ R_{(u,w)}(p)$$

for every $p \in \Omega_u - \{(0,0)\}$, where $R_{(u,w)}$ is a rotation around $(0,0)$ that identifies the edge $[s_u(u) = u', s_u(w)]$ of T_u with its edge $[u', u'_0]$, and $R^{-1}_{(w,u)}$ is a rotation around $(0,0)$ that identifies the edge $[s_w(w) = w', w'_0]$ of T_w with its edge $[w', w'_j]$, where $j \in \{0, 1, \ldots, m_w - 1\}$ and $s_w(u) = w'_j$.

Figure 4.3 shows the action of $g_{(u,w)}$ upon a point $p \in \Omega_u - \{(0,0)\}$.

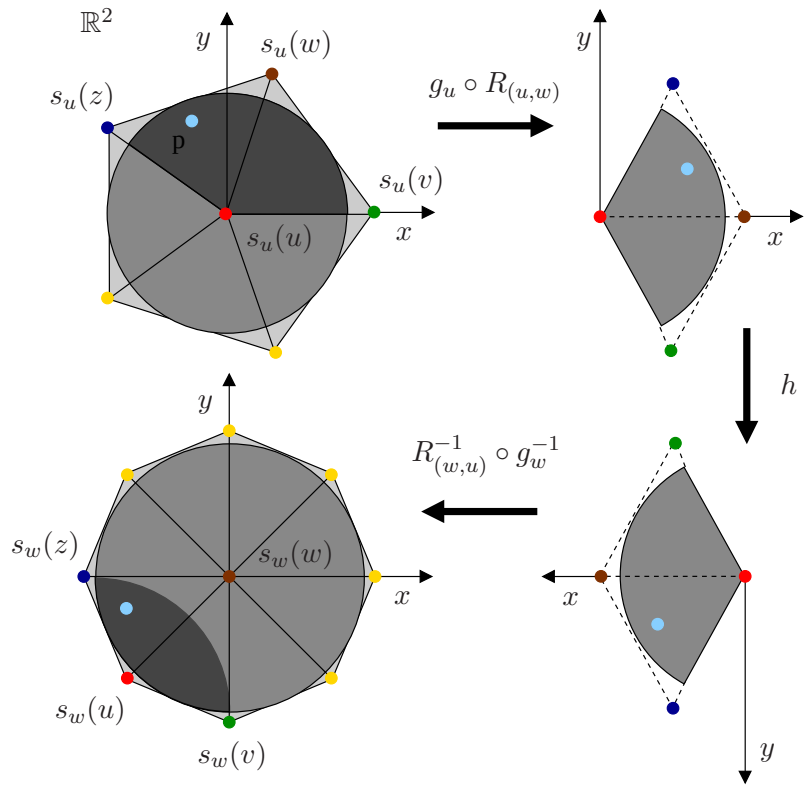

Figure 4.3: The action of $g_{(u,w)}$ upon a point $p \in \Omega_u - \{(0,0)\}$.

Note that $g_u \circ R_{(u,w)}$ maps $\Omega_u - \{(0,0)\}$ onto the set $\text{int}(C) - \{(0,0)\}$, where C is the circle of radius $\cos(\pi/6)$ and center $(0,0)$ (see Figure 4.4). In turn, function h maps $\text{int}(C) - \{(0,0)\}$ onto the set $\text{int}(D) - \{(1,0)\}$, where D is the circle of radius $\cos(\pi/6)$ and center $(1,0)$. Finally, by definition, the composite

function $R^{-1}_{(w,u)} \circ g_w^{-1}$ maps $\text{int}(C) - \{(0,0)\}$ onto $\Omega_w - \{(0,0)\}$. So, only the points in $(\text{int}(C) - \{(0,0)\}) \cap (\text{int}(D) - \{(1,0)\})$ are mapped by $R^{-1}_{(w,u)} \circ g_w^{-1}$ to $\Omega_w - \{(0,0)\}$. The set $E = (\text{int}(C) - \{(0,0)\}) \cap (\text{int}(D) - \{(1,0)\})$ is called the *canonical lens*, and it is contained in the quadrilateral, Q, given by the vertices $(0,0)$, $(1/2, -\sqrt{3}/2)$, $(1,0)$, and $(1/2, \sqrt{3}/2)$. Note that $\Omega_w - (0,0)$ is *not* the image of $\text{int}(D) - \{(0,0)\}$ by $R^{-1}_{w,u} \circ g_w^{-1}$, but the image of $\text{int}(C) - \{(0,0)\}$.

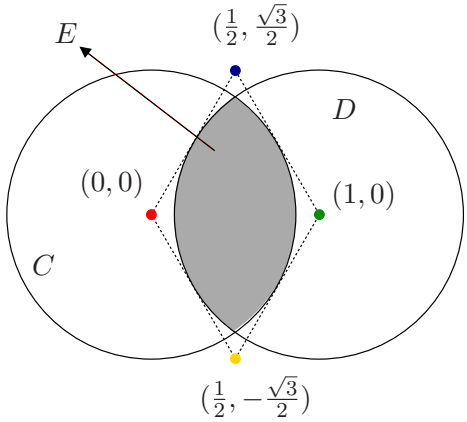

Figure 4.4: The circles C and D, the canonical lens E, and the quadrilateral Q (drawn with dotted line).

Suppose that $[u,w,v]$ and $[u,w,z]$ are the two triangles of $\mathcal{K}$ sharing the edge $[u,w]$, where v and z are vertices of $\mathcal{K}$, with $v \neq z$. Let Q_u be the quadrilateral given by the vertices $s_u(u) = u'$, $s_u(v)$, $s_u(w)$, and $s_u(z)$. Then, the composite function $g_u \circ R_{(u,w)}$ maps the intersection $Q_u \cap (\Omega_u - \{(0,0)\})$ onto the intersection set $Q \cap (\text{int}(C) - \{(0,0)\})$. In turn, function h maps $Q \cap (\text{int}(C) - \{(0,0)\})$ onto $Q \cap (\text{int}(D) - \{(0,0)\})$. From the definition of h, the points in the upper (resp. lower) half of Q are mapped to the lower (resp. upper) half of Q. Next, the composite function $R^{-1}_{(w,u)} \circ g_w^{-1}$ maps the set $Q \cap (\text{int}(C) - \{(0,0)\})$ onto the set $Q_w \cap (\Omega_w - \{(0,0)\})$, where Q_w is the quadrilateral given by the vertices $s_w(w) = w'$, $s_w(z)$, $s_w(u)$, and $s_w(v)$. However, since only the points of $Q \cap (\text{int}(C) - \{(0,0)\})$ that belong to the canonical lens, E, are mapped by $R^{-1}_{(w,u)} \circ g_w^{-1}$ to $Q_w \cap (\Omega_w - \{(0,0)\})$, not all points of $Q_u \cap (\Omega_u - \{(0,0)\})$ get mapped by $g_{(u,w)}$ to $Q_w \cap (\Omega_w - \{(0,0)\})$. Finally, function $g_{(u,w)}$ is bijective and its inverse,

$$g^{-1}_{(u,w)} : g_{(u,w)}(\Omega_u - \{(0,0)\}) \to \Omega_u - \{(0,0)\}\,,$$

is given by

$$g^{-1}_{(u,w)}(q) = R^{-1}_{(u,w)} \circ g_u^{-1} \circ h \circ g_w \circ R_{(w,u)}(q)\,,$$

for every $q \in g_{(u,w)}(\Omega_u - \{(0,0)\})$.

The following propositions state several useful properties of $g_{(u,w)}$:

Proposition 4.1.1. For any two $u, w \in I$ such that $[u, w]$ is an edge of $\mathcal{K}$, function $g_{(u,w)}$ is C^∞.

Proof. By definition,

$$g_{(u,w)}(p) = R^{-1}_{(w,u)} \circ g_w^{-1} \circ h \circ g_u \circ R_{(u,w)}(p)\,,$$

for every $p \in \Omega_u - \{(0,0)\}$. Since $R^{-1}_{(w,u)}$, g_w^{-1}, h, g_u, and $R_{(u,w)}$ are all C^∞ functions, so is $g_{(u,w)}$. □

Proposition 4.1.2. For any two vertices, u and w, of $\mathcal{K}$ such that $[u, w]$ is an edge of $\mathcal{K}$, we have that $(0,0) \notin g_{(u,w)}(\Omega_u - \{(0,0)\})$.

Proof. If $[u, w]$ is an edge of $\mathcal{K}$ then $u \neq w$ and $g_{(u,w)}(p) = R^{-1}_{(w,u)} \circ g_w^{-1} \circ h \circ g_u \circ R_{(u,w)}(p)$, for every $p \in \Omega_u - \{(0,0)\}$. By definition of $g_u \circ R_{(u,w)}$, the point $q = g_u \circ R_{(u,w)}(p)$ is such that $\Pi(q) = (\theta, r)$, where $\theta \in (-\pi/3, \pi/3)$ and $r \in (0, \cos(\pi/6))$. So, the x coordinate of q is in the open interval $(0, \cos(\pi/6))$, which means that the x coordinate of $h(q)$ is in the open interval $(1 - \cos(\pi/6), 1)$. So, $h(q) \in \mathbb{R}^2 - \{(0,0)\}$. But, $R^{-1}_{(w,u)} \circ g_w^{-1}(\mathbb{R}^2 - \{(0,0)\}) = \mathbb{R}^2 - \{(0,0)\}$, and thus our claim is true. This is consistent with the fact that g_w^{-1} is undefined at $(0,0)$. □

Proposition 4.1.3. For any two vertices, u and w, of $\mathcal{K}$ such that $[u, w]$ is an edge of $\mathcal{K}$, we have that $g_{(u,w)}(\Omega_u - \{(0,0)\}) \cap (\Omega_w - \{(0,0)\})$ is non-empty and open in $\mathbb{R}^2$. Furthermore, $g^{-1}_{(u,w)} = g_{(w,u)}(p)$, for every p in $g_{(u,w)}(\Omega_u - \{(0,0)\}) \cap \Omega_w$.

Proof. By definition, we have that $g_{(u,w)}(p) = R^{-1}_{(w,u)} \circ g_w^{-1} \circ h \circ g_u \circ R_{(u,w)}(p)$, for every $p \in \Omega_u - \{(0,0)\}$. But, the composite function $h \circ g_u \circ R_{(u,w)}$ maps $\Omega_u - \{(0,0)\}$ onto the set $\text{int}(D) - \{(1,0)\}$, where D is the circle of radius $\cos(\pi/6)$ and center $(1,0)$. In turn, the composite function $R^{-1}_{(w,u)} \circ g_w^{-1}$ maps $\text{int}(C) - \{(0,0)\}$ onto $\Omega_w - \{(0,0)\}$, where C is the circle of radius $\cos(\pi/6)$ and center $(1,0)$. So, only the points of $\Omega_u - \{(0,0)\}$ that get mapped by $h \circ g_u \circ R_{(u,w)}$ to the canonical lens,

$$E = h \circ g_u \circ R_{(u,w)}(\Omega_u - \{(0,0)\}) \cap \text{int}(C) - \{(0,0)\}\,,$$

are mapped by $R^{-1}_{(w,u)} \circ g_w^{-1}$ to $\Omega_w - \{(0,0)\}$. But, since the functions $R_{(u,w)}$, g_u, h, $R^{-1}_{(w,u)}$, and g_w^{-1} are all bijective and the canonical lens are non-empty, we have that $R^{-1}_{(w,u)} \circ g_w^{-1}(E)$ must be a non-empty subset

of $\Omega_w - \{(0,0)\}$. So,

$$g_{(u,w)}(\Omega_u - \{(0,0)\}) \cap (\Omega_w - \{(0,0)\}) \neq \emptyset\,,$$

is true. To complete the proof of our first claim, we must show that the above set is open in $\mathbb{R}^2$. But, from Proposition 4.1.1, function $g_{(u,w)}$ is a homeomorphism. So, since the set $\Omega_u - \{(0,0)\}$ is open in $\mathbb{R}^2$, its image, $g_{(u,w)}(\Omega_u - \{(0,0)\})$, under $g_{(u,w)}$ is also open in $\mathbb{R}^2$. Because $\Omega_w - \{(0,0)\}$ is open in $\mathbb{R}^2$ and the intersection of open sets is again an open set, our claim follows.

Now, consider the second claim. By definition,

$$g^{-1}_{(u,w)}(p) = R^{-1}_{(u,w)}(p) \circ g_u^{-1} \circ h \circ g_w \circ R_{(w,u)}(p)\,,$$

for every $p \in g_{(u,w)}(\Omega_u - \{(0,0)\})$, and

$$g_{(w,u)}(q) = R^{-1}_{(u,w)}(p) \circ g_u^{-1} \circ h \circ g_w \circ R_{(w,u)}(q)\,,$$

for every $q \in \Omega_w - \{(0,0)\}$. So, $g^{-1}_{(u,w)}(t) = g_{(w,u)}(t)$, for every t in $g_{(u,w)}(\Omega_u - \{(0,0)\}) \cap (\Omega_w - \{(0,0)\})$. From Proposition 4.1.2,

$$(0,0) \notin g_{(u,w)}(\Omega_u - \{(0,0)\})\,.$$

So,

$$g_{(u,w)}(\Omega_u - \{(0,0)\}) \cap \Omega_w = g_{(u,w)}(\Omega_u - \{(0,0)\}) \cap (\Omega_w - \{(0,0)\})\,,$$

which implies that $g^{-1}_{(u,w)}(t) = g_{(w,u)}(t)$, for every t in $g_{(u,w)}(\Omega_u - \{(0,0)\}) \cap \Omega_w$, and thus our claim is true. □

Function $g_{(u,w)}$ plays a crucial role in the following definitions of gluing domains and transition functions:

Definition 4.1.9. For any $u, w \in I$, the *gluing domain* Ω_{uw} is defined as

$$\Omega_{uw} = \begin{cases} \Omega_u & \text{if } u = w, \\ g_{(w,u)}(\Omega_w - \{(0,0)\}) \cap \Omega_u & \text{if } [u,w] \text{ is an edge of } \mathcal{K}, \\ \emptyset & \text{otherwise.} \end{cases}$$

As we shall see in Section 4.2, Definition 4.1.9 satisfies condition (2) of the definition of sets of gluing data (see Definition 3.4.1). Note that the requirement $\Omega_{uu} = \Omega_u$, for all $u \in I$, is true by definition. So, we

are left to prove that Ω_{uw} is open in $\mathbb{R}^2$ and $\Omega_{uw} \neq \emptyset$ if and only if $\Omega_{wu} \neq \emptyset$, for each $(u, w) \in I \times I$, with $u \neq w$.

Transition functions are bijective maps between non-empty gluing domains defined as follows:

Definition 4.1.10. Let K be the index set,

$$K = \{(u, w) \in I \times I \mid \Omega_{uw} \neq 0\}\,.$$

Then, for any pair $(u, w) \in K$, the *transition function*,

$$\varphi_{wu} : \Omega_{uw} \to \Omega_{wu}\,,$$

is such that, for every $p \in \Omega_{uw}$, we let

$$\varphi_{wu}(p) = \begin{cases} p & \text{if } u = w, \\ g_{(u,w)}(p) & \text{otherwise.} \end{cases}$$

Figure 4.5 illustrates Definition 4.1.10.

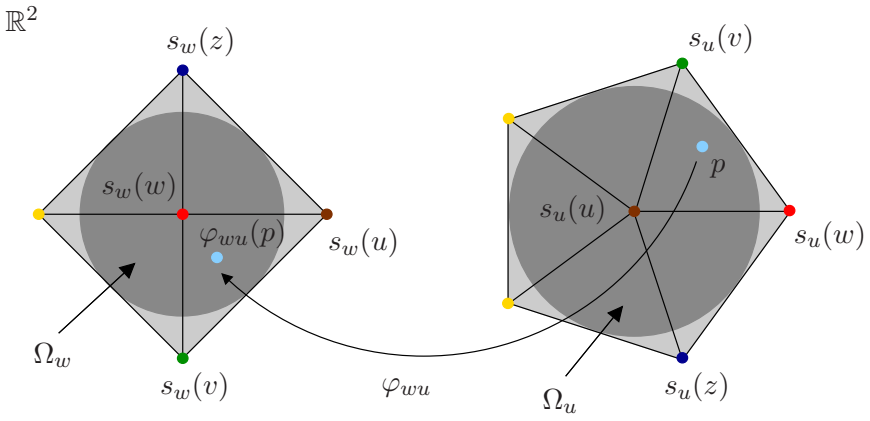

Figure 4.5: Illustration of Definition 4.1.10.

As we shall also see in Section 4.2, Definition 4.1.10 satisfies conditions (3) and (4) of the definition of sets of gluing data (see Definition 3.4.1). Note that condition 3(a), $\varphi_{uu} = \mathrm{id}_{\Omega_u}$, for all $u \in I$, is true by definition. So, we must prove condition 3(b), the *cocycle condition* (condition 3(c)), and the *Hausdorff condition* (condition (4)).

4.2 Construction Correctness

Propositions 4.2.1 and 4.2.2 below imply that Definition 4.1.9 satisfies condition (2) of Definition 3.4.1:

Proposition 4.2.1. Let Ω_u and Ω_w be any two p-domains of $(\Omega_v)_{v\in I}$. Then, $\Omega_{uw} \neq \emptyset$ if and only if $\Omega_{wu} \neq \emptyset$.

Proof. If $u = w$, our claim is trivially true. So, let us assume that $u \neq w$. Now, suppose that $\Omega_{uw} \neq \emptyset$. So, from Definition 4.1.9, we must have that $[u, w]$ is an edge of $\mathcal{K}$. Otherwise, Ω_{uw} would be empty. This implies that $g_{(u,w)}$ and its inverse, $g^{-1}_{(u,w)}$, are well-defined. Furthermore, Ω_{uw} and Ω_{wu} are defined as follows:

$$\Omega_{uw} = g_{(w,u)}(\Omega_w - \{(0,0)\}) \cap \Omega_u$$

and

$$\Omega_{wu} = g_{(u,w)}(\Omega_u - \{(0,0)\}) \cap \Omega_w \,.$$

From Proposition 4.1.2, we know that $(0,0) \notin g_{(w,u)}(\Omega_w - \{(0,0)\})$. So,

$$\Omega_{uw} = g_{(w,u)}(\Omega_w - \{(0,0)\}) \cap (\Omega_u - \{(0,0)\}) \,.$$

From Proposition 4.1.3, we know that $g_{(u,w)}$ and $g^{-1}_{(w,u)}$ coincide in Ω_{uw}. So,

$$g_{(u,w)}(\Omega_{uw}) = g^{-1}_{(w,u)}(\Omega_{uw}) = g^{-1}_{(w,u)}(g_{(w,u)}(\Omega_w - \{(0,0)\}) \cap (\Omega_u - \{(0,0)\})) \,.$$

Since $g^{-1}_{(w,u)}$ is bijective, we have that

$$\begin{aligned} g^{-1}_{(w,u)}(g_{(w,u)}(\Omega_w - \{(0,0)\}) \cap \Omega_u - \{(0,0)\})) &= g^{-1}_{(w,u)}(g_{(w,u)}(\Omega_w - \{(0,0)\})) \cap g^{-1}_{(w,u)}(\Omega_u - \{(0,0)\}) \\ &= (\Omega_w - \{(0,0)\}) \cap g^{-1}_{(w,u)}(\Omega_u - \{(0,0)\}) \\ &= g_{(u,w)}(\Omega_u - \{(0,0)\}) \cap (\Omega_w - \{(0,0)\}) \\ &= g_{(u,w)}(\Omega_u - \{(0,0)\}) \cap \Omega_w \\ &= \Omega_{wu} \,. \end{aligned}$$

Since $\Omega_{uw} \neq \emptyset$ and $g_{(u,w)}$ is bijective, the set $\Omega_{wu} = g_{(u,w)}(\Omega_{uw})$ cannot be empty either, and hence our claim follows. □

Proposition 4.2.2. Let Ω_u and Ω_w be any two p-domains of $(\Omega_v)_{v\in I}$. Then, the gluing domain Ω_{uw} is an open set of $\mathbb{R}^2$.

Proof. If $u = w$ then our claim is trivially true, as $\Omega_{uu} = \Omega_u$ and Ω_u is open in $\mathbb{R}^2$ (by definition). So, assume that $u \neq w$. If $\Omega_{uw} = \emptyset$ then our claim is trivially true. So, assume that $\Omega_{uw} \neq \emptyset$. From Definition 4.1.9, if $\Omega_{uw} \neq \emptyset$ then

$$\Omega_{uw} = g_{(w,u)}(\Omega_w - \{(0,0)\}) \cap \Omega_u \,.$$

From Proposition 4.1.2, we know that $(0,0) \notin g_{(u,w)}(\Omega_u - \{(0,0)\})$. So,

$$\Omega_{uw} = g_{(w,u)}(\Omega_w - \{(0,0)\}) \cap (\Omega_u - \{(0,0)\}) \,.$$

Finally, Proposition 4.1.3 states that the above set is non-empty and open in $\mathbb{R}^2$. □

In what follows, we show that the transition functions, as defined before, satisfy conditions (3) and (4) of Definition 3.4.1. Although conditions (3)(a) and (3)(b) follow from Condition (3)(c), the exposition of our proof of Condition (3)(c) assumes that (3)(a) and 3(b) are true, so we first show that condition (3)(b) holds.

Proposition 4.2.3. For any $(u, w) \in K$, we have that $\varphi_{wu}(p) = \varphi_{uw}^{-1}(p)$, for all $p \in \Omega_{uw}$.

Proof. From Definition 4.1.10, if $u = w$ then $\varphi_{wu} = \varphi_{uw} = \mathrm{id}_{\Omega_u}$. Otherwise, we have $\varphi_{wu} = g_{(u,w)}$ and $\varphi_{uw} = g_{(w,u)}$. In the former case, our claim is trivially true. In the latter case, Proposition 4.1.3 states that $g_{(u,w)}^{-1}(p) = g_{(w,u)}(p)$, for every $p \in \Omega_{uw}$. Since $\varphi_{uw}(p) = g_{(w,u)}(p) = g_{(u,w)}^{-1}(p) = \varphi_{uw}^{-1}(p)$, our claim follows. □

Our proof of Condition 3(c) relies on a property of function g_u, called *rotational symmetry*, which is stated below:

Proposition 4.2.4. Let $[u, w, z]$ be any triangle of $\mathcal{K}$. If $s_u(z)$ precedes $s_u(w)$ in a counterclockwise traversal of the vertices of P_u, then

$$M_{-\pi/3} \circ g_u \circ R_{(u,w)}(\Omega_{uw}) = g_u \circ R_{(u,w)}(\Omega_{uz}) \quad \text{and} \quad M_{\pi/3} \circ g_u \circ R_{(u,z)}(\Omega_{uz}) = g_u \circ R_{(u,z)}(\Omega_{uw}) \,,$$

where $M_{-\frac{\pi}{3}}$ (resp. $M_{\frac{\pi}{3}}$) is a rotation by $-\frac{\pi}{3}$ (resp. $\frac{\pi}{3}$) around the origin. Furthermore,

$$\Omega_{uz} = M_{-\frac{2\pi}{m_u}}(\Omega_{uw}) \qquad \text{and} \qquad \Omega_{uw} = M_{\frac{2\pi}{m_u}}(\Omega_{uz}) \,,$$

where $M_{-\frac{2\pi}{m_u}}$ is a rotation by $-\frac{2\pi}{m_u}$ around the origin, and m_u is the degree of vertex u in $\mathcal{K}$.

Proof. See Appendix A for a proof. □

We now show that the first implication of Condition 3(c) of Definition 3.4.1 holds:

Lemma 4.2.1. Let Ω_u, Ω_w, and Ω_x be any three p-domains in $(\Omega_v)_{v\in I}$. If the intersection

$$\Omega_{xu} \cap \Omega_{xw}$$

is nonempty, then

$$\varphi_{xu}^{-1}(\Omega_{xu} \cap \Omega_{xw}) \subseteq \Omega_{uw}\,.$$

Proof. See Appendix A for a proof. □

In what follows we show that the second and last implication of Condition 3(c) of Definition 3.4.1 also holds:

Lemma 4.2.2. Let Ω_u, Ω_w, and Ω_x be any three p-domains in $(\Omega_v)_{v\in I}$. If $\Omega_{xu} \cap \Omega_{xw} \neq \emptyset$, then

$$\varphi_{wu}(p) = \varphi_{wx} \circ \varphi_{xu}(p)\,,$$

for all $p \in \varphi_{xu}^{-1}(\Omega_{xu} \cap \Omega_{xw}) \subseteq \Omega_{uw}$.

Proof. See Appendix A for a proof. □

Lemma 4.2.3. Let (u, w) be any pair in K, with $u \neq w$. Then, for every $x \in \partial(\Omega_{uw}) \cap \Omega_u$ and every $y \in \partial(\Omega_{wu}) \cap \Omega_w$, there are open balls, V_x and V_y, centered at x and y, such that no point of $V_y \cap \Omega_{wu}$ is the image of any point $V_x \cap \Omega_{uw}$ under φ_{wu}.

Proof. By definition, each gluing domain, Ω_{uw}, is the image by $R_{(u,w)}^{-1} \circ g_u^{-1}$ of the canonical lens, E, given by

$$(\text{int}(C) - \{(0,0)\}) \cap (\text{int}(D) - \{(1,0)\})\,,$$

where C and D are the circles of radius $\cos(\pi/6)$ and centers $(0,0)$ and $(1,0)$, respectively. Furthermore, the gluing domain Ω_{uw} is also a lens-shaped set whose boundary, $\partial(\Omega_{uw})$, is the image by $R_{(u,w)}^{-1} \circ g_u^{-1}$ of the boundary, $\partial(E)$, of E. We can view $\partial(\Omega_{uw})$ as the union of two open and simple curve segments, C_{u_e}

and C_{u_i}, such that C_{u_e} belongs to $\partial(\Omega_{uw})$ and the interior, $\text{int}(C_{u_i})$, of C_{u_i} belongs to the interior of Ω_u, as shown in Figure 4.6. In addition, the pairs of endpoints of both curves, C_{u_e} and C_{u_i}, are the same, and each pair is the image by $R^{-1}_{(u,w)} \circ g_u^{-1}$ of the two intersection points of the boundaries, $\partial(C)$ and $\partial(D)$, of C and D.

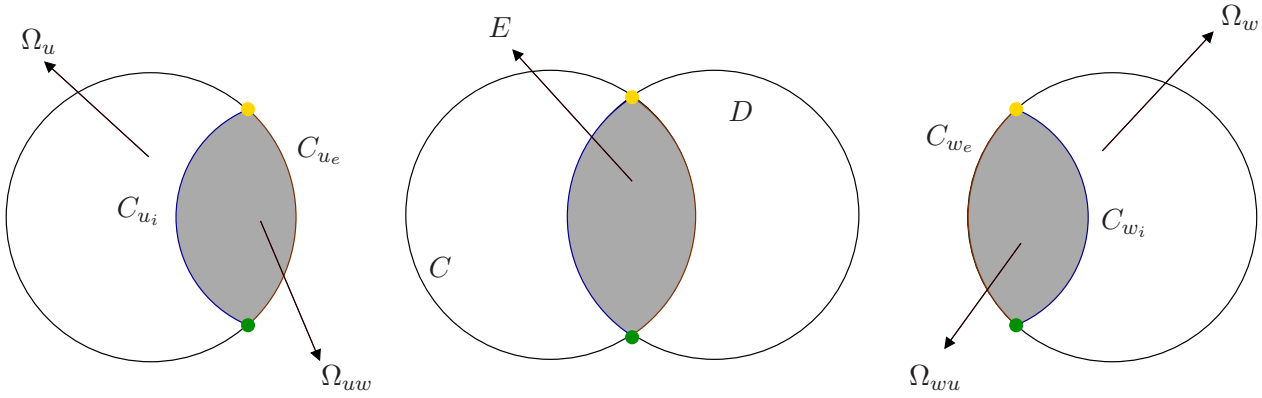

Figure 4.6: The image sets of the canonical lens, E, under $R^{-1}_{(u,w)} \circ g_u^{-1}$ and $R^{-1}_{(w,u)} \circ g_w^{-1}$.

Similarly, the boundary, $\partial(\Omega_{wu})$, of the gluing domain, Ω_{wu}, can be viewed as the union of two curves, C_{w_e} and C_{w_i}, such that C_{w_e} belongs to $\partial(\Omega_{wu})$ and the interior, $\text{int}(C_{w_i})$, of C_{w_i} belongs to the interior of Ω_w. In addition, the pairs of endpoints of both curves, C_{w_e} and C_{w_i}, are the same, and each pair is the image by $R^{-1}_{(w,u)} \circ g_w^{-1}$ of the two intersection points of the boundaries, $\partial(C)$ and $\partial(D)$, of C and D (see Figure 4.6).

Note that

$$\text{int}(C_{u_i}) = \partial(\Omega_{uw}) \cap \Omega_u \qquad \text{and} \qquad \text{int}(C_{w_i}) = \partial(\Omega_{wu}) \cap \Omega_w \,.$$

Note also that

$$g_{(u,w)}(C_{u_i}) = C_{w_e} \qquad \text{and} \qquad g_{(w,u)}(C_{w_i}) = C_{u_e} \,.$$

Indeed,

$$g_{(u,w)}(C_{u_i}) = R^{-1}_{(w,u)} \circ g_w^{-1} \circ h \circ g_u \circ R_{(u,w)}(C_{u_i}) \,.$$

By construction, we know that $g_u \circ R_{(u,w)}(C_{u_i}) \in \partial(C)$, which means that $h \circ g_u \circ R_{(u,w)}(C_{u_i}) \in \partial(D)$. So, we get

$$R^{-1}_{(w,u)} \circ g_w^{-1} \circ h \circ g_u \circ R_{(u,w)}(C_{u_i}) = C_{w_e} \,.$$

Finally, let x be any point in $\partial(\Omega_{uw}) \cap \Omega_u$. Since $\text{int}(C_{u_i}) = \partial(\Omega_{uw}) \cap \Omega_u$, we have that $x \in \text{int}(C_{u_i})$. From our discussion above, we also have that if $p = g_{(u,w)}(x)$ then $p \in \text{int}(C_{w_e})$. Since $\text{int}(C_{w_e}) \cap \text{int}(C_{w_i}) = \emptyset$, there exists an open ball, V_p, centered at p such that $V_p \cap \text{int}(C_{w_i}) = \emptyset$, which follows from the fact that $\mathbb{R}^2$ is a Hausdorff space.

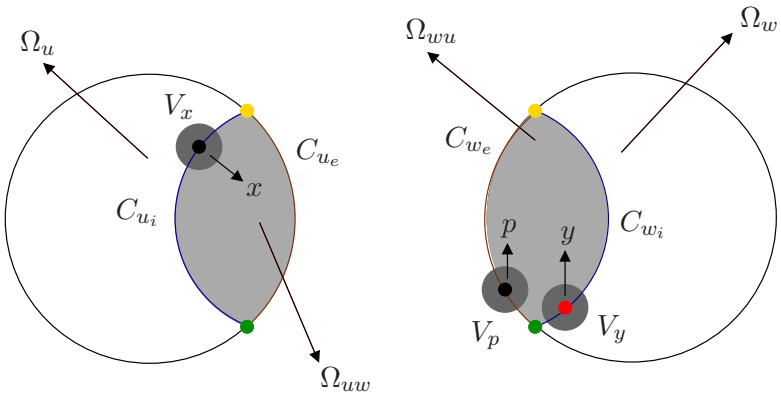

Figure 4.7: The open balls V_x, V_y, and V_p.

Since $\text{int}(C_{w_i}) = \partial(\Omega_{wu}) \cap \Omega_w$, we get that

$$V_p \cap (\partial(\Omega_{wu}) \cap \Omega_w) = \emptyset\,.$$

In turn, for any point $y \in \partial(\Omega_{wu}) \cap \Omega_w$, there exists an open ball, V_y, such that $V_y \cap V_p = \emptyset$ (see Figure 4.7). This also follows from the fact that $\mathbb{R}^2$ is a Hausdorff space. So, define V_x to be any open ball centered at x such that $V_x \subseteq g^{-1}_{(u,w)}(V_p)$. By construction, we know that $g_{(u,w)}(V_x) \cap V_y = \emptyset$. To conclude that our claim is true, it suffices to notice that $g_{(u,w)}(V_x \cap \Omega_{uw}) \subset \Omega_w$ and that $\varphi_{wu} = g_{(u,w)}$ for every point in Ω_{uw}, which implies that

$$\varphi_{wu}(V_x \cap \Omega_{uw}) \cap (V_y \cap \Omega_{wu}) = \emptyset\,.$$

□

The following theorem states the correctness of the construction in Section 4.1:

Theorem 4.2.1. Given any given simplicial surface, $\mathcal{K}$, in $\mathbb{R}^3$, the triple

$$\mathcal{G} = ((\Omega_v)_{v\in I}, (\Omega_{uw})_{(u,w)\in I\times I}, (\varphi_{uw})_{(u,w)\in K})\,,$$

where

- $(\Omega_v)_{v\in I}$ is any set of p-domains for $\mathcal{K}$,
- $(\Omega_{uw})_{(u,w)\in I\times I}$ is the set of gluing domains for $\mathcal{K}$ with respect to $(\Omega_v)_{v\in I}$,
- $(\varphi_{uw})_{(u,w)\in K}$ is the set of transition functions defined by Definition 4.1.10, and
- $K = \{(u,w) \in I \times I \mid \Omega_{uw} \neq \emptyset\}$,

is a set of gluing data according to Definition 3.4.1.

Proof. Our claim follows immediately from the facts that our construction yields p-domains, gluing domains, and transition functions that satisfy conditions (1)-(4) of the definition of a set of gluing data (see Definition 4.1.10). Indeed, the p-domains are open sets in $\mathbb{R}^2$; Proposition 4.2.1 and Proposition 4.2.2 ensure that the gluing domains satisfy condition (2) of Definition 4.1.10; Proposition 4.2.3, Lemma 4.2.1, and Lemma 4.2.2 ensure that the transition functions satisfy condition (3); and Lemma 4.2.3 states that condition (4) also hold. □

From now on, we shall refer to

$$\mathcal{G} = ((\Omega_v)_{v\in I}, (\Omega_{uw})_{(u,w)\in I\times I}, (\varphi_{uw})_{(u,w)\in K})$$

as a *set of gluing data for* $\mathcal{K}$.

Finally, we show that the transition functions are all C^∞ functions:

Lemma 4.2.4. For any pair $(u,w) \in K$, the transition function φ_{wu} is C^∞.

Proof. From Definition 4.1.10, we know that φ_{wu} is the identity function if $u = w$ and the function $g_{(u,w)}$ otherwise. In the former case, our claim is trivially true. In the latter case, our claim follows from Proposition 4.1.1. □

Chapter 5

Building Parametrizations

This chapter describes a new construction for defining a parametric pseudo-surface, $\mathcal{M} = (\mathcal{G}, (\theta_i)_{i\in I})$, from a set of gluing data,

$$\mathcal{G} = ((\Omega_i)_{i\in I}, (\Omega_{ij})_{(i,j)\in I\times I}, (\varphi_{ij})_{(i,j)\in K}),$$

for a given simplicial surface, $\mathcal{K}$, in $\mathbb{R}^3$. The set $\mathcal{G}$ is assumed to be defined from the topology of $\mathcal{K}$, as described in Chapter 4. Here, we show how to define the family of parametrizations, $(\theta_i)_{i\in I}$, from the geometry of the underlying surface, $|\mathcal{K}|$, of $\mathcal{K}$. We also show that the image, M, of $\mathcal{M}$ is guaranteed to be a surface in $\mathbb{R}^3$, which is homeomorphic to $|\mathcal{K}|$, whenever the θ_i's are bijective and satisfy conditions (C') and (C") in Section 3.5.

5.1 Parametric Pseudo-Surfaces

Let $\mathcal{K}$ be any given simplicial surface in $\mathbb{R}^3$, and let

$$\mathcal{G} = ((\Omega_v)_{v\in I}, (\Omega_{uw})_{(u,w)\in I\times I}, (\varphi_{uw})_{(u,w)\in K})$$

be a set of gluing data for $\mathcal{K}$.

We wish to define a parametric C^k pseudo-surface, $\mathcal{M} = (\mathcal{G}, (\theta_v)_{v\in I})$, in $\mathbb{R}^3$, so that the image,

$$M = \bigcup_{v\in I} \theta_v(\Omega_v),$$

of $\mathcal{M}$ is a surface in $\mathbb{R}^3$ that approximates the underlying surface, $|\mathcal{K}|$, of $\mathcal{K}$. To that end, we assume we are given a surface, $S' \subset \mathbb{R}^3$, that approximates the underlying surface, $|\mathcal{K}|$, of $\mathcal{K}$. More specifically, we assume that the surface to be approximated, S', is the union of finitely many parametric surface patches, i.e.,

$$S' = \bigcup_{\sigma \in \mathcal{K}} b_\sigma(\triangle)\,,$$

where each patch is associated with a triangle, σ, of $\mathcal{K}$ and is the image of a triangle, $\triangle$, in $\mathbb{R}^2$ by a function $b_\sigma : \mathbb{R}^2 \to \mathbb{R}^3$. In addition, we require S' be at least C^0-continuous. We can view S' as describing the geometry we want to locally approximate with the parametrizations. To define each parametrization θ_v, we specify a family, $\{\psi_v\}_{v \in I}$, of *shape functions* and a family, $\{\gamma_v\}_{v \in I}$, of *weight functions*. In particular, each shape function, ψ_v, is a rectangular Bézier patch that locally approximates S' on Ω_v. In turn, each γ_v is a non-negative function with compact support equal to the closure, $\overline{\Omega}_v$, of Ω_v. Finally, each parametrization, θ_v, is defined as a convex sum of shape functions. The weights associated with the shape functions are given by the weight functions.

In particular, for every point $p \in \Omega_v$, we let

$$\theta_v(p) = \sum_{u \in J_v(p)} \omega_{uv}(p) \cdot (\psi_u \circ \varphi_{uv}(p))\,, \tag{5.1}$$

where

$$\omega_{uv}(p) = \frac{\gamma_u \circ \varphi_{uv}(p)}{\sum_{w \in J_v(p)} \gamma_w \circ \varphi_{wv}(p)}$$

and

$$J_v(p) = \{u \mid p \in \Omega_{vu}\} \subseteq I\,.$$

The set $J_v(p)$ contains the index of each p-domain, Ω_u, that is "glued" to Ω_v by φ_{uv} at p. Note that $\varphi_{uv}(p)$ is the point in Ω_u identified with p by φ_{uv}. The former point is assigned a weight, $\omega_{uv}(p)$, which can be viewed as its contribution to $\theta_v(p)$. So, $\theta_v(p)$ adds up the contribution of each shape function, ψ_u, defined in a p-domain that contains a point, $\varphi_{uv}(p)$, identified with p in the gluing process. By construction, we have that

$$\sum_{u \in J_v(p)} \omega_{uv}(p) = 1, \quad \text{with } \omega_{uv}(p) \geq 0, \text{ for all } u \in J_v(p)\ \ ,$$

which ensures that $\theta_v(p)$ is indeed a convex sum of shape functions. The reason we define $\theta_v(p)$ as in Eq. (5.1) is that we are guaranteed to satisfy Condition (C) of Definition 3.5.1: $\theta_v(p) = \theta_u \circ \varphi_{uv}(p)$, for all

$u \in J_v(p)$ (see Figure 5.1). We will prove this claim later. For the time being, recall that Condition (C) ensures that

$$S = \bigcup_{v \in I} \theta_v(\Omega_v)$$

is the image of a parametric pseudo surface.

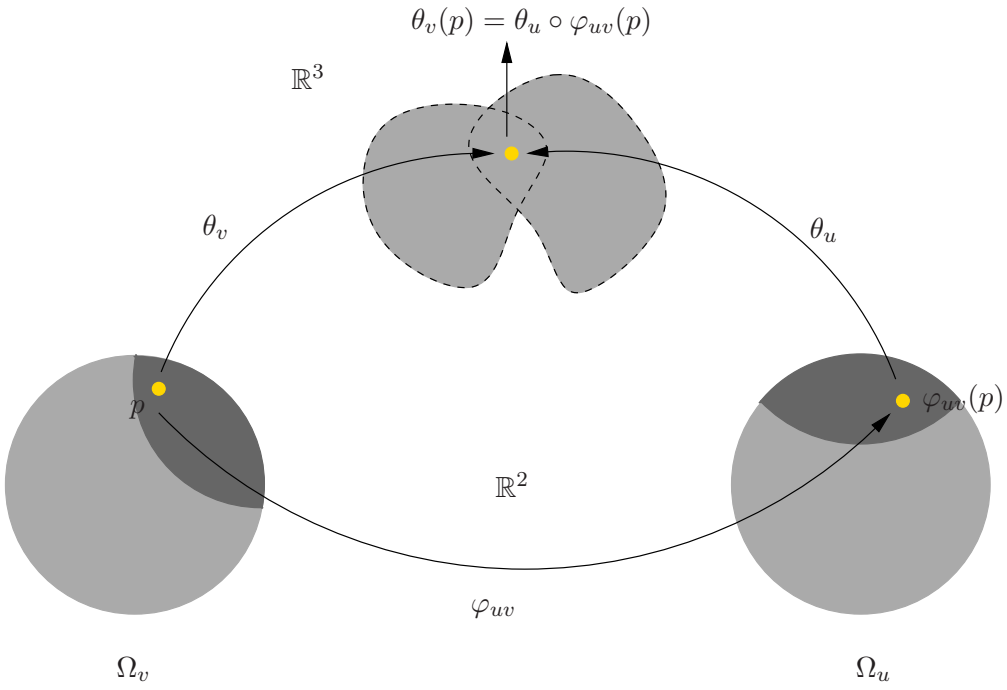

Figure 5.1: Illustration of Condition (C) of Definition 3.5.1.

5.2 Shape Functions

Definition 5.2.1. For each $v \in I$, we define the *shape function,*

$$\psi_v : \square_v \subset \mathbb{R}^2 \to \mathbb{R}^3 \,,$$

associated with Ω_v as the Bézier surface patch of bi-degree (l, l),

$$\psi_v(p) = \sum_{0 \le j \le l} \sum_{0 \le k \le l} b^v_{j,k} \cdot B^l_j(x) \cdot B^l_k(y) \,,$$

where $\square_v = [-L, L]^2$, with $L = \cos(\pi/m_v)$, (x, y) are the coordinates of $p \in \square_v$, $\{b^v_{j,k}\} \subset \mathbb{R}^3$ are the *control points*, and

$$B^l_i(t) = \binom{l}{i} \left(\frac{L-t}{2 \cdot L}\right)^{l-i} \left(\frac{t+L}{2 \cdot L}\right)^{i}$$

is the *i-th Bernstein polynomial of degree l over the interval* $[-L, L] \subset \mathbb{R}$, for every $i \in \{0, 1, \ldots, l\}$.

The controls points are determined by solving a least squares fitting problem. In particular, we have that $\{b^v_{j,k}\}$ is the family of control points that uniquely defines a Bézier patch of bi-degree (l, l) (i.e., ψ_v) which best fits (*in a least squares sense*) a finite set, P, of pairs, (q, p), of points, where q belongs to P_v and p belongs to the surface S'. Recall that S' is an input parameter of our construction, which is given as the union

$$S' = \bigcup_{\sigma \in \mathcal{K}} b_\sigma(\triangle)\,,$$

where $b_\sigma(\triangle)$ is a surface patch defined as the image of a triangle, $\triangle \subset \mathbb{R}^2$, by a parametric function, $b_\sigma : \mathbb{R}^2 \to \mathbb{R}^3$. Each surface patch $b_\sigma(\triangle)$ is associated with a distinct triangle, σ, of $\mathcal{K}$. It is worth mentioning that we impose no restriction on the way function b_σ is defined, but the surface patch, $b_\sigma(\triangle)$, is expected to be homeomorphic to a closed disk in $\mathbb{R}^2$. Finally, we compute P by starting with $P = \emptyset$ and then proceeding as follows:

- We uniformly sample the domain of ψ_v (i.e., the quadrilateral $\square_v = [-L, L]^2$) to generate a set, $Q \subset P_v$, with $4 \cdot l^2$ points. Note that $\square_v$ is the smallest quadrilateral that contains Ω_v. Note also that a uniform sampling of $\square_v$ will contain points that are not in P_v. These points are not placed into Q.
- For each point $q \in Q$, we find the triangle σ of $\mathcal{K}$ such that q is contained in the triangle $s_v(\sigma)$ of T_v. Then, we compute the barycentric coordinates, (λ, ν, η), of q with respect to $s_v(\sigma)$ and use these coordinates to compute a point, $r = \lambda \cdot a + \nu \cdot b + \eta \cdot c$, in $\triangle = [a, b, c]$, where $\triangle$ is the common affine frame of all parametric patches defining S'. Next, we compute $b_\sigma(r)$, let $p = b_\sigma(r)$, and add the pair, (q, p), to P.

Figure 5.2 illustrates the computation of q and p.

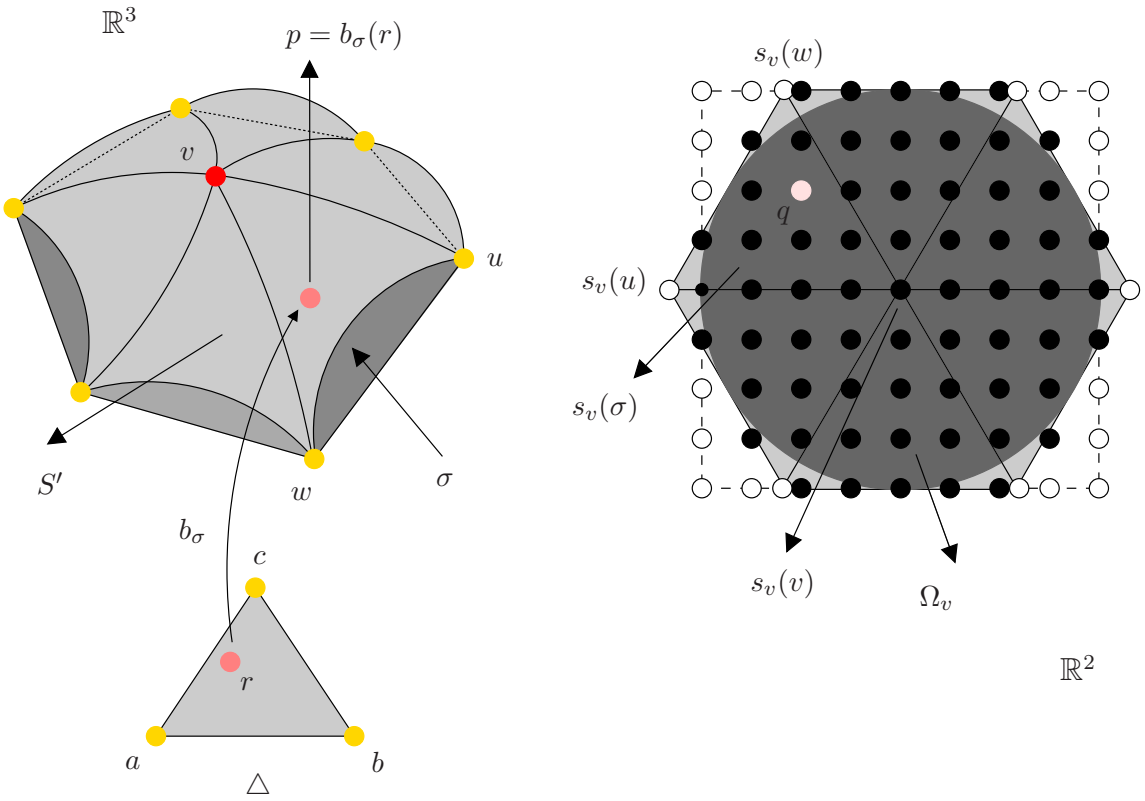

Figure 5.2: Local sampling of S' (white-filled vertices are not in Q).

Once P is computed, we use a standard least squares fitting procedure to compute $\{b^v_{j,k}\}$ (see [68], p. 278). More specifically, let $n = 4 \cdot l^2$, and let R be a sequence, $R = \{q_i\}_{i=1}^n$, where each q_i is a distinct point from Q, with $i \in \{1, \ldots, n\}$. Then, we can define n linear equations in l^2 unknowns,

$$\psi_v(q_i) = \sum_{0 \le j \le l} \sum_{0 \le k \le l} b^v_{j,k} \cdot B^l_j(x_i) \cdot B^l_k(y_i)\,,$$

where $q_i = (x_i, y_i)$. These equations give rise to three linear systems,

$$A \cdot X^{(h)} = D^{(h)}\,, \qquad \text{with } h = 1, 2, 3,$$

where

$$A_{i,j \times l + k + 1} = B^l_j(x_i) \cdot B^l_k(y_i)\,,$$
$$D^{(h)}_i = p^{(h)}_i\,,$$

and

$$X^{(h)}_{j \times l + k + 1} = b^v_{j,k,h}\,,$$

where $p_i^{(h)}$ is h-th coordinate of the point in P associated with q_i, and $b_{j,k,h}^v$ is h-th coordinate of $b_{j,k}^v$, for every $i \in \{1, \ldots, n\}$ and every $j, k \in \{0, \ldots, l\}$. Note that each system has $4l^2$ equations in l^2 unknowns, which implies that they are in general unsolvable. So, we commonly seek a vector $X^{(h)}$ that minimizes the length $\|A \cdot X^{(h)} - D^{(h)}\|$ of the residual vector $A \cdot X^{(h)} - D^{(h)}$. This is a least squares fitting problem, whose solution can be found by solving the system of normal equations, $A^{\mathrm{T}} A X^{(h)} = A^{\mathrm{T}} D^{(h)}$ [69]. The unknown vector $X^{(h)}$ is unique if $A^{\mathrm{T}} A$ has full rank. Note that A and $D^{(h)}$ depend only on Q and P, respectively.

Note that the larger l is the better each $\psi_v(\Omega_v)$ approximates the surface S'. On the other hand, the larger l is the longer the computation of the control points of each ψ_v will take. Furthermore, we should refrain from choosing very large values for l in order to avoid the well-known "undulation" phenomenon, which typically occur in high degree polynomial based fitting approaches [70]. In the implementation of our construction, we defined l to be $\max\{m_v + 1, 7\}$, where m_v is the degree of vertex v in $\mathcal{K}$. This choice was decided empirically and by taking into account the aforementioned tradeoff between accuracy and speed.

5.3 Weight Functions

To define the family, $\{\gamma_v\}_{v \in I}$, of weight functions, we first specify a scalar function:

Definition 5.3.1. For every $t \in \mathbb{R}$, we define

$$\xi : \mathbb{R} \to \mathbb{R}$$

as

$$\xi(t) = \begin{cases} 1 & \text{if } t \leq H_1 \\ 0 & \text{if } t \geq H_2 \\ 1/(1 + e^{2 \cdot s}) & \text{otherwise} \end{cases} \tag{5.2}$$

where H_1, H_2 are constant, with $0 < H_1 < H_2 < 1$,

$$s = \left(\frac{1}{\sqrt{1 - H}} \right) - \left(\frac{1}{\sqrt{H}} \right) \quad \text{and} \quad H = \left(\frac{t - H_1}{H_2 - H_1} \right).$$

Figure 5.3 shows a plot of function $\xi(t)$, for t in $[0,1] \subset \mathbb{R}$.

Note that $\xi(t)$ is constant for $t \leq H_1$ and $t \geq H_2$, and it is strictly decreasing when t varies from H_1 to H_2. Function[1] $\xi(t)$ is C^∞, and its i-th derivative, $\mathrm{D}^i\xi(t)$, vanishes for $t \leq H_1$ and $t \geq H_2$, and it is nonzero for $t \in (H_1, H_2) \subset \mathbb{R}$.

We can now define the weight functions:

Definition 5.3.2. For each $v \in I$, the *weight function,*

$$\gamma_v : \mathbb{R}^2 \to \mathbb{R}\,,$$

associated with Ω_v is given by

$$\gamma_v(p) = \xi\left(\sqrt{x^2+y^2}\right)\,,$$

for every $p = (x, y) \in \mathbb{R}^2$, where $\sqrt{x^2+y^2}$ is the Euclidean distance from p to the center point, $(0,0)$, of Ω_v. The constants H_1 and H_2 (in the definition of ξ) are experimentally chosen to be $0.25 \cdot H_2$ and $\cos(\pi/m_v)$, respectively.

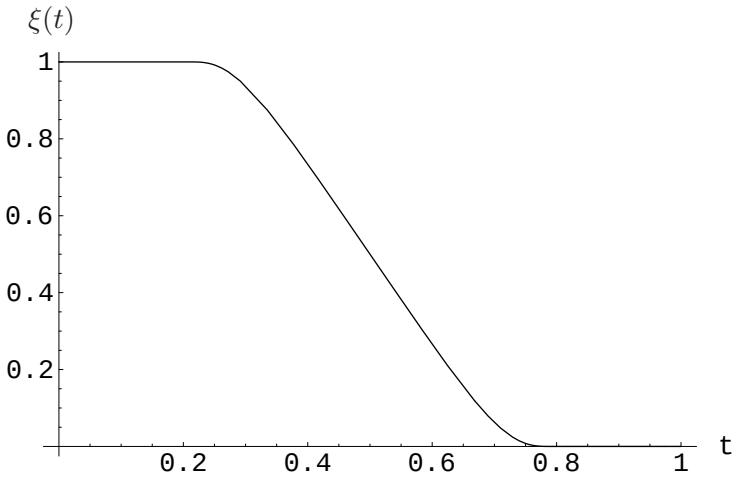

Figure 5.3: Plot of $\xi(t)$ for $t \in (0,1) \subset \mathbb{R}$, using $H_1 = 0.2$ and $H_2 = 0.8$.

Figure 5.4 shows a plot of the graph of $\gamma_v(p)$ for $p \in [-1,1]^2 \subset \mathbb{R}^2$.

By construction, function γ_v is positive for all points inside its *support*, *supp*(γ_v), which is the p-domain Ω_v. Note that γ_v attains its maximum, which is equal to 1, at $p = (0,0)$ and in the neighborhood of p given

[1] Peer Stelldinger provided us with function $\xi(t)$.

by $\{q \in \Omega_v \mid \|p - q\| < H_1\}$. Moreover, function γ_v decreases as p moves towards the boundary of Ω_v and vanishes outside Ω_v. This is because $\|p - q\| \geq H_2$, for every point $q \in \mathbb{R}^2$ on the boundary of Ω_v or outside it. So, γ_v is non-negative and its support, $supp(\gamma_v) = \Omega_v$, is compact. Finally, function γ_v is C^∞, as ξ is C^∞.

For the sake of simplicity and numerical robustness, it may be better to define $\gamma_v(p)$ using a different function ξ. For instance, we can replace the function ξ in Definition 5.3.1 with a polynomial function, such as $h(t) = (1 - t^{\alpha_1})^{\alpha_2}$, where α_1 and α_2 are positive integers, or even a C^k Hermite spline curve [71], for some large, positive integer k. Both a polynomial function and a C^k Hermite spline function yield a simpler weight function, $\gamma_v(p)$, whose derivatives of any order and order up to k, respectively, can be computed in a more efficient and robust way than the derivatives of the exponential function in Definition 5.3.1.

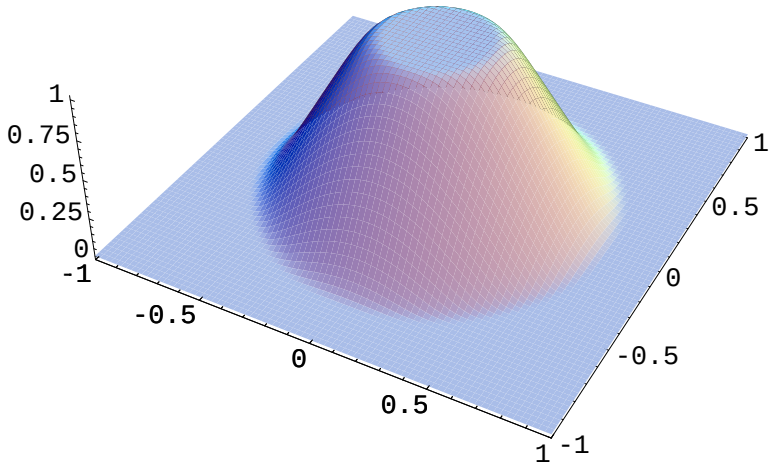

Figure 5.4: Plot of $\gamma_v(p)$, for every $p \in [-1, 1]^2 \subset \mathbb{R}^2$, with $H_1 = 0.2$ and $H_2 = 0.8$.

5.4 Parametrizations

Once we have computed ψ_v and γ_v, for each $v \in I$, we can define all parametrizations in $(\theta_v)_{v\in I}$, as described in Section 5.1. It remains to show that the pair $\mathcal{M} = (\mathcal{G}, (\theta_v)_{v\in I})$ is indeed a parametric C^k pseudo-surface. To do so, we first rewrite the expressions for the parametrization in $(\theta_v)_{v\in I}$ in order to simplify the exposition of our proof. More specifically, we define each θ_v in terms of the following two functions:

Definition 5.4.1. Let Ω_u and Ω_w be any two p-domains of $(\Omega_v)_{v\in I}$. Then, we define the functions

$$\Gamma_{wu} : \mathbb{R}^2 \to \mathbb{R} \qquad \text{and} \qquad \Psi_{wu} : \mathbb{R}^2 \to \mathbb{R}^3$$

such that

$$\Gamma_{wu}(p) = \begin{cases} \gamma_w \circ \varphi_{wu}(p) & \text{if } p \in \Omega_{uw} \\ \\ 0 & \text{otherwise} \end{cases}$$

and

$$\Psi_{wu}(p) = \begin{cases} \psi_w \circ \varphi_{wu}(p) & \text{if } p \in \Omega_{uw} \\ \\ (0,0,0) & \text{otherwise}\,, \end{cases}$$

for every point $p \in \mathbb{R}^2$.

Note that the value of the function Γ_{wu} (resp. Ψ_{wu}) at $p \in \Omega_{wu}$ is equal to the value of γ_w (resp. ψ_w) at $q \in \Omega_w$, where $q = \varphi_{wu}(p)$, i.e., q is the point p with respect to the local coordinate system of Ω_w. Note also that the function Ψ_{wu} (resp. Γ_{wu}) is not necessarily continuous in $\mathbb{R}^2$, but its restriction to Ω_{uw} is a C^∞ (resp. C^k, including $k = \infty$) function whenever $\Omega_{uw} \neq \emptyset$. This claim follows immediately from the fact that the transition functions are C^∞ and the weight functions are C^k (including $k = \infty$) (see Definition 5.3.2).

Definition 5.4.2. Let Ω_v be any p-domain of $(\Omega_v)_{(\sigma,v)\in I}$. Then, for every point $p \in \Omega_v$, we define the *parametrization associated with* Ω_v,

$$\theta_v : \Omega_v \to \mathbb{R}^3\,,$$

as the convex combination given by the expression

$$\theta_v(p) = \frac{\sum_{u \in I} (\Gamma_{uv}(p) \cdot \Psi_{uv}(p))}{\sum_{u \in I} \Gamma_{uv}(p)} .$$

From the construction of $\mathcal{G}$ in Chapter 4, we know that at most two p-domains can "overlap" with Ω_v at any given point $p \in \Omega_v$. So, both sums in the expression defining $\theta_v(p)$ in Definition 5.4.2 has at most three terms, one of which is $\Gamma_{vv}(p) \cdot \Psi_{vv}(p)$ (resp. $\Gamma_{uv}(p)$). This also means that both sums must have at least one term. In what follows, we show that $\mathcal{M} = (\mathcal{G}, (\theta_{(\sigma,v)})_{(\sigma,v)\in I})$ is indeed a parametric pseudo-surface:

Theorem 5.4.1. Given any simplicial surface, $\mathcal{K}$, in $\mathbb{R}^3$, let

$$\mathcal{G} = ((\Omega_v)_{v\in I}, (\Omega_{uw})_{(u,w)\in I\times I}, (\varphi_{uw})_{(u,w)\in K})$$

be a set of gluing data for $\mathcal{K}$ and let $(\theta_v)_{v\in I}$ be the family of parametrizations associated with the p-domains of $\mathcal{G}$. Then, the pair,

$$\mathcal{M} = (\mathcal{G}, (\theta_v)_{v\in I}) ,$$

is a parametric C^k (including $k = \infty$) pseudo-surface in $\mathbb{R}^3$.

Proof. We already know that (1) the function Ψ_{vu} is C^∞, and (2) the function Γ_{vu} is C^k (including $k = \infty$). So, it remains to show that θ_v satisfies condition (C) of Definition 3.5.1, namely: for all $(u, w) \in I \times I$, we have that $\theta_u(q) = \theta_w \circ \varphi_{wu}(q)$, for every $q \in \Omega_{uw}$. So, let Ω_u and Ω_w be any two distinct p-domains such that $\Omega_{uw} \neq \emptyset$ (resp. $\Omega_{wu} \neq \emptyset$). Let p be any point of Ω_{uw}. Since $\Omega_{uw} \neq \emptyset$, the transition function, φ_{wu}, is well-defined. Similarly, since $\Omega_{wu} \neq \emptyset$, the function φ_{uw} is also well-defined. Then, from Definition 5.4.1, we have

$$\begin{aligned}
\Gamma_{uu}(p) &= \gamma_u(\varphi_{uu}(p)) \\
&= \gamma_u(p) \\
&= \gamma_u(\varphi_{uw}(\varphi_{wu}(p))) \\
&= \Gamma_{uw}(\varphi_{wu}(p)) ,
\end{aligned}$$

$$\begin{aligned}
\Psi_{uu}(p) &= \psi_u(\varphi_{uu}(p)) \\
&= \psi_u(p) \\
&= \psi_u(\varphi_{uw}(\varphi_{wu}(p))) \\
&= \Psi_{uw}(\varphi_{wu}(p)) ,
\end{aligned}$$

$$\begin{aligned}\Gamma_{wu}(p) &= \gamma_w(\varphi_{wu}(p)) \\ &= \gamma_w(\varphi_{ww}(\varphi_{wu}(p))) \\ &= \Gamma_{ww}(\varphi_{wu}(p))\,,\end{aligned}$$

and

$$\begin{aligned}\Psi_{wu}(p) &= \psi_w(\varphi_{wu}(p)) \\ &= \psi_w(\varphi_{ww}(\varphi_{wu}(p))) \\ &= \Psi_{ww}(\varphi_{wu}(p))\,,\end{aligned}$$

where we used the facts that $\varphi_{wu} = \varphi_{uw}^{-1}$ (see Proposition 4.2.3) and that $\varphi_{uu} = \mathrm{id}_{\Omega_u}$ (see Definition 3.3.2). Now, let Ω_z be another p-domain such that $\Omega_{uz} \neq \emptyset$, for some $z \in I$, with $z \neq u$ and $z \neq w$. Further, suppose that $p \in \Omega_{uz}$. Since $p \in \Omega_{uw}$, Lemma 4.2.1 tells us that $\Omega_{wz} \neq \emptyset$. So, the transition functions φ_{zu} and φ_{zw} are well-defined. Then, from Definition 5.4.1, we also have that

$$\Gamma_{zu}(p) = \gamma_z(\varphi_{zu}(p)) = \gamma_z(\varphi_{zw}(\varphi_{wu}(p))) = \Gamma_{zw}(\varphi_{wu}(p))$$

and

$$\Psi_{zu}(p) = \psi_z(\varphi_{zu}(p)) = \psi_z(\varphi_{zw}(\varphi_{wu}(p))) = \Psi_{zw}(\varphi_{wu}(p))\,,$$

where we used the fact that

$$\varphi_{zw}(q) = \varphi_{zu}(\varphi_{uw}(q))\,,$$

for all points $q \in \varphi_{wu}(\Omega_{uw} \cap \Omega_{uz})$ (cocycle condition, Lemma 4.2.2). In particular, by letting $q = \varphi_{wu}(p)$, we get

$$\varphi_{zw}(\varphi_{wu}(p)) = \varphi_{zu}(\varphi_{uw}(\varphi_{wu}(p))) = \varphi_{zu}(\varphi_{uu}(p)) = \varphi_{zu}(p)\,.$$

From the above discussion, we get

$$\begin{aligned}
\theta_v(r) &= \frac{\sum_{u\in I}\Gamma_{uv}(r)\cdot\Psi_{uv}(r)}{\sum_{u\in I}\Gamma_{uv}(r)} \\
&= \frac{\sum_{u\in J}\Gamma_{uv}(r)\cdot\Psi_{uv}(r)}{\sum_{u\in I}\Gamma_{uv}(r)} \\
&+ \frac{\Gamma_{wv}(r)\cdot\Psi_{wv}(r)+\Gamma_{vv}(r)\cdot\Psi_{vv}(r)}{\sum_{u\in I}\Gamma_{uv}(r)} \\
&= \frac{\sum_{u\in J}\Gamma_{uw}(\varphi_{wv}(r))\cdot\Psi_{uw}(\varphi_{wv}(r))}{\sum_{u\in I}\Gamma_{wu}(\varphi_{uv}(r))} \\
&+ \frac{\Gamma_{ww}(\varphi_{wv}(r))\cdot\Psi_{ww}(\varphi_{wv}(r))}{\sum_{u\in I}\Gamma_{uw}(\varphi_{uv}(r))} \\
&+ \frac{\Gamma_{vw}(\varphi_{wv}(r))\cdot\Psi_{vw}(\varphi_{wv}(r))}{\sum_{u\in I}\Gamma_{uw}(\varphi_{uv}(r))} \\
&= \theta_w(\varphi_{wv}(r))\,,
\end{aligned}$$

where $J, H \subseteq I$, with $J = I - \{w, v\}$. So, for every $p \in \Omega_{vw}$, we have $\theta_v(r) = \theta_w \circ \varphi_{wv}(r)$. □

Recall from Section 3.5 that condition (C) of Definition 3.5.1 implies that

$$\theta_v(\Omega_{vw}) = \theta_w(\Omega_{wv})\,,$$

for all $v, w \in I$. This means that θ_v and θ_w are consistent parametrizations of the overlap, $\theta_v(\Omega_{vw}) = \theta_w(\Omega_{wv})$. Thus, the image, $M = \bigcup_{v\in I}\theta_v(\Omega_v)$, of $\mathcal{M}$ is covered by the pieces, $U_v = \theta_v(\Omega_v)$, such that each U_v is parametrized by θ_v and the overlapping pieces, $U_v \cap U_w$, are parametrized consistently. The local structure of M is given by the θ_v's and the global structure is given by the gluing data.

The image, $M = \bigcup_{v\in I}\theta_v(\Omega_v)$, of $\mathcal{M}$ is our approximation for the given simplicial complex, $\mathcal{K}$. Recall from Section 3.5 that M is guaranteed to be a surface in $\mathbb{R}^3$ if the θ_v's are bijective and conditions (C′) and (C″) hold:

(C′) For all $(u, w) \in K$,

$$\theta_u(\Omega_u) \cap \theta_w(\Omega_w) = \theta_u(\Omega_{uw}) \cap \theta_w(\Omega_{wu}) \,.$$

(C″) For all $(u, w) \notin K$,

$$\theta_u(\Omega_u) \cap \theta_w(\Omega_w) = \emptyset \,.$$

Informally, conditions (C′) and (C″) prevents self-intersections of surface patches and singularities caused by intersections among distinct surface patches. Unfortunately, the strategy we chose for defining the control points of the shape functions does not ensure that the θ_v's are bijective nor conditions (C′) and (C″). So, we cannot guarantee that the set M is a surface (i.e., a 2-manifold). However, if the θ_v's are bijective and conditions (C′) and (C″) happen to be true, then we can easily define a homeomorphism from $|\mathcal{K}|$ to M.

Chapter 6

Implementation and Experimental Results

This chapter describes the main algorithms and data structures in a C++ class library that implement our construction for building parametric pseudo-surfaces. It also presents some surfaces generated by this library. The chapter ends with a discussion about the displayed surfaces and other practical aspects of our construction.

6.1 Implementation Details

We implemented a C++ class library, called `PPS`, that provides the user with a class, called `tPPS`, that implements our construction to build parametric C^k pseudo-surfaces, as described in chapters 4 and 5. Currently, the class `tPPS` has a single argument constructor, `tPPS::tPPS()`, that takes in a simplicial surface, $\mathcal{K}$. The constructor `tPPS::tPPS()` builds the family of parametrizations, $(\theta_v)_{v\in I}$, from the given input $\mathcal{K}$.

The class `tPPS` also offers the user a method, called `tPPS::eval()`, that computes a point on the surface

$$M = \bigcup_{v\in I} \theta_v(\Omega_v)\,,$$

which is the image in $\mathbb{R}^3$ of the parametric C^k pseudo-surface, $\mathcal{M} = (\mathcal{G}, (\theta_v)_v)$. The input parameters of the method `tPPS::eval()` are a triangle, $\sigma = [u, v, w]$, of the simplicial surface, $\mathcal{K}$, and three integers, λ,

μ, and ν, where $\lambda, \mu, \nu \geq 0$ and $\lambda + \mu + \nu = 1$, which are the barycentric coordinates of p with respect to the vertices of σ. Next, the method finds a point, say q, in either Ω_u, Ω_v, or Ω_w. Finally, `tPPS::eval()` returns the point $\theta_i(q)$ in $\mathbb{R}^3$, where i is the index of the p-domain that contains the point q, i.e., i is one of u, v, and w.

At first glance, the method `tPPS::eval()` may seem a little awkward. However, it provides the user with a very natural way of sampling M. The reason is that `tPPS::eval()` provides the user with an "indirect" way of selecting a p-domain, Ω_v, and a point, q, from Ω_v. This indirect way is based only on $\mathcal{K}$, which means that the user does not have to be aware of the existence of p-domains, P-polygons, transition maps, and parametrizations. In addition, we will see that the point q is uniquely determined by the choice of σ and the barycentric coordinates, (λ, μ, ν), of p *whenever the surfaces* $|\mathcal{K}|$ *and* M *are homeomorphic*. This means that each quadruple, $(\sigma, \lambda, \mu, \nu)$, corresponds to a unique point on M. Conversely, each point on M can be defined by a unique quadruple, $(\sigma, \lambda, \mu, \nu)$. So, `tPPS::eval()` allows us to sample M in a very simple way, which is quite similar to the way that traditional parametric and subdivision surfaces are sampled.

6.1.1 The Augmented DCEL

We represent $\mathcal{K}$ as an augmented version of the Doubly Connected Edge List (DCEL) data structure [72]. The DCEL has three basic elements, triangles, edges, and vertices, and it is built around the concept of the edge element in a slightly non-intuitive way. The reason is that every edge is not naturally represented by its two endpoints, but by two *half-edges*. The two half-edges of an edge are said to be "mates". If the endpoints of an edge are the vertices u and w, then u is the *origin vertex* of one half-edge and w is the origin vertex of the other. Conversely, vertex w is the *destination vertex* of the former half-edge, while vertex u is the destination vertex of the latter half-edge. This means that every half-edge has an orientation, and that orientation is opposite to the orientation of its mate. Furthermore, each half-edge belongs to only one triangle, and if a given half-edge belongs to a triangle, t, then its mate belongs to the other triangle that shares the edge (consisting of the two half-edges) with t. Figure 6.1 illustrates the relationships among the DCEL elements.

All half-edges belonging to a given triangle have the same orientation, which is the orientation of the

edges with respect to the triangle. Each half-edge has a pointer to its mate, to its origin vertex, and to the half-edge that has its destination vertex as origin vertex. In turn, each triangle has a pointer to only one of its half-edges, which is chosen arbitrarily. Likewise, each vertex has a pointer to one of the half-edges that has the vertex as origin vertex. This half-edge is also chosen arbitrarily. All these pointers allow us to derive the essential topological information of $\mathcal{K}$. By storing the position of a vertex in the corresponding vertex element of the DCEL, we also have the essential geometric information of $\mathcal{K}$. The DCEL also contains the element *surface*, which keeps a pointer to a list of triangles of $\mathcal{K}$ and another pointer to the list of all vertices of $\mathcal{K}$.

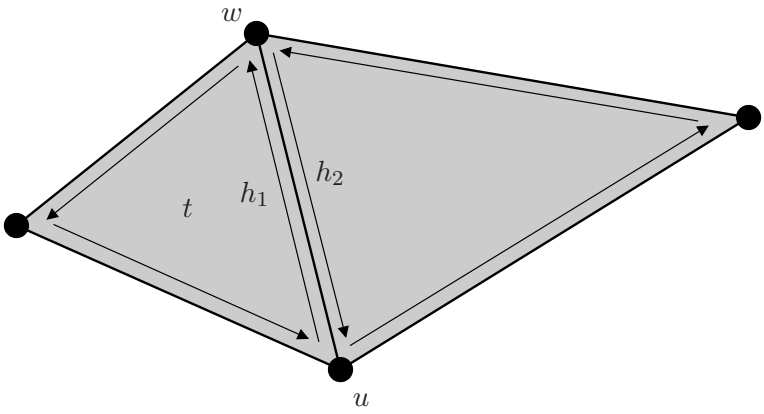

Figure 6.1: Half-edges h_1 and h_2 are mates. The origin vertex of h_1 (resp. h_2) is u (resp. w), and its destination vertex is w (resp. u). Half-edge h_1 belongs to triangle t, while h_2 belongs to the triangle that shares the edge consisting of h_1 and h_2 with t.

We augmented the DCEL to store information related to the parametric pseudo-surface. To that end, we added an *attribute* pointer to each of the DCEL element classes (i.e., vertex, half-edge, edge, face, or surface class). Each attribute pointer of a DCEL element class points to an object of an attribute class containing the parametric pseudo-surface data related to the element. By using these attribute pointers, we decouple the simplicial surface data from the parametric pseudo-surface data, and we can reuse the code of the DCEL classes for other applications as it is. In what follows, we describe the main elements of each attribute class of the augmented DCEL and present pieces of the C++ code corresponding to those elements:

- The vertex attribute class, `tVertexAttribute`, stores the degree of the DCEL vertex that owns

the attribute and a pointer to the Bézier patch associated with the vertex, as can be seen in the code below:

```
class tVertexAttribute {
    /**
     * Degree of  the origin  vertex of the  half-edge that  owns this
     * attribute.
     */
    unsigned m_d;

    /**
     * A pointer  to the rectangular Bezier patch  associated with the
     * vertex that owns this attribute.
     */
    bzPointer m_pat;
};
```

- The half-edge attribute class, `tHalfEdgeAttribute`, stores a unique identifier for the half-edge, say h, that owns the attribute. This identifier is a number from the range $\{0, \ldots, m_v\}$, where m_v is the degree of the origin vertex, v, of h. As we shall see later, this number is an explicit representation of the isomorphism $s_v : st(v, \mathcal{K})^{(0)} \rightarrow T_v^{(0)}$. The code for the `tHalfEdgeAttribute` class is given below:

```
class tHalfEdgeAttribute {
    /**
     * Id of the  half-edge with respect to the  set of halfedges that
     * share the origin vertex with this halfedge.
     */
    unsigned m_id;
};
```

- The face attribute class, `tFaceAttribute`, has a pointer to the parametric patch, $b_\sigma : \triangle \rightarrow \mathbb{R}^3$, associated with the triangle σ of $\mathcal{K}$ that owns the attribute, where $\triangle \subset \mathbb{R}^2$ is the affine frame on

which b_σ is defined. Recall from Chapter 5 that $S' = \bigcup_{\sigma \in \mathcal{K}} b_\sigma(\triangle)$ is the surface being approximated by M.

The augmented DCEL edge and surface elements have no associated attributes.

6.1.2 The Constructor `tPPS::tPPS()`

Given $\mathcal{K}$, the constructor `tPPS::tPPS()` carries out the following major steps:

(1) Create the DCEL data structure from $\mathcal{K}$.

(2) Add the half-edge attributes.

(3) Add the face attributes.

(4) Add the vertex attributes.

Step (1) consists of defining the isomorphism s_v, for each vertex v of $\mathcal{K}$. This is done by simply enumerating all half-edges whose origin vertex is v and assigning a unique integer from $\{0, \ldots, m_v - 1\}$ to each of them, where m_v is the degree of v. We can use a clockwise traversal of the edges incident to v to do the enumeration. The unique integer is stored in the attribute `m_id` of the `tHalfEdgeAttribute` class. Now, if we are given a vertex u in $st(v, \mathcal{K})$, the image of u under s_v is simply the identifier of the half-edge, h, with origin vertex v and destination vertex u. This simple labeling scheme enables us to implicitly represent the P-polygon, P_v, which means that we need not compute and store the vertices of P_v explicitly. Whenever we need the coordinates of $s_v(u)$, we recover the identifier of h, say i, and compute the coordinates of $s_v(u)$, i.e.,

$$s_v(u) = \left(\cos\left(\frac{2\pi \cdot i}{m_v}\right), \sin\left(\frac{2\pi \cdot i}{m_v}\right) \right),$$

as described in Chapter 4.

The face and vertex attributes are also easy to compute. However, the computation of the vertex attributes is the most time-consuming step of our construction. This is because the computation of the control points of the shape functions requires the solution of a linear system of $4 \cdot l^2$ equations on l^2

unknowns, where $l = \max\{m_v + 1, 7\}$ and m_v is the degree of the vertex that owns the attribute (see Chapter 6).

6.1.3 Transition Maps and Weight Functions

By definition, each transition function, φ_{wu}, of our construction is associated with a pair, (u, w), of vertices, u and w, of $\mathcal{K}$ such that $[u, w]$ is an edge of $\mathcal{K}$. If $u = w$ then φ_{wu} is simply the identity function. Otherwise, function φ_{wu} is defined as function $g_{(u,w)}$, which in turn is given by an expression that depends only on the degrees, m_u and m_w, of u and w, respectively, and on the identifiers of the half-edges with origin vertex u (resp. w) and destination vertex w (resp. u). These half-edges are mates of each other. So, we can naturally represent $g_{(u,w)}$ by a method of the `tHalfEdgeAttribute` class. In particular, whenever the method is invoked for a half-edge h, we recover the identifiers of h and its mate and the degrees of the origin vertices of both half-edges. Next, we apply the expression for $g_{(u,w)}$ using the recovered information.

The transition maps, $(\varphi_{wu})_{(u,w)\in K}$, are represented by a method of the `tPPS` class. This method is given two vertices, say u and w, and a point p in $\mathbb{R}^2$. If $u = w$ then the method returns p. Otherwise, it recovers the half-edge, h, with origin vertex u and destination vertex w and invokes the method representing $g_{(u,w)}$ for h. It is important to remark that p is expected to belong to Ω_{uw}. The method that computes φ_{wu} does not use any explicit information regarding Ω_{uw}. Instead, it computes the point $h \circ g_u(p)$, and then checks if $h \circ g_u \circ R_{(u,w)}(p)$ belongs to the canonical lens (see Chapter 4). This verification is trivial to implement, and we know that $p \in \Omega_{uw}$ if and only if $h \circ g_u \circ R_{(u,w)}(p)$ belongs to the canonical lens. So, we need not compute Ω_{uw}, which otherwise would involve more expensive calculations of planar region intersections.

The weight functions, $(\gamma_v)_{v\in I}$, are also represented by a method of the `tPPS` class. This is because the weight functions depend only on the radius, r_v, of the circle defined by the closure, $\overline{\Omega}_v$, of the associated p-domain, Ω_v. But, this radius is given in terms of the degree, m_v, of v only. In particular, we have that $r_v = \cos(\pi/m_v)$. So, given a vertex v and a point $p \in \mathbb{R}^2$, the method can recover m_v from the vertex attribute object associated with v and then use the expression defining γ_v to compute $\gamma_v(p)$ (see Definition 5.3.2).

It is worth reinforcing that the above implementation of our construction does not explicitly compute P-polygons and their associated triangulations. In addition, gluing domains are never (implicitly or explicitly) computed. So, although our construction may seem complicated, its implementation is actually fairly simple, and the space required to store the augmented DCEL is only slightly larger than the one for storing $\mathcal{K}$.

6.1.4 The Method `tPPS::eval()`

The method `tPPS::eval()` takes in a triangle σ of $\mathcal{K}$ and three integers, λ, μ, and ν, where $\lambda, \mu, \nu \geq 0$ and $\lambda + \mu + \nu = 1$, which are the barycentric coordinates of a point p of σ. As we pointed out in Section 6.1.1, the class representing the triangles of $\mathcal{K}$ in the augmented DCEL contains a pointer to one of its three half-edges. The choice of this half-edge is completely arbitrary, and the chosen half-edge is said to be the *first* half-edge of the triangle. This arbitrary choice is made by the method `tPPS::tPPS()` during the step (1) of the DCEL construction process (see Section 6.1.2). If `he` is a pointer to the first halfedge of a triangle, then `he->m_next` and `he->m_prev` are pointers to the *second* and *third* half-edges of the same triangle.

The ordering of the half-edges of a triangle imposes an ordering on its the vertices: we say that v_i is the i-th vertex of a triangle if v_i is the origin vertex of its i-th half-edge, for each $i = 1, 2, 3$. Using this vertex ordering, we can compute a point, p, in the triangle by viewing λ, μ, ν as the barycentric coordinates of p with respect to the triangle vertices v_1, v_2, and v_3, respectively. The method `tPPS::eval()` makes use of the half-edge ordering of the given triangle σ to compute a point q in either Ω_{v_1}, Ω_{v_2}, or Ω_{v_3}. Once q is computed, the method computes $\theta_j(q)$, where $j \in \{v_1, v_2, v_3\}$ is the index of the gluing domain containing q.

The choice of the p-domain, Ω_j, containing q is a crucial point of `tPPS::eval()`. To make our description simpler, let us rename the vertices v_1, v_2, and v_3 of σ u, w, and x, respectively. The method `tPPS::eval()` maps p to a point, q', in the equilateral triangle, t, with vertices $a = (0, 0)$, $b = (\frac{1}{2}, -\frac{\sqrt{3}}{2})$, and $c = (1, 0)$, as shown in Figure 6.2. If λ, μ, and ν are the barycentric coordinates of p with respect to u, w, and x, then

$$q' = \lambda \cdot a + \mu \cdot b + \nu \cdot c\,.$$

The above barycentric mapping is a bijection from σ to t, which implies that q' is uniquely determined by λ, μ, and ν.

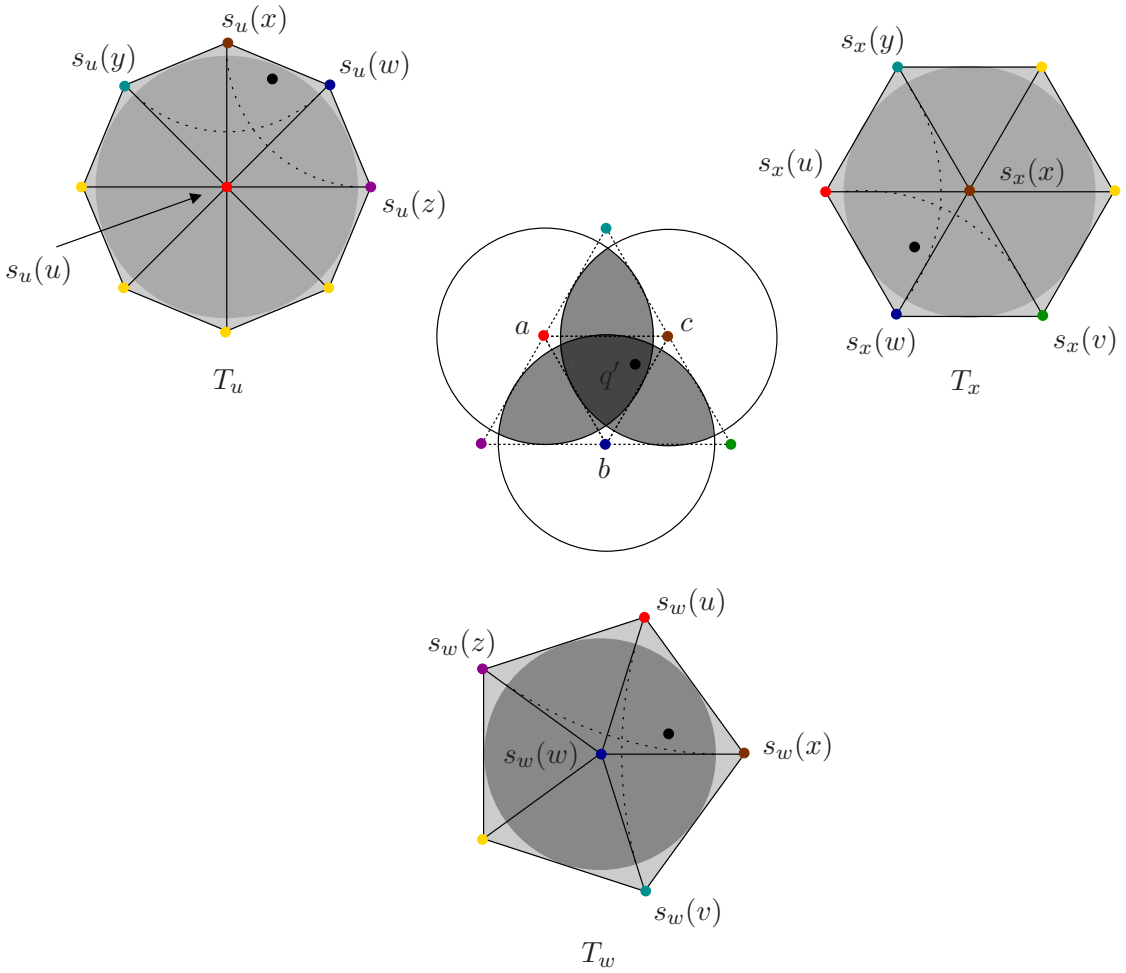

Figure 6.2: Illustration of the mapping carried out by `tPPS::eval()`.

Note that vertex a of t is the center of the circle C of radius $\cos(\pi/6)$, whose interior is the image of Ω_u by the map $g_u \circ R_{(u,x)}$. If point q' belongs to the interior, $int(C)$, of C, the method `tPPS::eval()` maps q' to the point $q = R^{-1}_{(u,x)} \circ g_u^{-1}(q')$ of Ω_u. Otherwise, the method `tPPS::eval()` maps q' to either Ω_x or Ω_w.

Suppose that q' does not belong to $int(C)$. Then, the method `tPPS::eval()` tries to map q' to Ω_x. Note that vertex c of t is the center of the circle D of radius $\cos(\pi/6)$, whose interior is the image of Ω_x by the map $h \circ g_x \circ R_{(x,u)}$. If point q' belongs to the interior, $int(D)$, of D, the method `tPPS::eval()` maps

q' to the point $q = R^{-1}_{(x,u)} \circ g_x^{-1} \circ h^{-1}(q')$ of Ω_x. Otherwise, the method `tPPS::eval()` maps point q' to Ω_w.

Suppose that q' does not belong to $int(C) \cup int(D)$. Then, point q' must belong to the interior, $int(E)$, of the circle E with radius $\cos(\pi/6)$ and centered at vertex b of t. This is because t is contained in $int(C) \cup int(D) \cup int(E)$. To map q' to Ω_w, the method `tPPS::eval()` uses the map $R^{-1}_{(w,u)} \circ g_w^{-1} \circ h^{-1} \circ M_{\frac{\pi}{3}}$, as $int(E)$ is the image of Ω_w by the map $M_{-\frac{\pi}{3}} \circ h \circ g_w \circ R_{(w,u)}$. So, the method `tPPS::eval()` lets $q = R^{-1}_{(w,u)} \circ g_w^{-1} \circ h^{-1} \circ M_{\frac{\pi}{3}}(q')$.

The above strategy used by `tPPS::eval()` to choose a p-domain is consistent. By that, we mean that if we have more than one choice of p-domain (e.g., if $q' \in (int(C) \cap int(D))$), then any valid choice maps q' to corresponding points (in distinct domains) with respect to the gluing process. Indeed, consider the following cases:

(1) $q' \in (int(C) \cap int(D))$

(2) $q' \in (int(C) \cap int(E))$

(3) $q' \in (int(D) \cap int(E))$

(4) $q' \in (int(C) \cap int(D) \cap int(E))$

In case (1), we can map q' to either Ω_u or Ω_x. The method `tPPS::eval()` picks the former p-domain, i.e., $q = R^{-1}_{(u,x)} \circ g_u^{-1}(q')$. We want to show that $\varphi_{xu}(q)$ is the same point as $R^{-1}_{(x,u)} \circ g_x^{-1} \circ h^{-1}(q')$, which is the point resulting from choosing to map q' to Ω_x. Indeed, from Definition 3.3.2, we know that $\varphi_{xu}(q)$ is given as

$$R^{-1}_{(x,u)} \circ g_x^{-1} \circ h \circ g_u \circ R_{(u,x)}(q)\,.$$

Since $q = R^{-1}_{(u,x)} \circ g_u^{-1}(q')$, we get

$$\begin{aligned}
\varphi_{xu}(q) &= R^{-1}_{(x,u)} \circ g_x^{-1} \circ h \circ g_u \circ R_{(u,x)}(q) \\
&= R^{-1}_{(x,u)} \circ g_x^{-1} \circ h \circ g_u \circ R_{(u,x)} \circ R^{-1}_{(u,x)} \circ g_u^{-1}(q') \\
&= R^{-1}_{(x,u)} \circ g_x^{-1} \circ h(q') \\
&= R^{-1}_{(x,u)} \circ g_x^{-1} \circ h^{-1}(q')\,.
\end{aligned}$$

In case (2), we can map q' to either Ω_u or Ω_w. The method `tPPS::eval()` picks the former p-domain, i.e., $q = R^{-1}_{(u,x)} \circ g_u^{-1}(q')$. We want to show that $\varphi_{wu}(q)$ is the same point as $q = R^{-1}_{(w,u)} \circ g_w^{-1} \circ h^{-1} \circ M_{\frac{\pi}{3}}(q')$, which is the point resulting from choosing to map q' to Ω_w. Indeed,

$$\begin{aligned}
\varphi_{wu}(q) &= R^{-1}_{(w,u)} \circ g_w^{-1} \circ h \circ g_u \circ R_{(u,w)}(q) \\
&= R^{-1}_{(w,u)} \circ g_w^{-1} \circ h \circ g_u \circ R_{(u,w)} \circ R^{-1}_{(u,x)} \circ g_u^{-1}(q') \\
&= R^{-1}_{(w,u)} \circ g_w^{-1} \circ h \circ g_u \circ M_{\frac{\pi}{3}} \circ g_u^{-1}(q') \\
&= R^{-1}_{(w,u)} \circ g_w^{-1} \circ h \circ M_{\frac{\pi}{3}}(q') \\
&= R^{-1}_{(w,u)} \circ g_w^{-1} \circ h^{-1} \circ M_{\frac{\pi}{3}}(q') \,.
\end{aligned}$$

In case (3), we can map q' to either Ω_x or Ω_w. The method `tPPS::eval()` picks the former p-domain, i.e., $q = R^{-1}_{(x,u)} \circ g_x^{-1} \circ h^{-1}(q')$. We want to show that $\varphi_{wx}(q)$ is the same point as $q = R^{-1}_{(w,u)} \circ g_w^{-1} \circ h^{-1} \circ M_{\frac{\pi}{3}}(q')$, which is the point resulting from choosing to map q' to Ω_w. Indeed,

$$\begin{aligned}
\varphi_{wx}(q) &= R^{-1}_{(w,x)} \circ g_w^{-1} \circ h \circ g_x \circ R_{(x,w)}(q) \\
&= R^{-1}_{(w,u)} \circ g_w^{-1} \circ M_{-\frac{\pi}{3}} \circ h \circ g_x \circ R_{(x,w)}(q) \\
&= R^{-1}_{(w,u)} \circ g_w^{-1} \circ M_{-\frac{\pi}{3}} \circ h \circ g_x \circ R_{(x,w)} \circ R^{-1}_{(x,u)} \circ g_x^{-1} \circ h^{-1}(q') \\
&= R^{-1}_{(w,u)} \circ g_w^{-1} \circ M_{-\frac{\pi}{3}} \circ h \circ g_x \circ R_{(x,w)} \circ R^{-1}_{(x,w)} \circ g_x^{-1} \circ M_{-\frac{\pi}{3}} \circ h^{-1}(q') \\
&= R^{-1}_{(w,u)} \circ g_w^{-1} \circ M_{-\frac{\pi}{3}} \circ h \circ M_{-\frac{\pi}{3}} \circ h^{-1}(q') \\
&= R^{-1}_{(w,u)} \circ g_w^{-1} \circ h \circ M_{-\frac{\pi}{3}}(q') \,,
\end{aligned}$$

where we used Proposition 4.2.4 to conclude that

$$R^{-1}_{(w,x)} \circ g_w^{-1} = R^{-1}_{(w,u)} \circ g_w^{-1} \circ M_{-\frac{\pi}{3}}$$

and

$$R^{-1}_{(x,u)} \circ g_x^{-1} = R^{-1}_{(x,w)} \circ g_x^{-1} \circ M_{-\frac{\pi}{3}} \,,$$

and the facts that

$$h = h^{-1} \qquad \text{and} \qquad h = M_{-\frac{\pi}{3}} \circ h \circ M_{-\frac{\pi}{3}} \circ h \circ M_{-\frac{\pi}{3}}$$

to conclude that

$$h \circ M_{\frac{\pi}{3}} = M_{-\frac{\pi}{3}} \circ h \circ M_{-\frac{\pi}{3}} \circ h^{-1} \,.$$

Finally, case (4) follows from cases (1), (2), and (3).

6.2 Results

The input to our implementation consists of $\mathcal{K}$ and the surface, S', to be approximated. In our experiments, we defined the surface S' either as a PN triangle surface [73] or as a Loop subdivision surface [22]. In the latter case, we replaced the function b_σ with the algorithm for exact evaluation of Loop subdivision surfaces at any parameter point of its base mesh, $\mathcal{K}$ (see [74]). We ran our implementation on the mesh models shown in Table 6.1. For each mesh, we generated two PPSs, one of which approximates a PN triangle surface defined from the mesh, while the other one approximates a Loop subdivision surface also defined from the same mesh.

Table 6.2 shows the CPU time for the construction of each PPS, which is highly dominated by the least squares procedure that computes the control points of the shape functions. This procedure is executed n_v times, where n_v is the number of vertices of the input mesh model. Each execution solves a system of about $4 \cdot (m_u + 1)^2$ linear equations using LU decomposition and substitution, where m_u is the valence of the vertex associated with the shape function. Later, we used the method `tPPS::eval()` to sample the PPSs in a triangle midpoint subdivision manner. We also sampled the corresponding PN triangles and subdivision surfaces.

Model ID	n_v	n_e	n_f	n_h	n_C
1	172	512	344	1	1
2	50	144	96	0	1
3	3,674	11,016	7,344	0	1
4	60,880	183,636	122,424	173	7

Table 6.1: Mesh model identifier (first column) and the number of vertices (second column), edges (third column), faces (fourth column), holes (fifth column), and connected components (sixth column) of the mesh.

Figure 6.3 shows the mesh models in Table 6.1. Figures 6.4-6.7 show Gaussian curvature plots for the PN triangle, Loop subdivision, and PPSs in Table 6.2. These plots demonstrate two important features of our surfaces. Firstly, they show that the image of our PPSs "mimics" closely the shape of the PN triangle or Loop subdivision surface being approximated, which are somewhat different from each other. Secondly, they also show the smoothing effect of the PPSs around the vertices and edges of the PN triangles surfaces

and around the so-called extraordinary vertices of the Loop's scheme (i.e., mesh vertices not incident to six edges). In general, PN triangles surfaces are only C^0-continuous around mesh vertices and edges, while Loop subdivision surfaces are C^2 everywhere, except around extraordinary vertices where they are only C^1.

Model ID	Approximated surface	CPU time (ms)
1	PN triangle	540
1	Loop	577
2	PN triangle	1,971
2	Loop	2,112
3	PN triangle	41,160
3	Loop	44,274
4	PN triangle	679,588
4	Loop	735,221

Table 6.2: CPU time in milliseconds for the construction of the PPS surfaces from the models in the first column and the approximated surfaces in the second column. The timing was measured on a Dell Precision 670 with Duo Pentium Xeon 3.2 GHz processors (single-core), 3Gb RAM, and running Fedora core 9.

The model meshes are mostly regular, i.e., the degree of most vertices is six. This is not a requirement for generating a PPS using our construction, but it yields surfaces with better visual quality. This is because transition maps involving vertices with low (i.e., 3 or 4) or high degree (i.e., > 8) cause too much distortion. Furthermore, meshes with vertices of high degree are likely to contain badly-shaped triangles. Since `tPPS::eval()` maps points from those triangles to regular shaped triangles of the P-polygons, distortions are also inevitable.

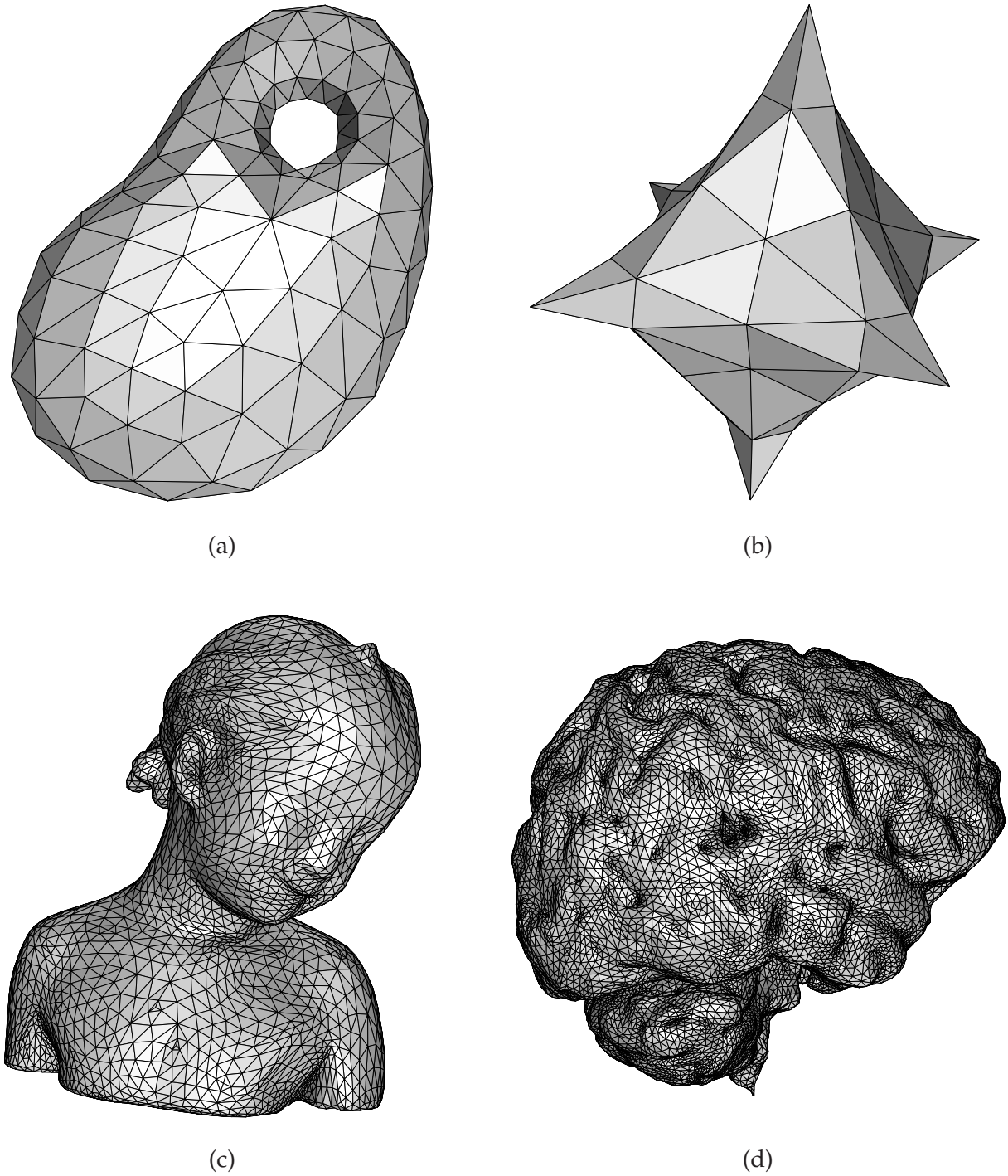

(a) (b)

(c) (d)

Figure 6.3: Mesh models (a) 1, (b) 2, (c) 3, and (d) 4 from Table 6.1.

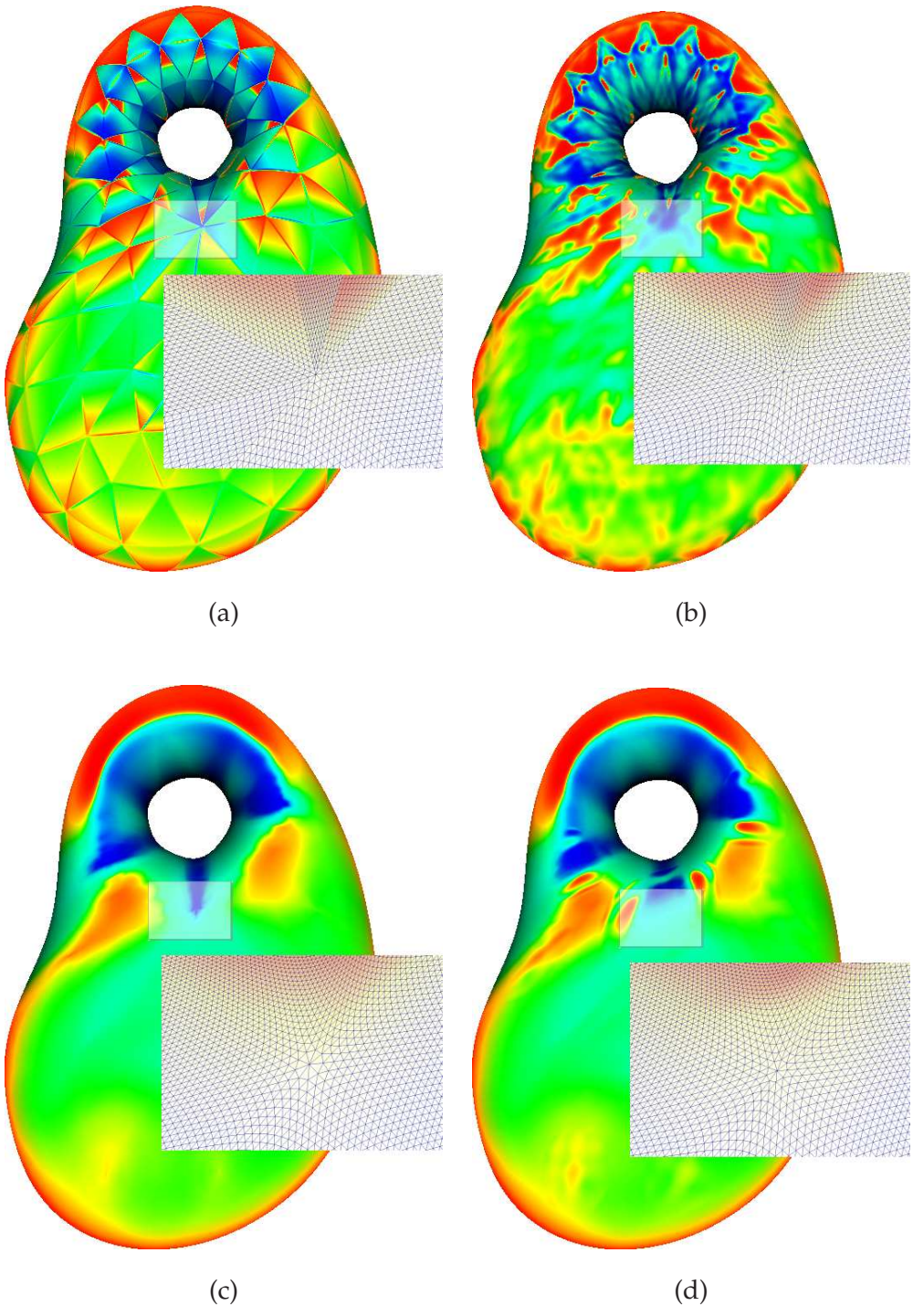

(a) (b)

(c) (d)

Figure 6.4: Curvature plots for the surfaces generated from mesh model 1: (a) PN triangle; (b) PPS from the surface in (a); (c) Loop; and (d) PPS from the surface in (c).

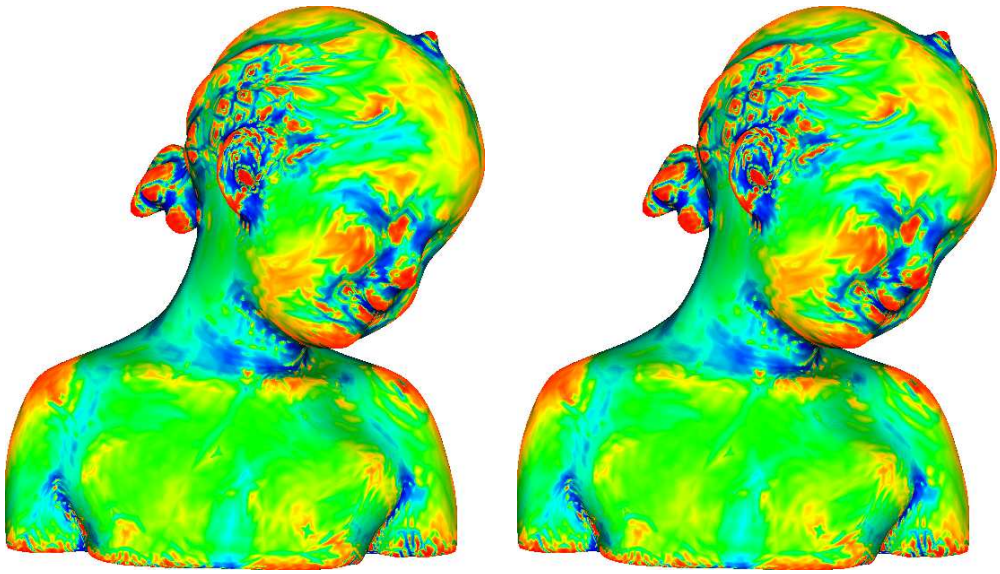

(a) (b)

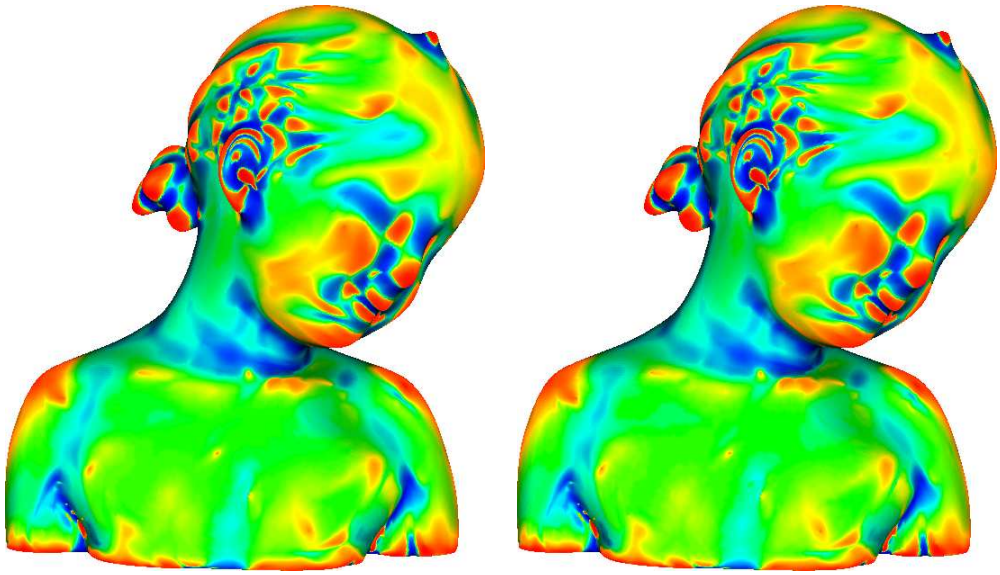

(c) (d)

Figure 6.5: Curvature plots for the surfaces generated from mesh model 3: (a) PN triangle; (b) PPS from the surface in (a); (c) Loop; and (d) PPS from the surface in (c).

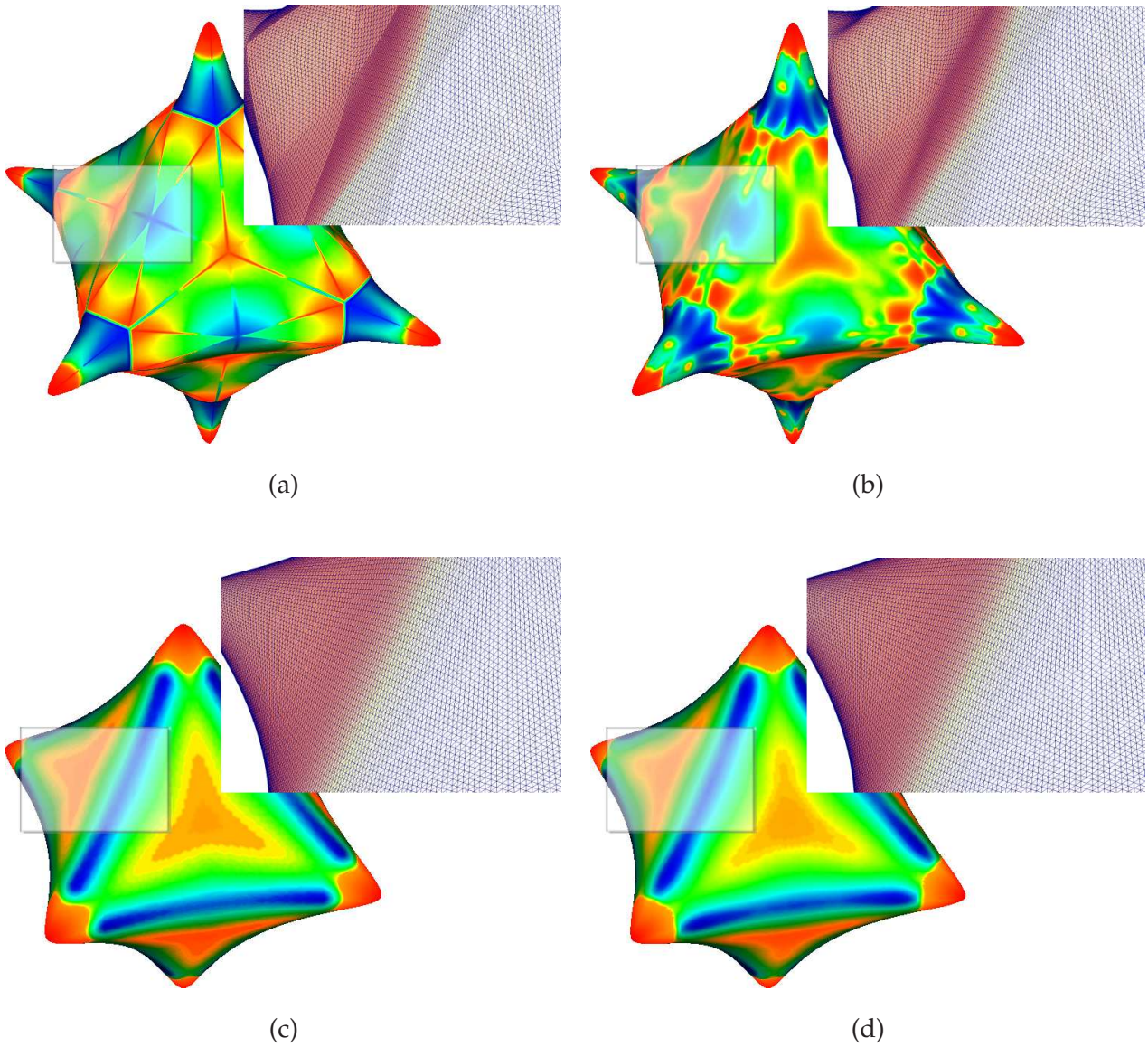

(a) (b)

(c) (d)

Figure 6.6: Curvature plots for the surfaces generated from mesh model 2: (a) PN triangle; (b) PPS from the surface in (a); (c) Loop; and (d) PPS from the surface in (c).

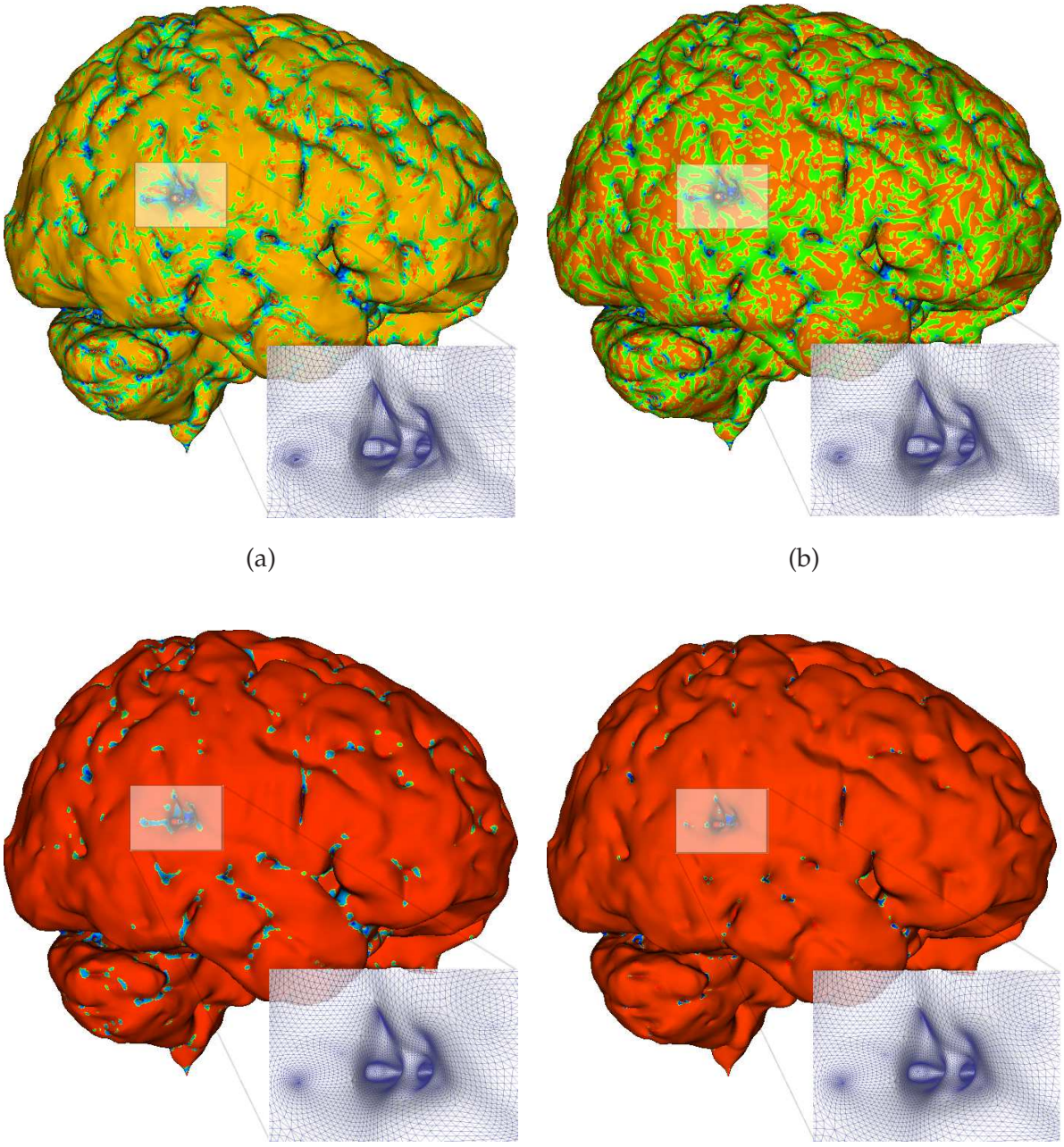

(a) (b)

(c) (d)

Figure 6.7: Curvature plots for the surfaces generated from mesh model 4: (a) PN triangle; (b) PPS from the surface in (a); (c) Loop; and (d) PPS from the surface in (c).

Chapter 7

Conclusion

We introduced a new manifold-based construction for fitting a smooth surface to a triangle mesh of arbitrary topology. Our construction combines in the same framework most of the best features of previous constructions, and thus it fills the gap left by other methods. In fact, the manifold structure produced by our construction is more compact and effective than the ones in [44, 45, 48], because it has only one type of p-domain and transition function, the gluing domains are larger, and the number of p-domains is smaller. Like the construction in [46], ours produces C^∞-continuous surfaces and is very flexible in ways of defining their geometry. However, different from the construction in [46], ours generates surfaces from triangle meshes, rather than quadrilateral meshes, and the surfaces are contained in the convex hull of all control points used to define their geometry.

Unlike the surfaces produced by the triangle-based constructions in [47, 66, 48], the ones produced by our construction are not given by purely (rational) polynomial functions. However, our surfaces are free of singular points, and thus they do not present the visual artifacts caused by the hole-filling techniques used by [47, 66] to deal with those points. Our manifold-based construction is also based on a solid theoretical framework, which is an improvement upon the one in [44, 63] and ensures the construction correctness. In addition, we provided experimental examples and concrete evidences of the effectiveness of our construction.

7.1 On-going and Future Work

There are three natural extensions of the work presented here, namely:

- surface construction from very large triangle meshes,
- parametric pseudo-manifolds with non-empty boundaries, and
- the incorporation of sharp features.

The construction of smooth surfaces from very large meshes (i.e., simplicial surfaces with hundreds of thousands or millions of triangles) has already been studied before (see [75, 76, 3, 6], to name a few). In particular, extensions of the manifold-based constructions in [47] and [44] to fit smooth surfaces to very large simplicial surfaces are described in [7] and [77], respectively. Here, the goal is to define surface patches that cover regions of the input surface containing many small triangles, as opposed to only one triangle or the star of a vertex. By doing so, it is possible to obtain a reasonably small smooth surface representation for the input surface. Currently, we are developing an extension of our manifold-based construction to deal with very large simplicial surfaces.

The extension of our construction to very large simplicial surface has the following three main steps:

(1) Let $\mathcal{K}$ be a very large simplicial surface. We apply the mesh simplification algorithm devised by Velho [78] to obtain another simplicial surface, $\mathcal{K}'$, with the same topology as $\mathcal{K}$ but a smaller number of triangles. Later, we apply a set of *stellar* operations to $\mathcal{K}'$ in order to give $\mathcal{K}'$ a semi-regular multiresolution structure [79]. The resulting simplicial surface, $\mathcal{K}''$, can be represented by a powerful data structure for the representation of geometric objects at multiple levels of details [80]. Moreover, the simplicial surface, $\mathcal{K}''$, can be locally coarsened or refined by further applying stellar operations supported by the data structure. The stellar operations do not change the topological type of $\mathcal{K}'$. So, we have $|\mathcal{K}'| \approx |\mathcal{K}''|$. In addition, the set of vertices of $\mathcal{K}'$ (resp. $\mathcal{K}''$) is a subset of the set of vertices of $\mathcal{K}$.

(2) We identify the vertices of $\mathcal{K}''$ with their counterparts in $\mathcal{K}$, and then embed the edges of $\mathcal{K}''$ in $\mathcal{K}$. Each embedding is a map from an edge of $\mathcal{K}''$ to a curve in the underlying space, $|\mathcal{K}|$, of $\mathcal{K}$. The

curve is defined by an algorithm for computing geodesics on simplicial surfaces given in [81]. The output of this step is a network of geodesic curves connecting each pair of vertices of $\mathcal{K}$ defining an edge in $\mathcal{K}''$. This network of curves and their endpoints induce a triangulation, T, on $|\mathcal{K}|$, whose "triangles" are curved, triangular-shaped regions of $|\mathcal{K}|$ called *macro patches*. The topology of T is the topology of $\mathcal{K}''$.

(3) We construct a C^∞-continuous surface from $\mathcal{K}$, $\mathcal{K}''$, and T using our manifold-based construction. Briefly, we assign a p-domain, a shape function, and a weight function with each vertex v of T. The control points of the shape functions are also determined by a fitting procedure. However, instead of using points on a given surface defined on $\mathcal{K}$ or $\mathcal{K}''$ (see Section 5.2), we choose the sample points to be the vertices of $\mathcal{K}$ inside the macro patches of T incident to v. If the error on approximating the sample points by a Bézier patch is equal to or larger than a fixed threshold, we locally refine $\mathcal{K}''$ using stellar operations, update T and the set of gluing data, and compute the shape functions again. This step is repeated until the approximation error is below the threshold. Note that the resulting surface is defined from the topology of $\mathcal{K}''$ (which is the same as the one of $\mathcal{K}$) and the geometry of $|\mathcal{K}|$.

The overall idea of the above solution is very similar to the one used in [6]. However, the strategies adopted in each step are significantly different and yield a simpler, faster, and more accurate surface approximation.

In several applications involving the surface fitting problem the input simplicial complex, $\mathcal{K}$, may not have an empty boundary. In this case, our manifold-based construction cannot be used *as it is* to define the smooth, approximating surface. In particular, there is no extension of our theoretical framework to define manifolds with boundaries from sets of gluing data. Nevertheless, by using an *implementation* strategy similar to the one devised by Tosun and Zorin [82], it is still possible to adapt our construction to build surfaces with boundary. However, we feel that a more natural solution should be preceded by the development of the aforementioned theoretical framework. So, we intend to develop such a framework instead of adapting our manifold-based construction to build surfaces with boundaries using the strategy described in [82].

Although the manifold-based approach is meant to be used to construct smooth surfaces, there are several 3D shapes whose boundary is a smooth surface everywhere, but along certain curves and corners known as *sharp features*. For modeling such boundaries, it would be appropriate to apply a manifold-based construction that is capable of generating C^k-continuous surfaces where $k = 0$ along sharp features and $k > 0$ or $k = \infty$ everywhere else. Sharp features can be extracted from the input simplicial surface, $\mathcal{K}$, using existing tools for feature detection on triangle meshes [83]. Next, we map the features from $\mathcal{K}$ to the p-domains. Finally, we define shape functions that are not smooth at points and lines of the p-domains corresponding to the features. Currently, we are investigating the details of the last two steps of this approach.

Bibliography

[1] Mario Botsch, Mark Pauly, Christian Rössl, Stephan Bischoff, and Leif Kobbelt. Geometric modeling based on triangle meshes. In *SIGGRAPH Course Notes*. ACM, 2006.

[2] Les Piegl and Wayne Tiller. *The NURBS book*. Springer-Verlag, second edition, 1997.

[3] Venkat Krishnamurthy and Marc Levoy. Fitting smooth surfaces to dense polygon meshes. In *Proceedings of the 23rd ACM Annual Conference on Computer Graphics and Interactive Techniques (SIGGRAPH '96)*, pages 313–324, New Orleans, Louisiana, USA, August 4-9 1996.

[4] Gary Yngve and Greg Turk. Robust creation of implicit surfaces from polygonal meshes. *IEEE Transactions on Visualization and Computer Graphics*, 8(4):346–359, 2002.

[5] Chen Shen, James F. O'Brien, and Jonathan R. Shewchuk. Interpolating and approximating implicit surfaces from polygon soup. In *Proceedings of the 28th ACM Annual Conference on Computer Graphics and Interactive Techniques (SIGGRAPH '01)*, pages 896–904, Los Angeles, California, USA, July 31 - August 4 2004.

[6] Alex Yvart, Stefanie Hahmann, and Georges-Pierre Bonneau. Smooth adaptive fitting of 3D models using hierarchical triangular splines. In *Proceedings of the International Conference on Shape Modeling and Applications 2005 (SMI'05)*, pages 13–22, Cambridge, Massachusetts, USA, June 13-17 2005.

[7] Ying He, Kexiang Wang, Hongyu Wang, Xianfeng Gu, and Hong Qin. Manifold T-spline. In Myung-Soo Kim and Kenji Shimada, editors, *Proceedings of the 4th International Conference on Geometric Modeling and Processing (GMP 2006)*, volume 4077 of *Lecture Notes in Computer Science*, pages 409–422, Pittsburgh, Pennsylvania, USA, July 26-28 2006. Springer.

[8] Byoung K. Choi, Bo H. Kim, and Robert B. Jerard. Sculptured surface NC machining. In Gerald Farin, Josef Hoschek, and Myung-Soo Kim, editors, *Handbook of Computer Aided Geometric Design*. Elsevier Science, 2002.

[9] Cindy M. Grimm, Joseph J. Crisco, and David H. Laidlaw. Fitting manifold surfaces to three-dimensional point clouds. *Journal of Biomechanical Engineering*, 124(1):136–140, 2002.

[10] Lexing Ying, George Biros, and Denis Zorin. A high-order 3D boundary integral equation solver for elliptic PDEs in smooth domains. *Journal of Computational Physics*, 219(1):247–275, 2006.

[11] Michael J. D. Powell and Malcolm A. Sabin. Piecewise quadratic approximations on triangles. *ACM Transactions on Mathemaitical Software*, 3(4):316–325, 1977.

[12] Robert E. Barnhill and Gerald Farin. C^1 quintic interpolation over triangles: two explicit representations. *International Journal for Numerical Methods in Engineering*, 17(12):1763–1778, 1981.

[13] Gerald Farin. A construction for visual C^1 continuity of polynomial surface patches. *Computer Graphics and Image Processing*, 20(7):272–282, 1982.

[14] Bruce Piper. Visually smooth interpolation with triangular bézier patches. In Gerald Farin, editor, *Geometric Modeling: Algorithm and New Trends*, pages 221–234. SIAM, 1987.

[15] Thomas Jensen. Assembling triangular and rectangular patches and multivariate splines. In Gerald Farin, editor, *Geometric Modeling: Algorithm and New Trends*, pages 203–222. SIAM, 1987.

[16] Gregory M. Nielson. A transfinite, visually continuous triangular interpolant. In Gerald Farin, editor, *Geometric Modeling: Algorithm and New Trends*, pages 235–246. SIAM, 1987.

[17] Leon A. Shirman and Carlo H. Séquin. Local surface interpolation with bézier patches. *Computer Aided Geometric Design*, 4(4):279–295, 1987.

[18] Hans Hagen and Helmut Pottmann. Curvature continuous triangular interpolants. In Tom Lyche and Larry L. Schumaker, editors, *Mathematical Methods in Computer Aided Geometric Design*, pages 373–384. Academic Press, 1989.

[19] Charles T. Loop and Tony DeRose. A multisided generalization of bézier surfaces. *ACM Transactions on Graphics*, 8(3):204–234, 1989.

[20] Jörg Peters. Local cubic and bicubic C^1 surface interpolation with linearly varying boundary normal. *Computer Aided Geometric Design*, 7(6):499–516, 1990.

[21] Gunther Greiner and Hans-Peter Seidel. Modeling with triangular B-splines. *IEEE Computer Graphics and Applications*, 14(2):56–60, 1994.

[22] Charles T. Loop. A G^1 triangular spline surface of arbitrary topological type. *Computer Aided Geometric Design*, 11(3):303–330, 1994.

[23] Desmond J. Walton and Dereck S. Meek. A triangular G^1 patch from boundary curves. *Computer-Aided Design*, 28(2):113–123, 1996.

[24] Ramon F. Sarraga. A variational method to model G^1 surfaces over triangular meshes of arbitrary topology in R^3. *ACM Transactions on Graphics*, 19(4):279–301, 2000.

[25] Stefanie Hahmann and Georges-Pierre Bonneau. Polynomial surfaces interpolating arbitrary triangulations. *IEEE Transactions on Visualization and Computer Graphics*, 9(1):99–109, 2003.

[26] Hartmut Prautzsch and Georg Umlauf. Parameterization of triangular g^k spline surfaces of low degree. *ACM Transaction on Graphics*, 25(4):1281–1293, 2006.

[27] Edwin Catmull and Jim Clark. Recursively generated B-spline surfaces on arbitrary topological surfaces. *Computer-Aided Design*, 10(6):350–355, 1978.

[28] Daniel Doo and Malcolm Sabin. Behaviour of recursive subdivision surfaces near extraordinary points. *Computer-Aided Design*, 10(6):356–360, 1978.

[29] Charles T. Loop. Smooth subdivision surfaces based on triangles. Master's thesis, Department of Mathematics, University of Utah, Salt Lake City, Utah, USA, 1987.

[30] Nira Dyn, David Levine, and John A. Gregory. A butterfly subdivision scheme for surface interpolation with tension control. *ACM Transactions on Graphics*, 9(2):160–169, 1990.

[31] Jörg Peters and Ulrich Reif. The simplest subdivision scheme for smoothing polyhedra. *ACM Transactions on Graphics*, 16(4):420–431, 1997.

[32] Leif Kobbelt. $\sqrt{3}$ subdivision. In *Proceedings of the 27th annual conference on Computer graphics and interactive techniques (SIGGRAPH '00)*, pages 103–112, New Orleans, Louisiana, USA, July 23-28 2000.

[33] Luiz Velho and Denis Zorin. 4-8 subdivision. *Computer Aided Geometric Design*, 18(5):397–427, 2001.

[34] Jos Stam. Exact evaluation of Catmull-Clark subdivision surfaces at arbitrary parameter values. In *Proceedings of the 25th annual conference on Computer graphics and interactive techniques (SIGGRAPH '98)*, pages 395–404, Orl ando, FL, USA, July 19-24 1998.

[35] Jörg Peters and Ulrich Reif. Shape characterization of subdivision surfaces – basic principles. *Computer Aided Geometric Design*, 21(6):585–599, 2004.

[36] Kestutis Karciauskas, Jörg Peters, and Ulrich Reif. Shape characterization of subdivision surfaces – case studies. *Computer Aided Geometric Design*, 21(6):601–614, 2004.

[37] Ulrich Reif. A degree estimate for subdivision surfaces of higher regularity. *Proceedings of the American Mathematical Society*, 124(7):2167–2174, 2006.

[38] Hartmut Prautzsch and Ulrich Reif. Degree estimates for C^kpiecewise polynomial subdivision surfaces. *Advances in Computational Mathematics*, 10(2):209–217, 2004.

[39] Christoph M. Hoffman. Implicit curves and surfaces in CAGD. *IEEE Computer Graphics and Applications*, 13(1):79–88, 1993.

[40] J. C. Carr, R. K. Beatson, J. B. Cherrie, T. J. Mitchell, W. R. Fright, and B. C. McCallum. Reconstruction and representation of 3D objects with radial basis functions. In *SIGGRAPH 01: Proceedings of the 28th ACM Annual Conference on Computer Graphics and Interactive Techniques*, pages 67–76, August 12-17 2001.

[41] Yutaka Ohtake, Alexander Belyaev, Marc Alexa, Greg Turk, and Hans-Peter Seidel. Multi-level partition of unity implicits. *ACM Transactions on Graphics*, 22(3):463–470, 2003.

[42] Michael Kazhdan, Matthew Bolitho, and Hugues Hoppe. Poisson surface reconstruction. In *Proceedings of the 4th Eurographics Symposium on Geometry Processing (SGP '06)*, pages 61–70, June 26 - 28 2006.

[43] Ravikrishna Kolluri. Provably good moving least squares. In *Proceedings of the 2005 ACM-SIAM Symposium on Discrete Algorithms*, pages 1008–1018, Vancouver, British Columbia, Canada, January 23-25 2005.

[44] Cindy M. Grimm and John F. Hughes. Modeling surfaces of arbitrary topology using manifolds. In *Proceedings of the 22nd ACM Annual Conference on Computer Graphics and Interactive Techniques (SIGGRAPH 95)*, pages 359–368, August 6-11 1995.

[45] Josep Cotrina Navau and Núria Pla-Garcia. Modeling surfaces from meshes of arbitrary topology. *Computer Aided Geometric Design*, 7(1):643–671, 2000.

[46] Lexing Ying and Denis Zorin. A simple manifold-based construction of surfaces of arbitrary smoothness. *ACM Transactions on Graphics*, 23(3):271–275, 2004.

[47] Xianfeng Gu, Ying He, and Hong Qin. Manifold splines. *Graphical Models*, 68(3):237–254, 2006.

[48] G. D. Vecchia, B. Jüttler, and M.-S. Kim. A construction of rational manifold surfaces of arbitrary topology and smoothness from triangular meshes. *Computer Aided Geometric Design*, 25(9):801–815, 2008.

[49] Cindy M. Grimm and Denis Zorin. Surface modeling and parameterization with manifolds. In *ACM SIGGRAPH 2006 Courses (SIGGRAPH '06)*, pages 1–81, New York, NY, USA, 2006. ACM Press.

[50] Greg Turk. Generating textures on arbitrary surfaces using reaction-diffusion. In *Proceedings of the 18th Annual Conference on Computer Graphics and Interactive Techniques (SIGGRAPH '91)*, pages 289–298, July 28 - August 2 1991.

[51] Greg Turk. Texture synthesis on surfaces. In *Proceedings of the 28th Annual Conference on Computer Graphics and Interactive Techniques (SIGGRAPH '01)*, pages 347–354, August 12-17 2001.

[52] Li-Yi Wei and Marc Levoy. Texture synthesis over arbitrary manifold surfaces. In *Proceedings of the 28th Annual Conference on Computer Graphics and Interactive Techniques (SIGGRAPH '01)*, pages 355–360, August 12-17 2001.

[53] Jos Stam. Flows on surfaces of arbitrary topology. *ACM Transactions on Graphics*, 22(3):724–731, 2003.

[54] Doug L. James and Dinesh K. Pai. ArtDefo: accurate real time deformable objects. In *Proceedings of the 26th Annual Conference on Computer Graphics and Interactive Techniques (SIGGRAPH '99)*, pages 65–72, August 8-13 1999.

[55] Dennis Barden and Charles Thomas. *An introduction to differential manifolds*. Imperial College Press, 2003.

[56] Marcel Berger and Bernard Gostiaux. *Differential geometry, manifolds, curves, and surfaces*, volume 115 of *GTM*. Springer-Verlag, 2006.

[57] John M. Lee. *Introduction to smooth manifolds*, volume 218 of *GTM*. Springer-Verlag, 2002.

[58] André Weil. *Foundations of algebraic topology*, volume XXIX of *Colloquium Publications*. AMS, second edition, 1946.

[59] Norman Steenrod. *The topology of fibre bundles*, volume 14 of *Princeton Mathematics Series*. Princeton University Press, 1956.

[60] Raoul Bott and Loring W. Tu. *Differential forms in algebraic topology*, volume 82 of *GTM*. Springer-Verlag, first edition, 1986.

[61] Shigeyuki Morita. *Geometry of differential forms*, volume 201 of *Translations of Mathematical Monographs*. AMS, first edition, 2001.

[62] R. O. Wells. *Differential analysis on complex manifolds*, volume 65 of *GTM*. Springer-Verlag, second edition, 1980.

[63] Cindy M. Grimm. *Modeling surfaces of Arbitrary topology using manifolds*. PhD thesis, Department of Computer Science, Brown University, Providence, RI, USA, 1996.

[64] John Milnor and James D. Stasheff. *Characteristic classes*, volume 76 of *Annals of Mathematics Studies*. Princeton University Press, 1974.

[65] Xianfeng Gu and Shing-Tung Yau. Global conformal surface parameterization. In *Proceedings of the 2003 Eurographics/ACM SIGGRAPH Symposium on Geometry Processing (SGP '03)*, pages 127–137, June 23-25 2003.

[66] Xianfeng Gu, Ying He, Miao Jin, Feng Luo, Hong Qin, and Shing-Tung Yau. Manifold splines with single extraordinary point. In *Proceedings of the 2007 ACM Symposium on Solid and Physical Modeling (SPM '07)*, pages 61–72, June, 4-6 2007.

[67] Ethan D. Bloch. *A first course in geometric topology and differential geometry*. Birkhäuser, 1997.

[68] Gerald Farin. *Curves and surfaces for CAGD: a practical guide*. Morgan-Kaufmann, fifth edition, 2002.

[69] Jean Gallier. *Geometric methods and applications: for computer science and engineering* . Springer-Verlag, 2000.

[70] David Kincaid and Ward Cheney. *Numerical analysis: mathematics of scientific computing*. The Brooks/Cole Series in Advanced Mathematics. Brooks/Cole, third edition, 2002.

[71] Richard H. Bartels, John C. Beatty, and Brian A. Barsky. *An introduction to splines for use in computer graphics and geometric modeling*. Morgan-Kaumann, 1987.

[72] M. de Berg, M. van Kreveld, M. Overmars, and O. Schwarzkopf. *Computational geometry: algorithms and applications*. Springer-Verlag, second edition, 2000.

[73] Alex Vlachos, Jörg Peters, Chas Boyd, and Jason L. Mitchell. Curved PN triangles. In *Proceedings of the ACM Symposium on Interactive 3D Graphics*, pages 159–166, Research Triangle Park, NC, USA, March 19-21 2001.

[74] Jos Stam. Evaluation of Loop subdivision surfaces. In *ACM SIGGRAPH 1999 Courses (SIGGRAPH '99)*, pages 1–15, New York, NY, USA, August 8-13 1999. ACM Press.

[75] David R. Forsey and Richards H. Bartels. Surface fitting with hierarchical splines. *ACM Transactions on Graphics*, 14(2):134–161, 1995.

[76] Matthias Eck and Hugues Hoppe. Automatic reconstruction of B-spline surfaces of arbitrary topological type. In *Proceedings of the 23rd ACM Annual Conference on Computer Graphics and Interactive Techniques (SIGGRAPH '96)*, pages 325–334, New Orleans, Louisiana, USA, August 4-9 1996.

[77] Cindy Grimm, Tao Ju, Ly Phan, and John Hughes. Adaptive smooth surface fitting with manifolds. *The Visual Computer*, 25(5-7):589–597, 2009.

[78] Luiz Velho. Mesh simplification using four-face clusters. In *Proceedings of the International Conference on Shape Modeling & Applications (SMI'01)*, pages 200–208, Genoa, Italy, May 7-11 2001.

[79] Luiz Velho. A dynamic adaptive mesh library based on stellar operators. *Journal of Graphics Tools*, 9(2):1–29, 2004.

[80] Luiz Velho and Jonas Gomes. Variable resolution 4-k meshes: concepts and applications. *Computer Graphics Forum*, 19(4):195–214, 2000.

[81] Dimas M. Morera, Luiz Velho, and Paulo C. Carvalho. Computing geodesics on triangular meshes. *Computer & Graphics*, 29(5):667–675, 2005.

[82] Elif Tosun and Denis Zorin. Manifold-based surfaces with boundary. *submitted to publication*, 2008.

[83] Ulrich Clarenz, Martin Rumpf, and Alexandru Telea. Robust feature detection and local classification for surfaces based on moment analysis. *IEEE Transactions on Visualization and Computer Graphics*, 10(5):516–524, 2004.

Appendix A

Proofs and Counterexamples

A.1 Proofs

Proposition 4.2.4. Let $[u, w, z]$ be any triangle of $\mathcal{K}$. If $s_u(z)$ precedes $s_u(w)$ in a counterclockwise traversal of the vertices of P_u, then

$$M_{-\pi/3} \circ g_u \circ R_{(u,w)}(\Omega_{uw}) = g_u \circ R_{(u,w)}(\Omega_{uz}) \quad \text{and} \quad M_{\pi/3} \circ g_u \circ R_{(u,z)}(\Omega_{uz}) = g_u \circ R_{(u,z)}(\Omega_{uw}) \,,$$

where $M_{-\frac{\pi}{3}}$ (resp. $M_{\frac{\pi}{3}}$) is a rotation by $-\frac{\pi}{3}$ (resp. $\frac{\pi}{3}$) around the origin. Furthermore,

$$\Omega_{uz} = M_{-\frac{2\pi}{m_u}}(\Omega_{uw}) \qquad \text{and} \qquad \Omega_{uw} = M_{\frac{2\pi}{m_u}}(\Omega_{uz}) \,,$$

where $M_{-\frac{2\pi}{m_u}}$ is a rotation by $-\frac{2\pi}{m_u}$ around the origin, and m_u is the degree of vertex u in $\mathcal{K}$.

Proof. From Definition 4.1.9, we have that

$$\Omega_{uw} = g_{(w,u)}(\Omega_w - \{(0,0)\}) \cap \Omega_u \quad \text{and} \quad \Omega_{uz} = g_{(z,u)}(\Omega_z - \{(0,0)\}) \cap \Omega_u \,.$$

From Proposition 4.1.2, we know that $(0,0) \notin g_{(w,u)}(\Omega_w - \{(0,0)\})$ and $(0,0) \notin g_{(z,u)}(\Omega_z - \{(0,0)\})$. So,

$$\Omega_{uw} = g_{(w,u)}(\Omega_w - \{(0,0)\}) \cap (\Omega_u - \{(0,0)\}) \quad \text{and} \quad \Omega_{uz} = g_{(z,u)}(\Omega_z - \{(0,0)\}) \cap (\Omega_u - \{(0,0)\}) \,.$$

Since $g_u \circ R_{(u,w)}$ and $g_u \circ R_{(u,z)}$ are bijective, we also have that

$$g_u \circ R_{(u,w)}(g_{(w,u)}(\Omega_w - \{(0,0)\}) \cap (\Omega_u - \{(0,0)\})) = g_u \circ R_{(u,w)}(g_{(w,u)}(\Omega_w - \{(0,0)\})) \\ \cap\, g_u \circ R_{(u,w)}(\Omega_u - \{(0,0)\})$$

and

$$g_u \circ R_{(u,z)}(g_{(z,u)}(\Omega_z - \{(0,0)\}) \cap (\Omega_u - \{(0,0)\})) = g_u \circ R_{(u,z)}(g_{(z,u)}(\Omega_z - \{(0,0)\})) \\ \cap\, g_u \circ R_{(u,z)}(\Omega_u - \{(0,0)\})\,.$$

But,

$$g_u \circ R_{(u,w)}(\Omega_u - \{(0,0)\}) = \text{int}(C) - \{(0,0)\} \quad \text{and} \quad g_u \circ R_{(u,z)}(\Omega_u - \{(0,0)\}) = \text{int}(C) - \{(0,0)\}\,,$$

where C is the circle of radius $\cos(\pi/6)$ and center $(0,0)$,

$$\begin{aligned} g_u \circ R_{(u,w)}(g_{(w,u)}(\Omega_w - \{(0,0)\})) &= g_u \circ R_{(u,w)} \circ R^{-1}_{(u,w)} \circ g_u^{-1} \circ h \circ g_w \circ R_{(w,u)}(\Omega_w - \{(0,0)\}) \\ &= h \circ g_w \circ R_{(w,u)}(\Omega_w - \{(0,0)\}) \\ &= \text{int}(D) - \{(1,0)\}\,, \end{aligned}$$

where D is the circle of radius $\cos(\pi/6)$ and center $(1,0)$, and

$$\begin{aligned} g_u \circ R_{(u,w)}(g_{(z,u)}(\Omega_z - \{(0,0)\})) &= g_u \circ R_{(u,w)} \circ R^{-1}_{(u,z)} \circ g_u^{-1} \circ h \circ g_z \circ R_{(z,u)}(\Omega_w - \{(0,0)\}) \\ &= g_u \circ M_{-\frac{2\pi}{m_u}} \circ g_u^{-1} \circ h \circ g_w \circ R_{(w,u)}(\Omega_w - \{(0,0)\}) \\ &= M_{-\frac{\pi}{3}} \circ h \circ g_w \circ R_{(w,u)}(\Omega_w - \{(0,0)\}) \\ &= M_{-\frac{\pi}{3}}(\text{int}(D) - \{(1,0)\}) \\ &= \text{int}(F) - \{(1/2, \sqrt{3}/2)\}\,, \end{aligned}$$

where F is the circle of radius $\cos(\pi/6)$ and center $(1/2, \sqrt{3}/2)$, and $g_u \circ M_{-\frac{2\pi}{m_u}} \circ g_u^{-1} = M_{-\frac{\pi}{3}}$. So,

$$g_u \circ R_{(u,w)}(\Omega_{uw}) = (\text{int}(C) - \{(0,0)\}) \cap (\text{int}(D) - \{(1,0)\})$$

and

$$g_u \circ R_{(u,w)}(\Omega_{uz}) = (\text{int}(C) - \{(0,0)\}) \cap (\text{int}(F) - \{(1/2, \sqrt{3}/2)\})\,,$$

as shown in Figure A.1.

But, since $M_{-\frac{\pi}{3}}(\text{int}(D) - \{(1,0)\}) = \text{int}(F) - \{(1/2, \sqrt{3}/2)\}$, we get

$$M_{-\pi/3} \circ g_u \circ R_{(u,w)}(\Omega_{uw}) = g_u \circ R_{(u,w)}(\Omega_{uz})\,.$$

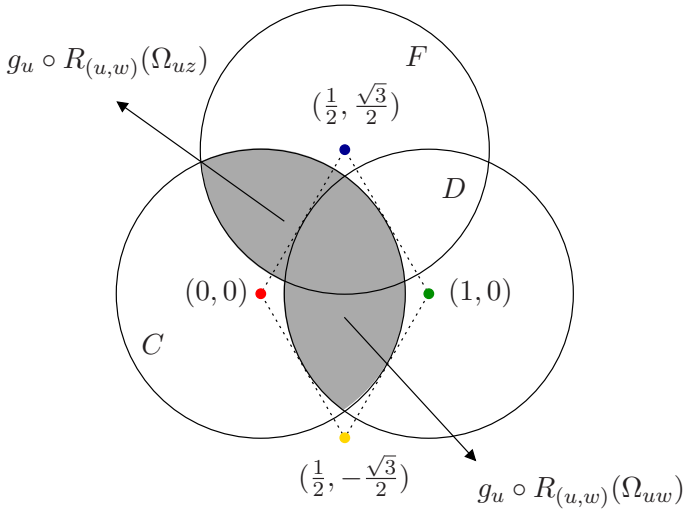

Figure A.1: The sets $g_u \circ R_{(u,w)}(\Omega_{uw})$ and $g_u \circ R_{(u,w)}(\Omega_{uz})$.

To show that $M_{\pi/3} \circ g_u \circ R_{(u,z)}(\Omega_{uz}) = g_u \circ R_{(u,z)}(\Omega_{uw})$, we can proceed as before, but noting that

$$R_{(u,z)} \circ R^{-1}_{(u,w)} = M_{\frac{2\pi}{m_u}} \quad \text{and} \quad g_u \circ M_{\frac{2\pi}{m_u}} \circ g_u^{-1} = M_{\frac{\pi}{3}}\,.$$

To prove the second claim, note that

$$\begin{aligned}
M_{-\frac{2\pi}{m_u}}(\Omega_{uw}) &= M_{-\frac{2\pi}{m_u}}(g_{(w,u)}(\Omega_w - \{(0,0)\}) \cap (\Omega_u - \{(0,0)\})) \\
&= M_{-\frac{2\pi}{m_u}} \circ g_{(w,u)}(\Omega_w - \{(0,0)\}) \cap M_{-\frac{2\pi}{m_u}}(\Omega_u - \{(0,0)\}) \\
&= M_{-\frac{2\pi}{m_u}} \circ R^{-1}_{(u,w)} \circ g_u^{-1} \circ h \circ g_w \circ R_{(w,u)}(\Omega_w - \{(0,0)\}) \cap (\Omega_u - \{(0,0)\}) \\
&= R^{-1}_{(u,z)} \circ g_u^{-1}(\text{int}(D) - \{(0,0)\}) \cap (\Omega_u - \{(0,0)\}) \\
&= \Omega_{uz} \cap (\Omega_u - \{(0,0)\}) \\
&= \Omega_{uz}\,.
\end{aligned}$$

To show that $M_{\frac{2\pi}{m_u}}(\Omega_{uz}) = \Omega_{uw}$ holds, we can proceed as before, but noting that $M_{\frac{2\pi}{m_u}} \circ R^{-1}_{(u,z)} = R^{-1}_{(u,w)}$. □

Lemma 4.2.1. Let Ω_u, Ω_w, and Ω_x be any three p-domains in $(\Omega_v)_{v\in I}$. If the intersection

$$\Omega_{xu} \cap \Omega_{xw}$$

is nonempty, then

$$\varphi_{xu}^{-1}(\Omega_{xu} \cap \Omega_{xw}) \subseteq \Omega_{uw}\,.$$

Proof. We distinguish three cases: (a) $u = w = x$, (b) $u = w$ and $u \neq x$, or $u = x$ and $u \neq w$, or $w = x$ and $u \neq w$, and (c) $u \neq w$, $u \neq x$, and $w \neq x$. Case (a) is trivial, as $\Omega_{xu} \cap \Omega_{xw} = \Omega_x$, and thus $\varphi_{xu}^{-1}(\Omega_{xu} \cap \Omega_{xw}) = \mathrm{id}_{\Omega_x}(\Omega_x) = \Omega_x = \Omega_{uw} \subseteq \Omega_{uw}$. Case (b) is also trivial. If $u = w$ and $u \neq x$ then $\Omega_{xu} \cap \Omega_{xw} = \Omega_{xu}$, and thus $\varphi_{xu}^{-1}(\Omega_{xu} \cap \Omega_{xw}) = \varphi_{xu}^{-1}(\Omega_{xu}) = \Omega_{ux} \subseteq \Omega_{uw}$. In turn, if $u = x$ and $u \neq w$ then $\Omega_{xu} \cap \Omega_{xw} = \Omega_{xx} \cap \Omega_{xw} = \Omega_x \cap \Omega_{xw} = \Omega_{xw}$, and thus $\varphi_{xu}^{-1}(\Omega_{xu} \cap \Omega_{xw}) = \mathrm{id}_{\Omega_x}^{-1}(\Omega_{xw}) = \Omega_{xw} = \Omega_{uw} \subseteq \Omega_{uw}$. Finally, if $w = x$ and $u \neq w$ then $\Omega_{xu} \cap \Omega_{xw} = \Omega_{xu} \cap \Omega_{xx} = \Omega_{xu} \cap \Omega_x = \Omega_{xu}$, and thus $\varphi_{xu}^{-1}(\Omega_{xu} \cap \Omega_{xw}) = \varphi_{xu}^{-1}(\Omega_{xu}) = \Omega_{ux} = \Omega_{uw} \subseteq \Omega_{uw}$. So, consider case (c) and assume that the edges $[u, w]$, $[u, x]$, and $[w, x]$ of $\mathcal{K}$ are shared by the triangles $[u, w, x]$ and $[u, w, z]$, $[u, w, x]$ and $[u, x, y]$, and $[u, w, x]$ and $[u, w, v]$ of $\mathcal{K}$, respectively.

The key idea behind our argument is to show that

$$g_{(u,x)}^{-1}(\Omega_{xu} \cap \Omega_{xw}) = \Omega_{ux} \cap \Omega_{uw}\,.$$

In fact, since $g_{(u,x)}^{-1}$ is bijective,

$$g_{(u,x)}^{-1}(\Omega_{xu} \cap \Omega_{xw}) = g_{(u,x)}^{-1}(\Omega_{xu}) \cap g_{(u,x)}^{-1}(\Omega_{xw}) = g_{(x,u)}(\Omega_{xu}) \cap g_{(x,u)}(\Omega_{xw}) = \Omega_{ux} \cap g_{(x,u)}(\Omega_{xw})\,.$$

By definition,

$$g_{(x,u)}(\Omega_{xw}) = R_{(u,x)}^{-1} \circ g_u^{-1} \circ h \circ g_x \circ R_{(x,u)}(\Omega_{xw})\,.$$

From Proposition 4.2.4, we have that

$$R_{(u,x)}^{-1} \circ g_u^{-1} \circ h \circ g_x \circ R_{(x,u)}(\Omega_{xw}) = R_{(u,x)}^{-1} \circ g_u^{-1} \circ h \circ M_{\frac{\pi}{3}} \circ g_x \circ R_{(x,u)}(\Omega_{xu})\,,$$

where $M_{\frac{\pi}{3}}$ is a rotation by $\frac{\pi}{3}$ around the origin. By construction, the composite function $g_x \circ R_{(x,u)}$ maps Ω_{xu} onto the canonical lens, E, which can be expressed by

$$E = (\mathrm{int}(C) - \{(0,0)\}) \cap (\mathrm{int}(D) - \{(1,0)\})\,,$$

where C is the circle of radius $\cos(\pi/6)$ and center $(0,0)$ and D is the circle of radius $\cos(\pi/6)$ and center $(1,0)$. So,

$$h \circ M_{\frac{\pi}{3}} \circ g_x \circ R_{(x,u)}(\Omega_{xu})$$

is the set

$$(\text{int}(D) - \{(1,0)\}) \cap \left(\text{int}(G) - \left\{\left(\frac{1}{2}, -\frac{\sqrt{3}}{2}\right)\right\}\right) ,$$

where G is the circle of radius $\cos(\pi/6)$ and center $(1/2, -\sqrt{3}/2)$. But, only the points of the above set which also belong to $\text{int}(C) - \{(0,0)\}$ are mapped by $R^{-1}_{(u,x)} \circ g_u^{-1}$ to Ω_u. So, we can say that $g_{(x,u)}(\Omega_{xw}) \cap \Omega_u$ is the image of

$$(\text{int}(C) - \{(0,0)\}) \cap (\text{int}(D) - \{(1,0)\}) \cap \left(\text{int}(G) - \left\{\left(\frac{1}{2}, -\frac{\sqrt{3}}{2}\right)\right\}\right)$$

under $R^{-1}_{(u,x)} \circ g_u^{-1}$ (see Figure A.2).

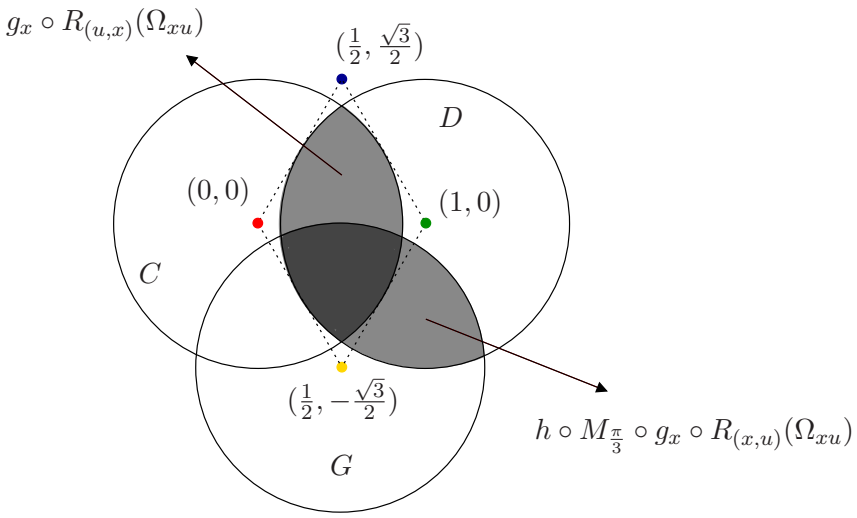

Figure A.2: The sets $h \circ M_{\frac{\pi}{3}} \circ g_x \circ R_{(u,x)} \circ g_u(\Omega_{xu})$ and $h \circ g_x \circ R_{(u,x)} \circ g_u(\Omega_{xu})$.

Now, we claim that the image of $\Omega_{ux} \cap \Omega_{uw}$ under $g_u \circ R_{(u,x)}$ is also equal to

$$(\text{int}(C) - \{(0,0)\}) \cap (\text{int}(D) - \{(1,0)\}) \cap \left(\text{int}(G) - \left\{\left(\frac{1}{2}, -\frac{\sqrt{3}}{2}\right)\right\}\right) .$$

In fact,

$$g_u \circ R_{(u,x)}(\Omega_{ux} \cap \Omega_{uw}) = g_u \circ R_{(u,x)}(\Omega_{ux}) \cap g_u \circ R_{(u,x)}(\Omega_{uw}) .$$

By definition,

$$g_u \circ R_{(u,x)}(\Omega_{ux}) = E = (\text{int}(C) - \{(0,0)\}) \cap (\text{int}(D) - \{(1,0)\})\,.$$

In turn, from Proposition 4.2.4, we know that $g_u \circ R_{(u,x)}(\Omega_{uw}) = M_{-\frac{\pi}{3}} \circ g_u \circ R_{(u,x)}(\Omega_{uw})$. So,

$$g_u \circ R_{(u,x)}(\Omega_{uw}) = M_{-\frac{\pi}{3}}(E) = (\text{int}(C) - \{(0,0)\}) \cap \left(\text{int}(G) - \left\{\left(\frac{1}{2}, -\frac{\sqrt{3}}{2}\right)\right\}\right)\,,$$

and hence

$$g_u \circ R_{(u,x)}(\Omega_{ux} \cap \Omega_{uw}) = (\text{int}(C) - \{(0,0)\}) \cap (\text{int}(D) - \{(1,0)\}) \cap \left(\text{int}(G) - \left\{\left(\frac{1}{2}, -\frac{\sqrt{3}}{2}\right)\right\}\right)\,.$$

This means that

$$\begin{aligned}
\Omega_{ux} \cap \Omega_{uw} &= g_{(x,u)}(\Omega_{xw}) \cap \Omega_u \\
&= g_{(x,u)}(\Omega_{xw}) \cap \Omega_{ux} \\
&= g_{(x,u)}(\Omega_{xw}) \cap g_{(x,u)}(\Omega_{xu}) \\
&= g_{(x,u)}(\Omega_{xw} \cap \Omega_{xu}) \\
&= g^{-1}_{(u,x)}(\Omega_{xw} \cap \Omega_{xu})\,.
\end{aligned}$$

Since $\varphi^{-1}_{xu}(p) = g^{-1}_{(u,x)}(p)$, for every $p \in \Omega_{xu}$, we get $\varphi^{-1}_{xu}(\Omega_{xw} \cap \Omega_{xu}) = \Omega_{ux} \cap \Omega_{uw}$, and hence our claim is true. □

Lemma 4.2.2 Let Ω_u, Ω_w, and Ω_x be any three p-domains in $(\Omega_v)_{v\in I}$. If $\Omega_{xu} \cap \Omega_{xw} \neq \emptyset$, then

$$\varphi_{wu}(p) = \varphi_{wx} \circ \varphi_{xu}(p)\,,$$

for all $p \in \varphi^{-1}_{xu}(\Omega_{xu} \cap \Omega_{xw}) \subseteq \Omega_{uw}$.

Proof. From Lemma 4.2.1, we know that φ_{wu} is well-defined for all points in $\varphi^{-1}_{xu}(\Omega_{xu} \cap \Omega_{xw}) \subseteq \Omega_{uw}$. So, we are left to show that $\varphi_{wu} = \varphi_{wx} \circ \varphi_{xu}$. We assume that u, w, and x are all distinct; otherwise, if two of them are equal or all of them are the same, our claim would be reduced to condition (3)(b) of Definition 3.4.1, which has already been proved. Since the indices u, w, and x are assumed to be pairwise distinct, Definition 4.1.10 tells us that $\varphi_{wu} = g_{(u,w)}$, $\varphi_{wx} = g_{(x,w)}$, and $\varphi_{xu} = g_{(u,x)}$. So, our task amounts to prove that

$$g_{(u,w)}(p) = g_{(x,w)} \circ g_{(u,x)}(p)\,,$$

for all $p \in g^{-1}_{(u,x)}(\Omega_{xu} \cap \Omega_{xw}) \subseteq \Omega_{uw}$.

From Definition 4.1.8, we know that

$$g_{(u,w)} = R^{-1}_{(w,u)} \circ g_w^{-1} \circ h \circ g_u \circ R_{(u,w)}\,, \tag{A.1}$$

$$g_{(x,w)} = R^{-1}_{(w,x)} \circ g_w^{-1} \circ h \circ g_x \circ R_{(x,w)}\,, \tag{A.2}$$

and

$$g_{(u,x)} = R^{-1}_{(x,u)} \circ g_x^{-1} \circ h \circ g_u \circ R_{(u,x)}\,. \tag{A.3}$$

So,

$$g_{(x,w)} \circ g_{(u,x)} = R^{-1}_{(w,x)} \circ g_w^{-1} \circ h \circ g_x \circ R_{(x,w)} \circ R^{-1}_{(x,u)} \circ g_x^{-1} \circ h \circ g_u \circ R_{(u,x)}\,. \tag{A.4}$$

To show that the right side of Eq. (A.4) is equal to the right side of Eq. (A.1), we make use of Proposition 4.2.4. So, consider the triangles $[s_u(u), s_u(w), s_u(x)]$, $[s_w(u), s_w(w), s_w(x)]$, and $[s_x(u), s_x(w), s_x(x)]$ of T_u, T_w, and T_x, respectively (see Figure A.3). Without loss of generality, suppose that $s_u(x)$ follows $s_u(w)$ in a counterclockwise traversal of the vertices of P_u. This means that $s_w(u)$ follows $s_w(x)$ in a counterclockwise traversal of the vertices of P_w, and that $s_x(w)$ follows $s_x(u)$ in a counterclockwise traversal of the vertices of P_x.

Let p be a point in $g^{-1}_{(u,x)}(\Omega_{xu} \cap \Omega_{xw})$. From Lemma 4.2.1, we know that $g^{-1}_{(u,x)}(\Omega_{xu} \cap \Omega_{xw}) \subseteq \Omega_{uw}$. From Proposition 4.2.4, we know that

$$g_u \circ R_{(u,x)}(\Omega_{uw}) = M_{-\frac{\pi}{3}} \circ g_u \circ R_{(u,w)}(\Omega_{uw})\,,$$

where $M_{-\frac{\pi}{3}}$ is a rotation by $-\pi/3$ around the origin.

Since $p \in g^{-1}_{(u,x)}(\Omega_{xu} \cap \Omega_{xw})$, we can conclude that

$$g_u \circ R_{(u,x)}(p) = M_{-\frac{\pi}{3}} \circ g_u \circ R_{(u,w)}(p)\,, \tag{A.5}$$

For the same reason, we also know that

$$g_w \circ R_{(w,x)}(q) = M_{\frac{\pi}{3}} \circ g_w \circ R_{(w,u)}(q)\,,$$

for every $q \in g^{-1}_{(w,x)}(\Omega_{xu} \cap \Omega_{xw}) \subseteq \Omega_{wx}$. So,

$$R^{-1}_{(w,x)} \circ g_w^{-1}(t) = R^{-1}_{(w,u)} \circ g_w^{-1} \circ M_{-\frac{\pi}{3}}(t)\,, \tag{A.6}$$

for every t such that $t = g_w \circ R_{(w,x)}(q)$, for some $q \in g^{-1}_{(w,x)}(\Omega_{xu} \cap \Omega_{xw})$.

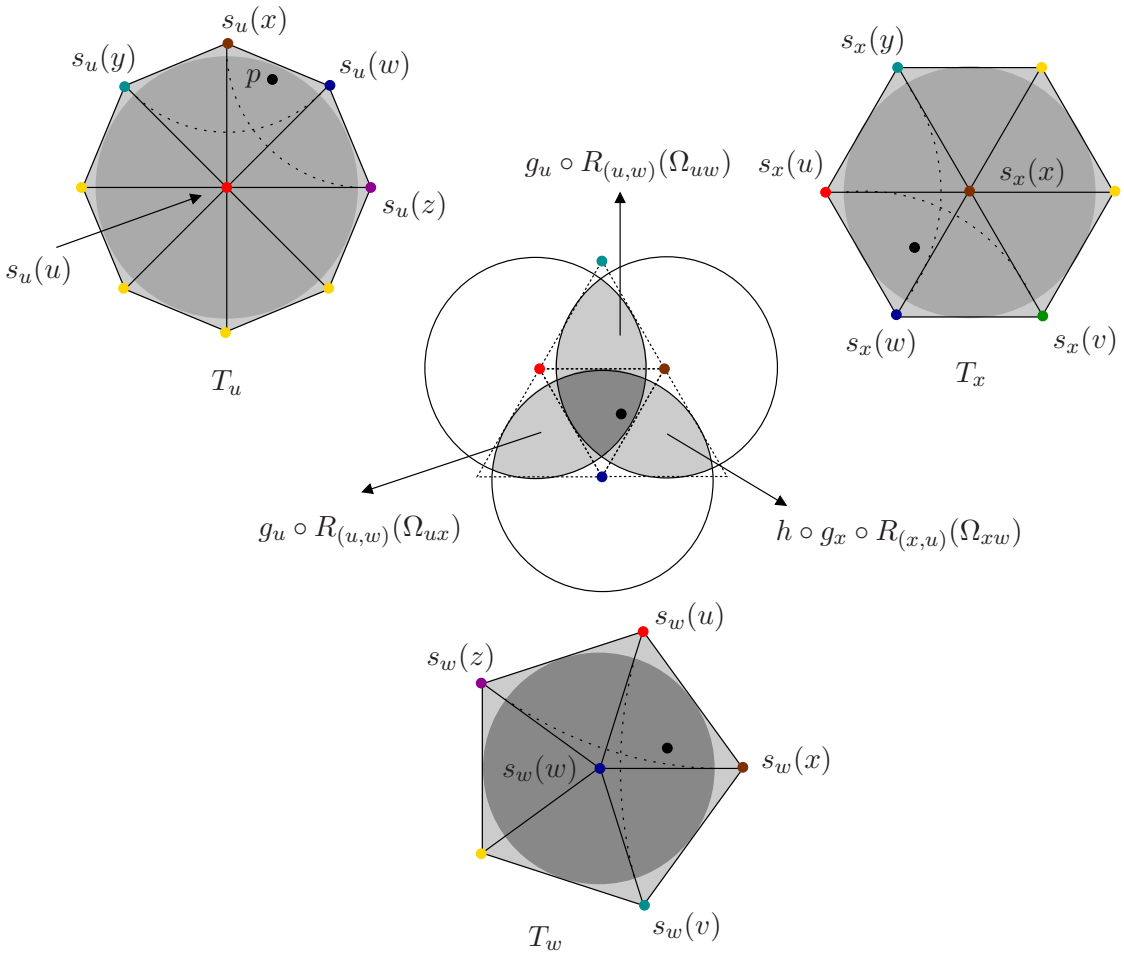

Figure A.3: Illustration of the cocycle condition.

Using the left side of the identities in Eq. (A.5) and Eq. (A.6) to replace their right side in Eq. (A.4), we get

$$g_{(x,w)} \circ g_{(u,x)} = R^{-1}_{(w,u)} \circ g_w^{-1} \circ M_{-\frac{\pi}{3}} \circ h \circ g_x \circ R_{(x,w)} \circ R^{-1}_{(x,u)} \circ g_x^{-1} \circ h \circ M_{-\frac{\pi}{3}} \circ g_u \circ R_{(u,w)} \,. \tag{A.7}$$

We claim that

$$g_x \circ R_{(x,w)} \circ R^{-1}_{(x,u)} \circ g_x^{-1}(q) = M_{-\frac{\pi}{3}}(q) \,,$$

where q is a point in the upper half of the canonical lens, E. To see why, note that

$$R_{(x,w)} \circ R^{-1}_{(x,u)} = M_{-\frac{2\pi}{m_x}} \,,$$

as $s_x(w)$ follows $s_x(u)$ in a counterclockwise traversal of P_x, where m_x is the degree of x. So,

$$g_x \circ R_{(x,w)} \circ R_{(x,u)}^{-1} \circ g_x^{-1}(q) = g_x \circ M_{-\frac{2\pi}{m_x}} \circ g_x^{-1}(q)\,.$$

But, if (β, s) and (α, t) are the polar coordinates of q and $g_x \circ M_{\frac{2\pi}{m_x}} \circ g_x^{-1}(q)$, respectively, then the definition of g_x tells us that

$$\alpha = \frac{m_x}{6} \cdot \left(-\frac{2\pi}{m_x} + \frac{6}{m_x} \cdot \beta \right) = -\frac{\pi}{3} + \beta$$

and

$$t = \frac{\cos(\pi/6)}{\cos(\pi/m_x)} \cdot \frac{\cos(\pi/m_x)}{\cos(\pi/6)} \cdot s = s\,.$$

This implies that

$$g_{(x,w)} \circ g_{(u,x)} = R_{(w,u)}^{-1} \circ g_w^{-1} \circ M_{-\frac{\pi}{3}} \circ h \circ M_{-\frac{\pi}{3}} \circ h \circ M_{-\frac{\pi}{3}} \circ g_u \circ R_{(u,w)}\,. \tag{A.8}$$

Finally, we can show that

$$h(p) = M_{-\frac{\pi}{3}} \circ h \circ M_{-\frac{\pi}{3}} \circ h \circ M_{-\frac{\pi}{3}}(p)\,,$$

for every point $p \in \mathbb{R}^2$. This is because

$$h \circ M_{-\frac{\pi}{3}} \circ h \circ M_{-\frac{\pi}{3}} \circ h \circ M_{-\frac{\pi}{3}}$$

is the identity function. But, since $h \circ h$ is the identity function, our claim follows. So,

$$g_{(x,w)} \circ g_{(u,x)}(p) = R_{(w,u)}^{-1} \circ g_w^{-1} \circ h \circ g_u \circ R_{(u,w)}(p) = g_{(u,w)}(p)\,, \tag{A.9}$$

for every $p \in g_{(u,x)}^{-1}(\Omega_{xu} \cap \Omega_{xw})$. □

A.2 The Cocycle and Hausdorff Conditions

The cocycle condition (condition 3(c) of Definition 3.4.1) may seem overly complicated, but it is actually needed to guarantee the transitivity of the relation, $\sim$, defined in the proof of Theorem 3.4.1. The problem is that $\varphi_{kj} \circ \varphi_{ji}$ is a partial function whose domain, $\varphi_{ji}^{-1}(\Omega_{ji} \cap \Omega_{jk})$, is not necessarily related to the domain, Ω_{ik}, of φ_{ki}. To ensure the transitivity of $\sim$, we must assert that whenever the composition $\varphi_{kj} \circ \varphi_{ji}$ has nonempty domain, this domain is contained in the domain of φ_{ki} and that $\varphi_{kj} \circ \varphi_{ji}$ and φ_{ki} agree.

Flawed versions of condition 3(c) of Definition 3.4.1 appear in the literature. In particular, Grimm and Hughes [44, 63] uses the following cocycle condition in their definition of a "proto-manifold" (the equivalent of what we call a set of gluing data): *For all* $x \in \Omega_{ij} \cap \Omega_{ik}$, *we have that* $\varphi_{ki}(x) = \varphi_{kj} \circ \varphi_{ji}(x)$. This condition is too weak to imply the transitivity of the relation $\sim$, as shown by the following counterexample:

Consider the open real line intervals $\Omega_1 = (0, 3)$, $\Omega_2 = (4, 5)$, $\Omega_3 = (6, 9)$, $\Omega_{12} = (0, 1)$, $\Omega_{13} = (2, 3)$, $\Omega_{21} = \Omega_{23} = (4, 5)$, $\Omega_{32} = (8, 9)$, and $\Omega_{31} = (6, 7)$, and the transition functions $\varphi_{21}(x) = x + 4$, $\varphi_{32}(x) = x + 4$, and $\varphi_{31}(x) = x + 4$. Note that the pairwise gluings yield Hausdorff spaces. Obviously, we have that $\varphi_{32} \circ \varphi_{21}(x) = x + 8$, for all $x \in \Omega_{12}$, but $\Omega_{12} \cap \Omega_{13} = \emptyset$. Thus, $0.5 \sim 4.5 \sim 8.5$, but $0.5 \not\sim 8.5$ since $\varphi_{31}(0.5)$ is undefined.

A similar and simple example can also be used to show that the Hausdorff condition (condition 4 of Definition 3.4.1) is necessary. Indeed, let $\Omega_1 = (-3, -1)$, $\Omega_2 = (1, 3)$, $\Omega_{12} = (-3, -2)$, $\Omega_{21} = (1, 2)$, and $\varphi_{21}(x) = x + 4$. The resulting space, M, is a curve looking like a "fork", and the problem is that the images of -2 and 2 in M, which are distinct points of M, cannot be separated. Indeed, the images of any two open intervals, $(-2 - \epsilon, -2 + \epsilon)$ and $(2 - \eta, 2 + \eta)$, for $\epsilon, \eta > 0$, always intersect since $(-2 - \min(\epsilon, \eta), -2)$ and $(2 - \min(\epsilon, \eta), 2)$ are identified. So, M is not Hausdorff. But, as we can clearly see, condition 4 of Definition 3.4.1 fails.